THE UNIVERSITY OF TEXAS AT AUSTIN

NAS9-13865
T-1002
3 MA-129T
75006

NASA CR-
144391

CHARACTERIZATION OF TYPICAL PLATELET INJECTOR FLOW CONFIGURATIONS

August, 1975

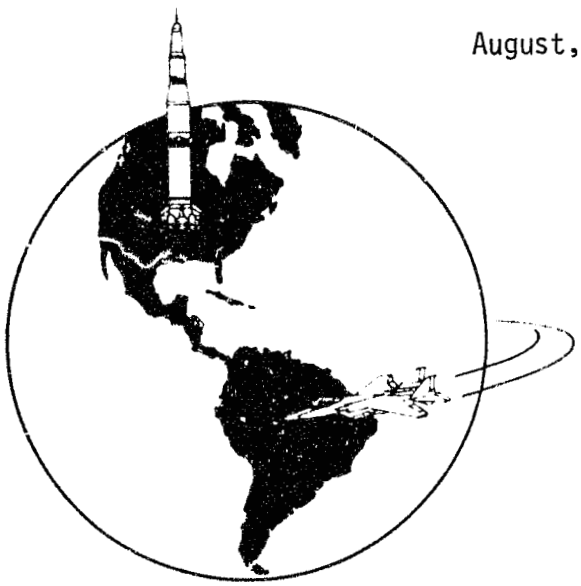

Department of Aerospace Engineering and Engineering Mechanics

NAS9-13865
T-1002
3 MA 129T

CHARACTERIZATION OF TYPICAL PLATELET INJECTOR FLOW CONFIGURATIONS

August, 1975

Submitted by

Charles E. Hickox

Department of Aerospace Engineering
and Engineering Mechanics

The University of Texas at Austin

DISTRIBUTION LIST

1. NASA Lyndon B. Johnson Space Center
Primary Propulsion Branch
Attn: Joseph Fries, Mail Code EP2
Houston, TX 77058
Mark for: Contract NAS 9-13865 — 19 copies

2. NASA Lyndon B. Johnson Space Center
Technical Library Branch
Attn: Retha Shirkey, Mail Code JM6
Houston, TX 77058
Mark for: Contract NAS 9-13865 — 4 copies

3. NASA Lyndon B. Johnson Space Center
Management Services Division
Attn: John T. Wheeler, Mail Code JM7
Houston, TX 77058
Mark for: Contract NAS 9-13865 — 1 copy

4. NASA Lyndon B. Johnson Space Center
R&T Procurement Branch
Attn: T. Lapko, Mail Code BC731
Houston, TX 77058
Mark for: Contract NAS 9-13865 — 1 copy

ACKNOWLEDGMENTS

The research described in this report was conducted for the National Aeronautics and Space Administration, Lyndon B. Johnson Space Center under contract NAS9-13865.

A number of persons provided invaluable assistance during the course of the investigation for which I am grateful. Mr. William R. Stump, Mr. William Greenlees, and Mr. Basil N. Antar contributed significantly to the experimental program. Mr. Frank J. Wise served as electronics technician. Mr. Everett Sims, Jr. assisted with all phases of the photographic studies and processed practically all the photographs. Finally, special thanks are due Ms. Pamela Rossano for so cheerfully handling the numerous details associated with the preparation of this report as well as the day-to-day accounting during the course of the study.

The Department of Aerospace Engineering and Engineering Mechanics of the University of Texas at Austin provided considerable machine shop time for the construction of the models used for testing.

The cooperation and supervision provided by the contract monitor, Mr. Joseph Fries was most helpful and is genuinely appreciated.

TABLE OF CONTENTS

TABLE OF CONTENTS continued

LIST OF SYMBOLS

A - Flow cross-sectional area

C_d - Injector discharge coefficient

D - Mean droplet diameter

g - Acceleration due to gravity

h - Vertical distance from injector face to spray collector

ℓ - Characteristic dimension of injector

$\dot{M}$ - Total mass flow rate from injector

$\dot{m}$ - Local mass flow rate in spray field

Δp - Pressure drop between plenum chamber and atmosphere

Q - Volumetric flow rate from injector

$\underset{\sim}{r}$ - Position vector of points located within the spray field

T - Reference time (or temperature)

t - Time

$\underset{\sim}{U}$ - Velocity vector

V - Reference velocity

w - Local width of spray field

x - Distance measured from center of spray

μ - Fluid viscosity

ρ - Fluid density

σ - Surface tension at liquid-gas interface

Subscripts

G - Refers to gas

I - Indicates injector

i - Initial conditions

L - Refers to liquid

m - Refers to model

p - Refers to prototype

T - Indicates total quantity

LIST OF TABLES

LIST OF FIGURES

LIST OF FIGURES continued

LIST OF FIGURES continued

1. INTRODUCTION

1.1 General Aspects of the Study

The study described in this report was undertaken in order to investigate the hydraulic atomization characteristics of several novel injector designs developed by the Aerojet Liquid Rocket Company for use in liquid propellant rocket engines. The injectors are manufactured from a series of thin stainless steel platelets through which orifices have been very accurately formed by a photoetching process. These individual platelets are then stacked together and the orifices aligned so as to produce flow passages of prescribed geometry. After alignment, the platelets are bonded into a single, "platelet injector," unit by a diffusion bonding process.

Two platelet injector concepts, the x-doublet and splash-plate, as illustrated by the Aerojet Liquid Rocket Company, are shown in Figures 1 and 2, respectively. During the early phases of the study, it was determined that the x-doublet held considerably more promise for future applications than did the splash-plate. Accordingly, this report is concerned almost exclusively with the detailed investigation of the x-doublet platelet injector as well as a number of modified versions of the basic design.

Only the hydraulic atomization characteristics were investigated, that is, the liquid atomization process exclusive of any combustion effects. Due to the complex nature of the flow associated with platelet injectors, it was necessary to use experimental techniques, exclusively, throughout the study. Large scale models of the injectors were constructed from aluminum plates and the appropriate fluids were modeled using a glycerol-water solution. Stop-action photographs using spark-shadowgraph or

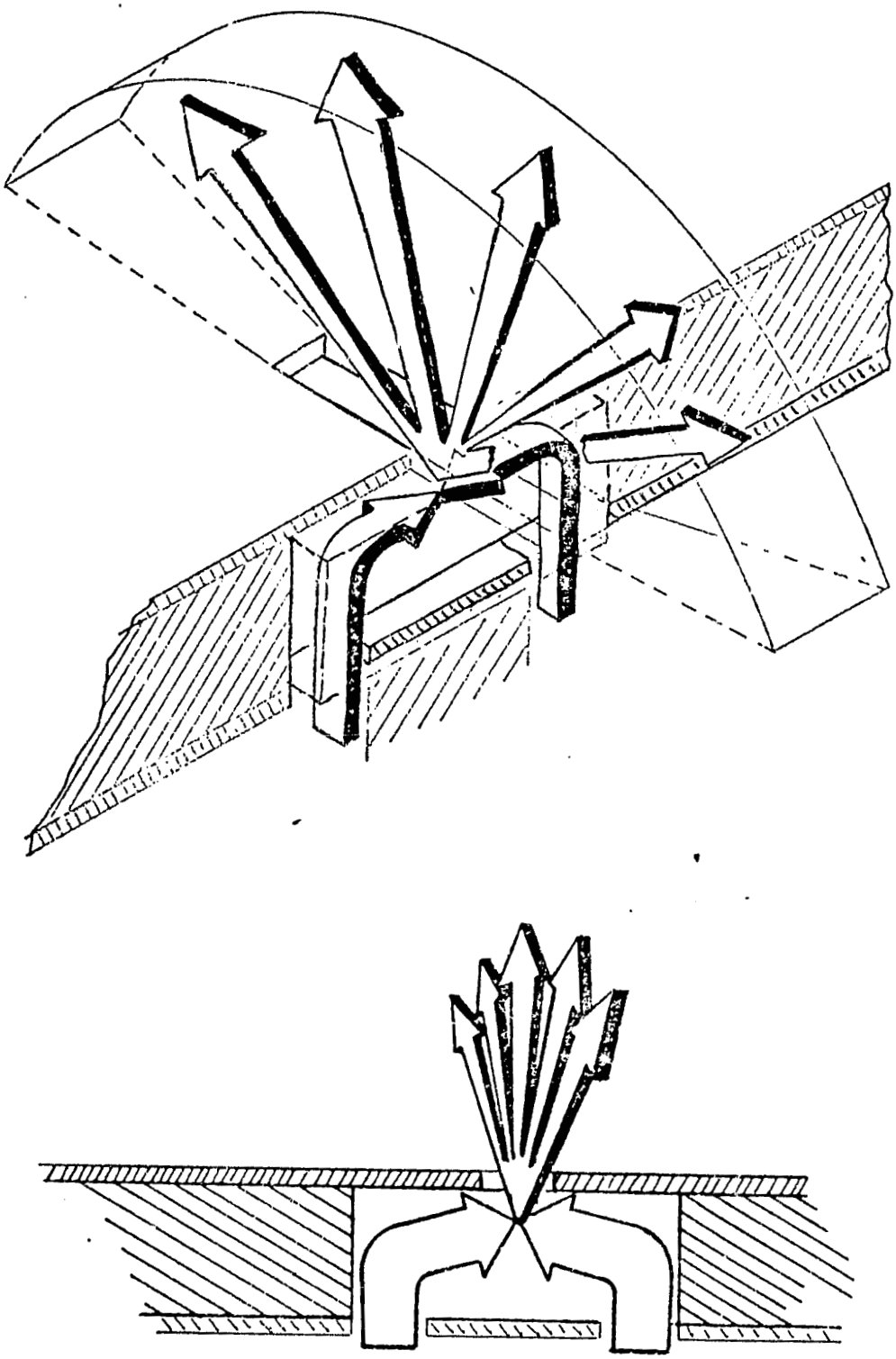

Figure 1. X-Doublet Platelet Injector

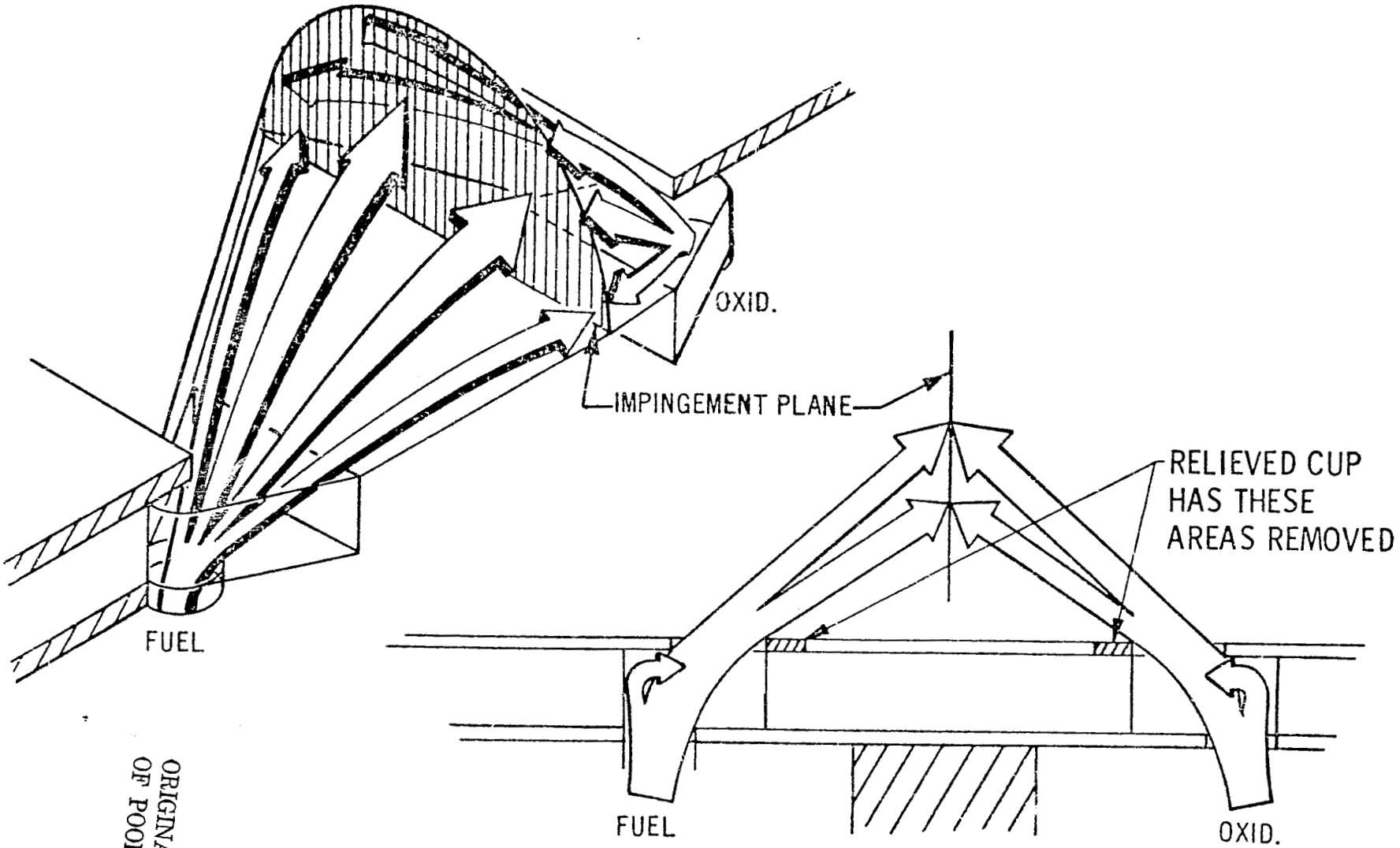

Figure 2. Splash-Plate Platelet Injector

stroboscopic back-lighting were made of the atomized spray fields produced by all configurations tested. High speed (4000 frames per second) movies were also made of several important basic configurations. From the photographs produced, certain fundamental characteristics of the atomization process could be inferred. Also, the photographs provided an effective method of comparison for the various injectors tested.

In summary, the information obtained from the study consists of: (1) photographs and movies showing typical atomization characteristics of all injector configurations tested, (2) the effect of inlet cross-flow on the performance of the x-doublet injector, (3) an investigation of the internal flow field of the x-doublet injector using a transparent plastic model and dye injection, (4) measurements of the mass distribution in the x-doublet spray field, and (5) an analysis and preliminary verification of the similarity requirements important in the modeling of atomization phenomena.

1.2 The Atomization of Liquids

A few general ideas concerning the atomization of liquids are put forth in this section in order to provide a basis for the interpretation of the data to be presented in subsequent sections of this report. Only the initial hydraulic characteristics associated with the atomization of a bulk liquid in ambient air are considered in this report. No effort was made to investigate the effects of heat transfer or secondary breakup of the atomized liquid. Although many of the effects which are of importance in an actual combustion process were not considered, an adequate procedure was established whereby the fundamental atomization characteristics of various injector designs could be readily evaluated.

Atomization of a liquid is generally understood to imply the disintegration and dispersal of a bulk liquid into a large number of droplets accompanied by a significant increase in surface area. The atomization of a liquid by mechanical means (as opposed to acoustic, vibrational, or electrostatic methods) is generally accomplished by one of the following techniques:

1. Hydraulic atomization
   (a) self-atomizing
   (b) jet impingement
   (c) swirl atomizer
2. Pneumatic atomization
3. Rotary atomizer.

Hydraulic atomization is accomplished by converting fluid pressure into kinetic energy by the passage of fluid through an orifice. Atomization then occurs as a result of fluid jet instability arising from the relative velocity between the liquid and ambient gas, impingement with another jet or solid surface, or due to the instability of a thin sheet produced by swirling action. Pneumatic atomization occurs when a high relative velocity between gas and liquid is achieved by the acceleration of the gas, instead of the liquid, to a high velocity. Rotary atomizers produce a thin sheet of fluid by centrifugal action. All of the injectors tested in the current study could, generally speaking, be included in the jet-impingement category.

Whatever the method of atomization, the kinetics of all such processes involve the following sequential steps, although any specific step may be absent under some circumstances:

1. Extension of a bulk liquid into sheets, jets, films, or streams by accelerating the liquid in some prescribed manner.
2. Initiation of small disturbances at the liquid surface in the form of local ripples, protuberances, or waves.
3. Formation of ligaments by the action of normal and shear forces.
4. Collapse of ligaments into drops due to the action of surface tension.
5. Further breakup of the drops as they move through the gaseous medium by the action of normal and shear forces.

Photographs of the spray fields produced by the injectors and included in Section 4 exhibit all of the characteristics except the last. The first four of the steps in the atomization process are depicted schematically in Figure 3.

The complete evaluation of the performance of an atomization device should consist of the consideration of the following items:

1. Geometry of the spray field
2. Energy required for effective atomization
3. Droplet size and distribution
4. Operational considerations such as erosion, corrosion, clogging, and upstream flow conditions.

All four items were investigated in varying degrees for each of the injectors tested under the current program.

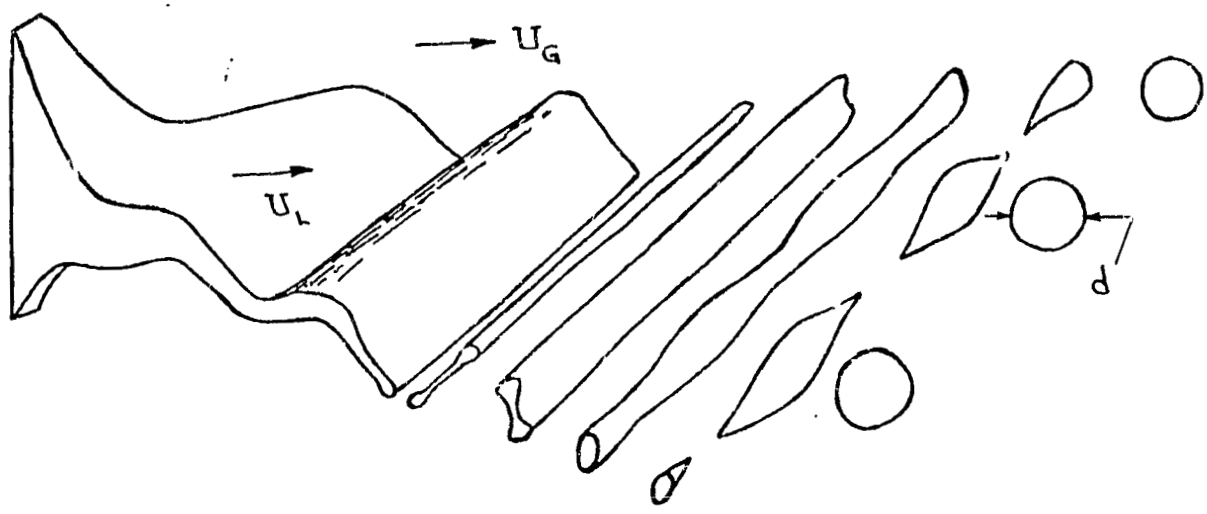

Growth of Waves on Sheet

Fragmentation and Formation of Ligaments

Breakdown of Ligaments into Drops

Figure 3. Schematic of the Atomization Process. (Adapted from Ref. 8)

1.3 Literature Survey

Throughout the study, numerous journals were consulted in an effort to determine if any previous work had been reported which would be useful in guiding the current investigation. It was originally intended to develop an extensive bibliography from the references obtained. However, several months after the initiation of this project, a report by Lapple, Henry, and Blake entitled "Atomization - A Survey and Critique of the Literature" was discovered. This report is an exhaustive, comprehensive survey of all literature pertaining to the subject of atomization published prior to 1967. Approximately 960 references along with abstracts were compiled. In addition, the results of all references were reduced to a common basis and compared in extensive tables. For reference, the abstract sources used in compiling this report are listed in the Bibliography.

Since Lapple's report is extensive and readily available for use, it was not considered worthwhile to attempt to improve on this work. References which were consulted during the course of the present investigation and which are not included in the report by Lapple are listed in the last section of the Bibliography. Also included in the Bibliography are a list of references which contains surveys of the atomization literature and a list of references which are felt to be either fundamental to the understanding of atomization phenomena or were of particular interest in the current injector study.

2. THEORY OF MODELING

2.1 Fundamental Similarity Parameters

All of the experimental data acquired during the course of this program were obtained from model studies of one kind or another. Accordingly, it is important, at this point, to examine the fundamental dimensionless parameters which are important in the description of an atomization process. The discussion to follow will be concerned specifically with the mechanical atomization of an incompressible liquid by hydraulic means as illustrated in Figure 3. Any gas velocites involved are assumed to be small enough so that compressibility effects are negligible.

As a first step, it is convenient to identify the various forces which are important in the atomization process and to express them, proportionally, in terms of the fundamental variables pertinent to atomization phenomena. Accordingly, the following proportionalities can be obtained:

$$\begin{aligned} &\text{viscous force} && \alpha && \mu V \ell \\ &\text{surface tension force} && \alpha && \sigma \ell \\ &\text{inertial force} && \alpha && \rho V^2 \ell^2 \\ &\text{pressure force} && \alpha && \Delta p \ell^2 \\ &\text{gravity force} && \alpha && \rho g \ell^3 \end{aligned} \qquad (1)$$

In the above, the quantitits V, ℓ, Δp, ρ, μ, σ, g are, respectively, a characteristic velocity, characteristic length, characteristic pressure drop, the density, viscosity, surface tension, and acceleration due to gravity. The fluid properties are taken to be those of the liquid. From the five forces identified in (1), the following four nondimensional ratios can be

formed:

$$\frac{\text{inertial force}}{\text{viscous force}} \alpha \frac{V\ell\rho}{\mu} : \text{Reynolds Number}$$

$$\frac{\text{surface tension force}}{\text{inertial force}} \alpha \frac{\sigma}{\rho V^2 \ell} : \text{Weber Number} \qquad (2)$$

$$\frac{\text{pressure force}}{\text{inertial force}} \alpha \frac{\Delta p}{\rho V^2} : \text{Euler Number}$$

$$\frac{\text{inertial force}}{\text{gravity force}} \alpha \frac{V}{\sqrt{g\ell}} : \text{Froude Number}$$

Similar force ratios can also be written for the gas in which case it is deduced that the ratios

$$\left(\frac{\rho}{\rho_G}\right) , \quad \left(\frac{\mu}{\mu_G}\right) , \qquad (3)$$

where the subscript G denotes a property of the gas, are also of importance. If the independent variables which describe spacial position and time are nondimensionalized with respect to a characteristic length ℓ and time T, there result the ratios

$$\left(\frac{\underset{\sim}{r}}{\ell}\right) , \quad \left(\frac{t}{T}\right) , \qquad (4)$$

where $\underset{\sim}{r}$ is the spacial position vector and t is the time. An additional nondimensional ratio which can be formed from the variables thus far introduced is

$$\left(\frac{\ell}{VT}\right) , \qquad (5)$$

and basically represents the ratio of local to convective acceleration in the fluid. The initial velocities in the liquid and gas prior to atomization have an important influence on the subsequent atomization process. In nondimensional form these initial velocities are

$$\left(\frac{\underset{\sim}{U}_{i,L}}{V}\right) \quad , \quad \left(\frac{\underset{\sim}{U}_{i,G}}{V}\right) \quad , \tag{6}$$

where the subscripts i, L, G indicate the initial condition, liquid, and gas, respectively. The vector $\underset{\sim}{U}$ represents the velocity.

From the previous discussion, it can be concluded that the atomization process is characterized by the following eleven nondimensional parameters:

$$\left(\frac{V\ell\rho}{\mu}\right), \left(\frac{\sigma}{\rho V^2 \ell}\right), \left(\frac{\Delta p}{\rho V^2}\right), \left(\frac{V}{\sqrt{g\ell}}\right), \left(\frac{\ell}{VT}\right), \left(\frac{\rho}{\rho_G}\right),$$

$$\left(\frac{\mu}{\mu_G}\right), \left(\frac{\underset{\sim}{r}}{\ell}\right), \left(\frac{t}{T}\right), \left(\frac{\underset{\sim}{U}_{i,L}}{V}\right), \left(\frac{\underset{\sim}{U}_{i,G}}{V}\right) \quad . \tag{7}$$

These same parameters can also be obtained from more elegant mathematical considerations if one renders nondimensional the differential equations and boundary conditions which describe the atomization process. In this case, the Navier-Stokes and continuity equations together with conditions on the normal and shear stresses between the liquid and gas, continuity of liquid and gas velocities at the interface, and initial conditions on liquid and gas velocities constitute the appropriate set of differential equations and boundary conditions.

2.2 Use of Similarity Parameters

The nondimensional parameters listed in (7) may be used in two ways. First, when conducting model studies of some prototype design, the principle of dynamic similarity requires that each of the parameters have the same numerical value in model and prototype. This insures that, in addition to the flows being kinematically similar, all forces are in the appropriate ratios and the flows are also dynamically similar, hence the origin of the term "similarity parameter". For complete similarity of model to prototype it is required that

$$\left(\frac{V\ell\rho}{\mu}\right)_m = \left(\frac{V\ell\rho}{\mu}\right)_p , \text{ etc.,} \tag{8}$$

for all eleven parameters, where the subscripts m, p indicate the model and prototype, respectively.

A second use for similarity parameters is in the formulation of prediction equations. From dimensional considerations, it is known that a flow process is described not by the numerous independent and dependent variables acting separately, but by a certain minimum number of nondimensional parameters. Hence, for the case of atomization under consideration, it can be shown that, in general, the mean droplet diameter D produced by a particular injector can be expressed in terms of the eleven parameters listed in (7), i.e.,

$$\frac{D}{\ell} = F\left[\frac{V\ell\rho}{\mu} , \frac{\sigma}{\rho V^2 \ell} , \ldots, \text{etc.}\right] , \tag{9}$$

where F denotes the functional relationship to be determined by analytical or experimental means.

2.3 Parameters Important in Platelet Injector Study

The platelet injector study considered in this report involved experimental investigations of large scale models of prototype injector designs. The scale chosen, 7.8 to 1.0, resulted in the smallest model that could be produced using conventional machining operations. Also, various geometry changes could be studied more conveniently with the models than with the relatively small prototype injectors. The prototype injectors had minimum orifice dimensions on the order of 0.020 inch and were manufactured by a special photoetching process.

It has been deduced that the hydraulic atomization of a liquid is described by the parameters listed in (7) and, furthermore, that any model study of such a process should be based on the conditions specified by (8). Since it is in general impossible to satisfy all eleven of the conditions required by (8), each of the individual parameters, as listed in (7), will be examined separately in order to determine their relative importance. From these considerations, criteria will be established for the interpretation of the experimental results. In the comments which follow, complete geometric similarity between model and prototype will be assumed.

$\left(\frac{\Delta p}{\rho V^2}\right)$: In general, for large Reynolds number (>10,000) flow of an incompressible liquid through an orifice, the ratio of pressure drop across the orifice to the terms ρV^2 is constant. Hence, this nondimensional parameter will have the same

numerical value in model and prototype so long as the Reynolds number is above some minimum critical value.

$\left(\frac{V}{\sqrt{g\ell}}\right)$: It is expected that, near the outlet of the injector where the atomization process is initiated, inertial effects will be of much more importance than gravitational effects. This parameter will thus be relatively unimportant and can safely be omitted in subsequent considerations.

$\left(\frac{\ell}{VT}\right)$: The numerical value of this parameter is dictated by the choice of reference quantities. If the reference time T for the process is taken equal to (ℓ/V), then this nondimensional parameter is identically equal to unity for both model and prototype. This choice of reference time is deemed appropriate for the process under consideration.

$\left(\frac{\rho}{\rho_G}\right)$: This parameter is important, but is not controllable in the current study since both model and prototype atomization occur in ambient air. Popov[14] has noted that an increase in the ratio (ρ_G/ρ) of 300% caused a decrease of 57% in the mean droplet diameter as measured for the atomization of a single jet of fluid. In the current

investigation, (ρ/ρ_G) varied by 10% between model and prototype, the prototype having the larger value.

$\left(\frac{\mu}{\mu_G}\right)$: This parameter is also important, but uncontrollable for the same reason stated above. Popov[14] found that the mean droplet diameter decreased by 8% when the ratio (μ_G/μ) was increased by 300%. In the current investigation, (μ/μ_G) varied by 300% between model and prototype, the prototype having the larger value.

$\left(\frac{\underset{\sim}{r}}{\ell}\right)$, $\left(\frac{t}{T}\right)$: These parameters indicate that, so long as all other conditions are satisfied, the atomization processes of model and prototype will have the same spatial relationship and time correspondence. In the model studies reported here, precise time correspondence between events was not demanded since only average or typical atomization processes were of concern.

$\left(\frac{\underset{\sim}{U}_{i,L}}{V}\right)$, $\left(\frac{\underset{\sim}{U}_{i,G}}{V}\right)$: These parameters express the requirement that the initial gas and liquid velocity distributions should be identical in model and prototype. In the current study, $\underset{\sim}{U}_{i,G}$ was negligible for both model and prototype. So long as the Reynolds numbers and internal flow passages are identical in model and prototype, it is anticipated that

$\underset{\sim}{U}_{i,L}$ will have the same average distribution in both instances.

From the previous considerations it is concluded that model studies of hydraulic atomization can be based on the requirements of equality of Reynolds and Weber numbers

$$\left(\frac{V\ell\rho}{\mu}\right)_m = \left(\frac{V\ell\rho}{\mu}\right)_p \quad , \quad \left(\frac{\sigma}{\rho V^2 \ell}\right)_m = \left(\frac{\sigma}{\rho V^2 \ell}\right)_p \quad . \tag{10}$$

From (10) the following transfer relations between model and prototype can be established

$$\begin{aligned} \frac{\ell_m}{\ell_p} &= \left(\frac{\mu_m}{\mu_p}\right)^2 \left(\frac{\sigma_p}{\sigma_m}\right) \left(\frac{\rho_p}{\rho_m}\right) \\ \frac{V_m}{V_p} &= \left(\frac{\mu_m}{\mu_p}\right) \left(\frac{\ell_p}{\ell_m}\right) \left(\frac{\rho_p}{\rho_m}\right) = \left(\frac{\mu_p}{\mu_m}\right) \left(\frac{\sigma_m}{\sigma_p}\right) \quad . \end{aligned} \tag{11}$$

The Euler number then yields the relationship between pressure drops

$$\frac{\Delta p_m}{\Delta p_p} = \left(\frac{\rho_m}{\rho_p}\right) \left(\frac{V_m}{V_p}\right)^2 \quad . \tag{12}$$

3. EXPERIMENTAL PROGRAM

3.1 Model Design

A model-to-prototype injector scale of 7.81-to-1.0 was adopted for use in the experimental program. This choice of scale was dictated by two opposing considerations. First, it was desired to have the model as small as possible in order that the modeling criteria set forth in Section 2 could be adhered to as closely as possible. On the other hand, it was necessary to have the model as large as possible to allow for ease of manufacture using conventional machining operations. Along this same line, it was necessary to choose a scale which would result in convenient dimensions for the model.

Prototype x-doublet and splash-plate injectors used in the program were supplied by the Aerojet Liquid Rocket Company. A photograph of a typical prototype x-doublet injector, as mounted for testing, is presented in Figure 4. Models of the x-doublet were constructed from aluminum plates using standard broaching and milling techniques. The plates were fastened together with machine screws. A photograph of a typical x-doublet model (XD-M1) is presented in Figure 5. The designation XD-M1 refers to "x-doublet model number 1", with similar designations used for other models. A prototype splash-plate was tested, but no splash-plate models were constructed. Sketches, together with the dimensions of all models tested, are included in Appendix A.

The fuel proposed for use with the prototype injectors was liquid MMH. So far as hydraulics are concerned, the fluid properties of liquid MMH at room termperature are very close to those of water. Accordingly, it

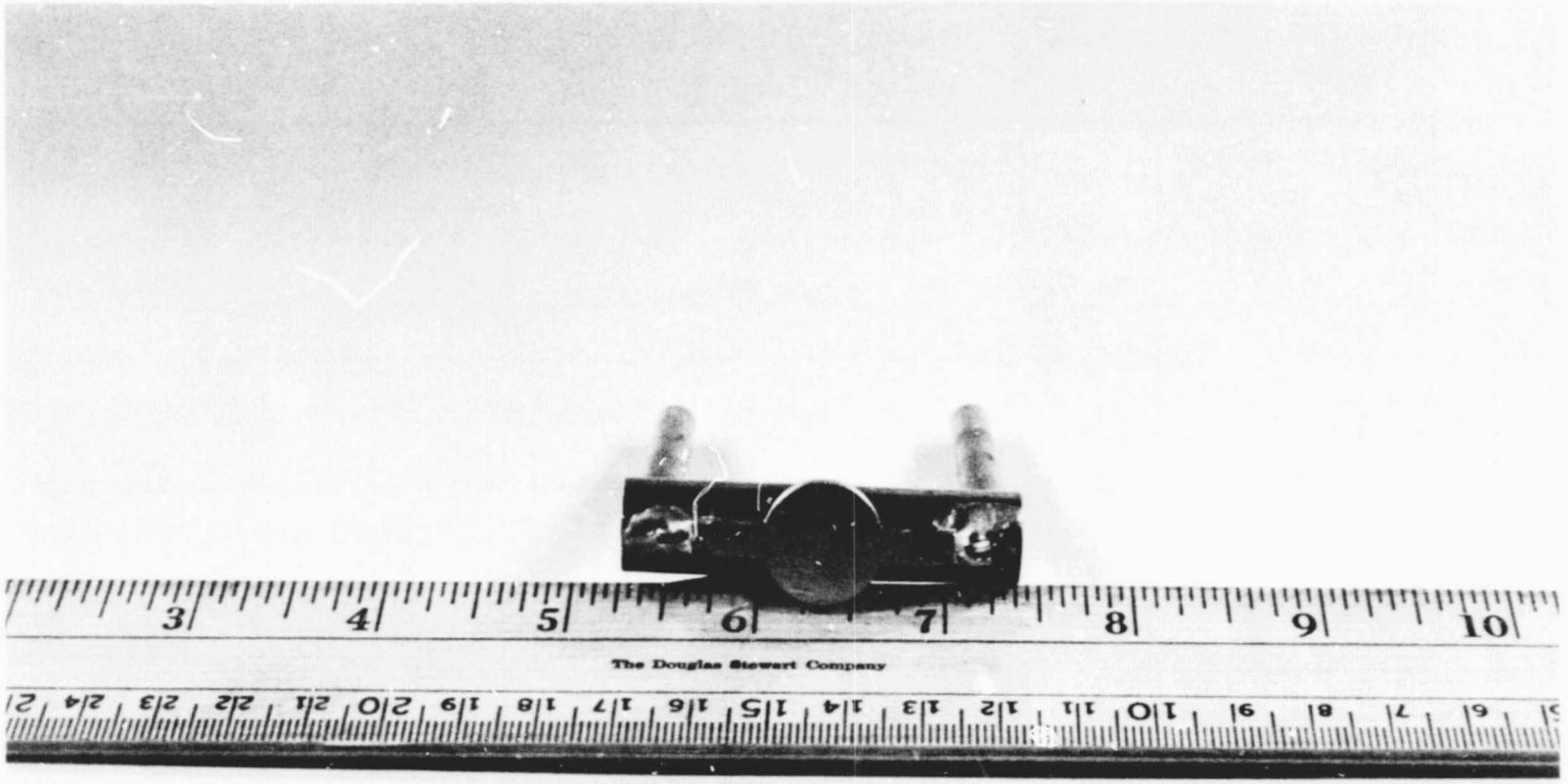

Figure 4. Typical Prototype X-Doublet Injector Mounted for Testing

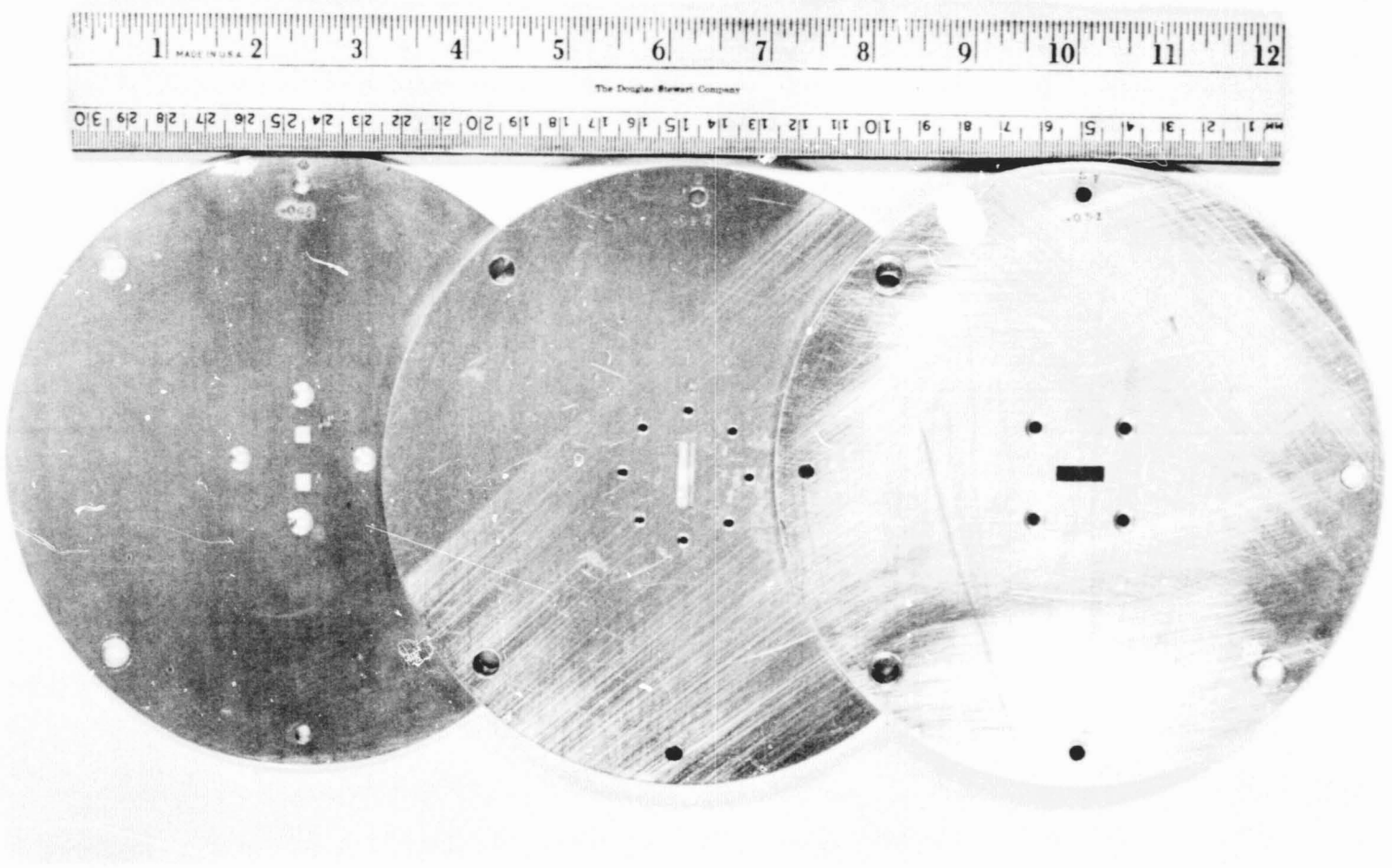

Figure 5. Typical X-Doublet MOdel (XD-Mi)

was decided to evaluate the hydraulic properties of the prototype injectors using water as the working fluid in the fuel side of the injector. For any scale other than unity, the first of equations (11) dictates that some fluid other than water must be used in the model tests. Glycerol-water solutions were used in the test program. For a scale of 7.81-to-1.0, the first of equations (11) is satisfied by a 34% aqueous glycerol solution. If the model is based on the actual fluid properties of liquid MMH at 200°F, then a 24% solution is appropriate. For comparison purposes, a 34% solution was used almost exclusively. Properties of all fluids used in the experiments are summarized in Appendix B.

3.2 Experimental Flow Facility

Photographs of the flow facility used in the tests are presented in Figures 6 through 8. A line diagram of the flow facility and associated equipment information is included in Appendix A. In the flow facility, the injector which is to be tested is bolted to a small plenum chamber which is in turn supplied with fluid from an 82 gallon reservoir. The reservoir is pressurized to an appropriate value (depending on the flow rate to be established) using 100 psig house air. The pressure in the plenum chamber is monitored with a Bourdon tube pressure gage and the volumetric flow rate is measured with a rotameter. A sketch of the plenum chamber is presented in Appendix A. The fluid is exhausted into air at ambient room conditions (generally 70 - 75°F, 30 - 40% relative humidity) and collected in a holding tank. A frequent check of specific gravity is made on the fluid in the holding tank and corrected if necessary before returning the fluid to the reservoir.

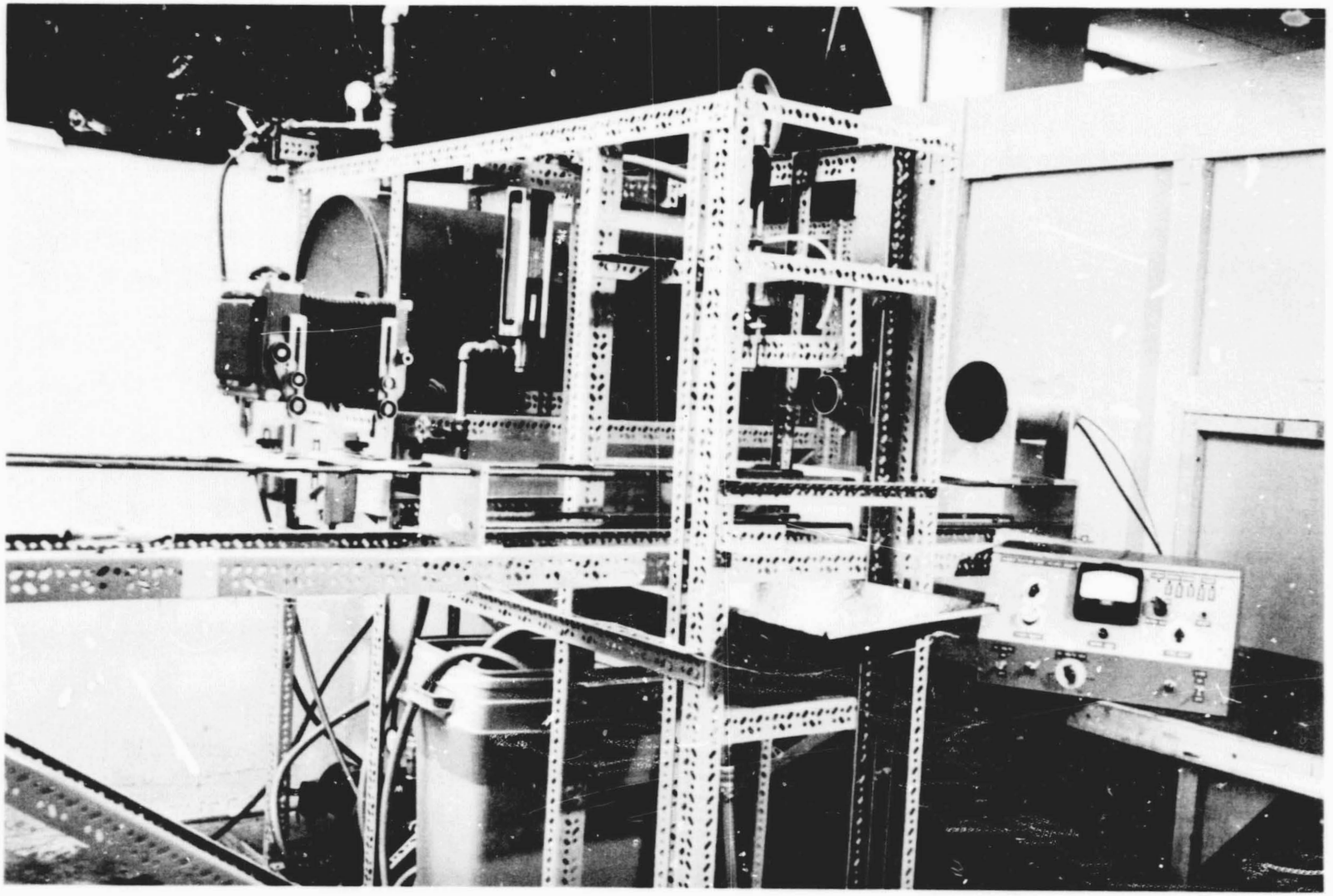

Figure 6. Flow Facility with Shadowgraph

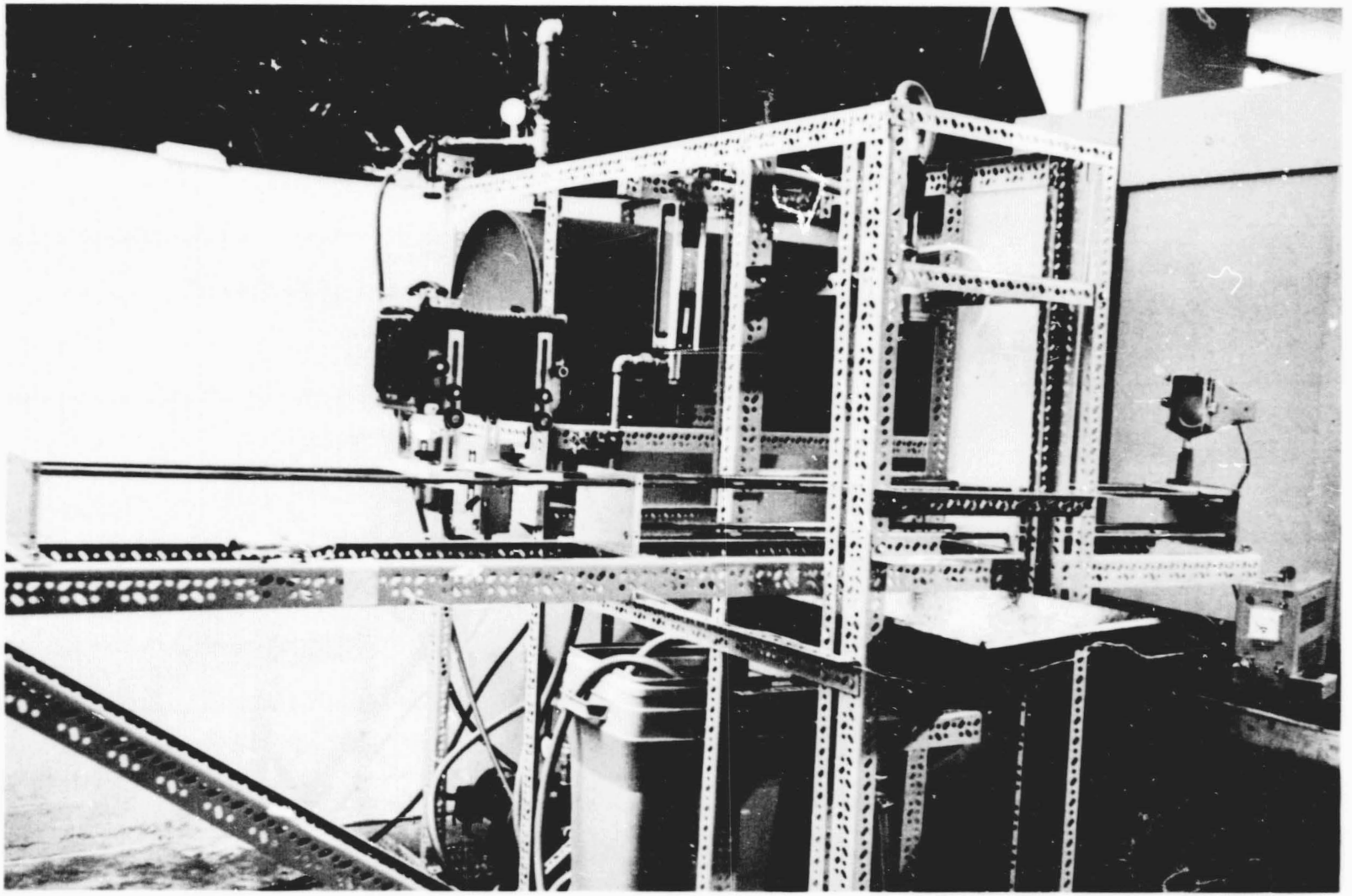

Figure 7. Flow Facility with Stroboscopic Back-Lighting

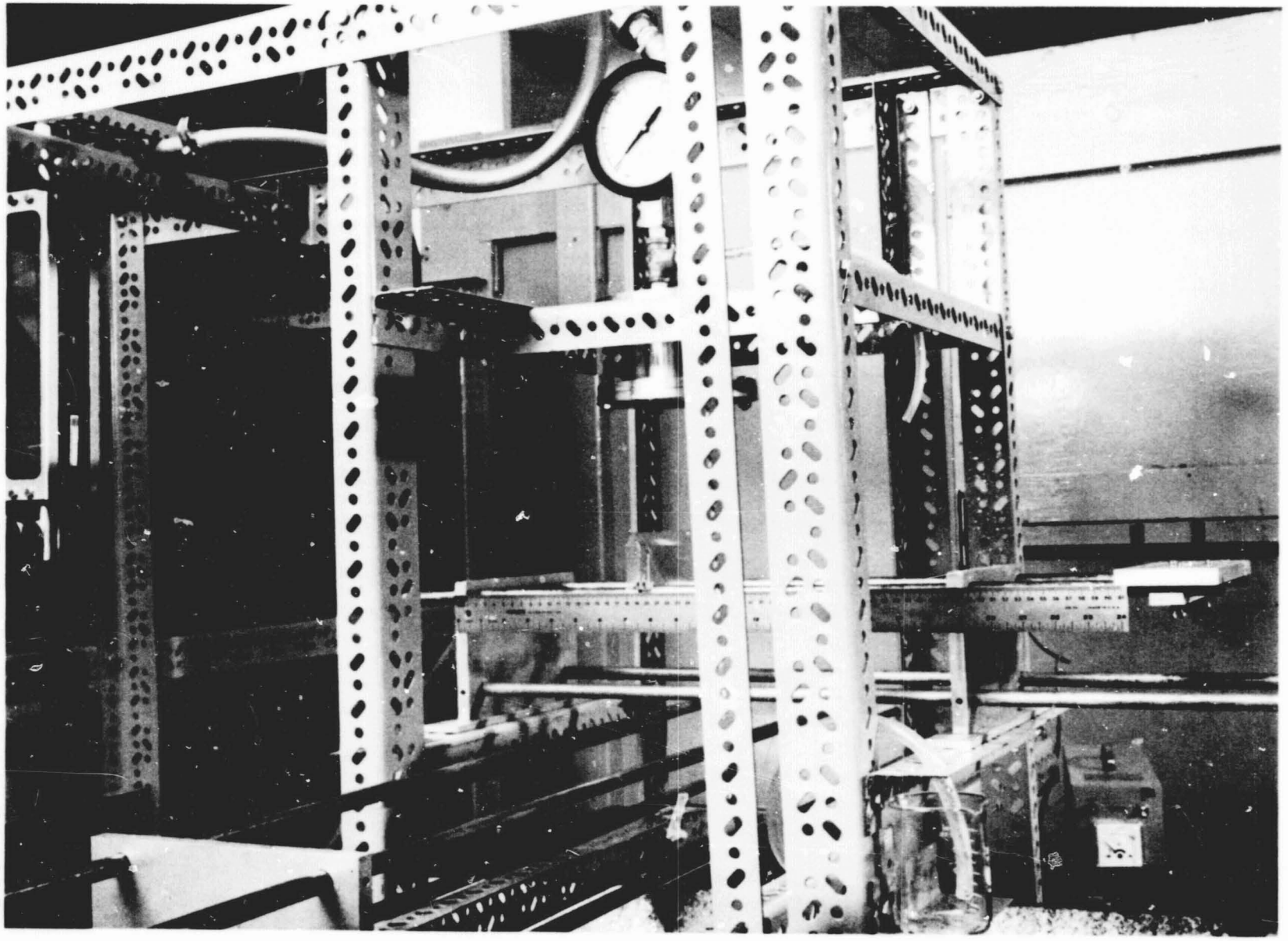

Figure 8. Flow Facility Showing Plenum Chamber and Mass Measurement Apparatus

3.3 Photographic Techniques

The photographic techniques used to produce the stop-action photographs included in this report are shown schematically in Figure 9. The actual systems are shown in Figures 6 and 7. Specific data on the important system components are tabulated in Appendix C.

The spark-shadowgraph technique was used for all prototype studies. The spray field produced by the injector was illuminated by an approximately collimated beam of light from a spark-discharge point source which was originally designed for use with a small ballistics tunnel in the laboratories of the Aerospace Engineering Department at the University of Texas at Austin. To generate a spark source, five .05 μf capacitors, wired in parallel, were charged to 4000 volts and then discharged across an ionized air gap. A spark duration of approximately 1.0 μ-sec was thus obtained. A complete analysis of the shadowgraph optical system is considered in Appendix C.

A stroboscopic back-lighted arrangement was adopted for use in the model studies. This change was necessitated by the relatively small field of view attainable with the shadowgraph system. The spray field produced by the model was illuminated from behind by a single flash, with a duration of approximately 50 μ-sec., from a stroboscopic lamp. Before reaching the spray, the light was diffused by passage through two 1/4-in. sheets of translucent acrylic plastic. The plastic sheets were rendered translucent by sand-blasting. The photographs obtained with this sytem did not have the clarity and depth of field exhibited by the shadowgraphs, but were of sufficient quality for qualitative comparison of various injector designs.

High speed movies (4000 frames/sec.) were successfully obtained for

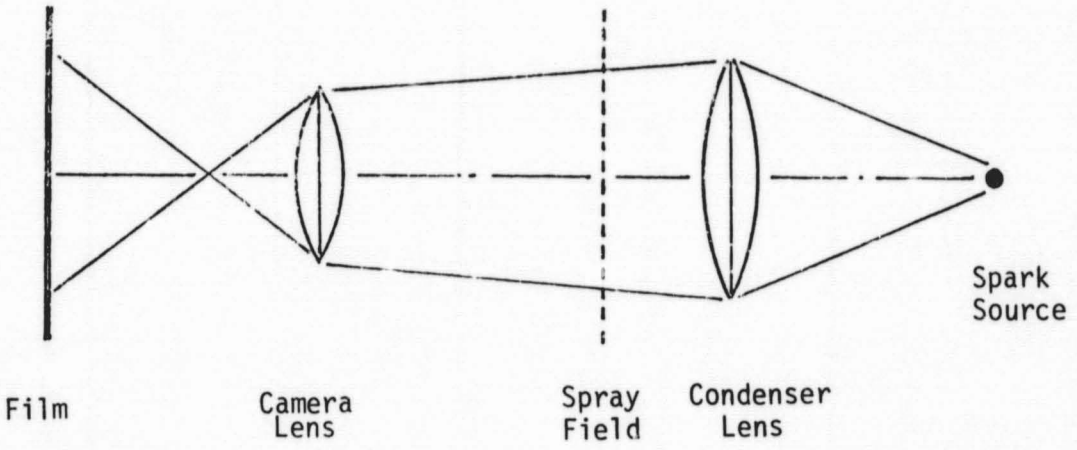

(a) Spark Shadowgraph

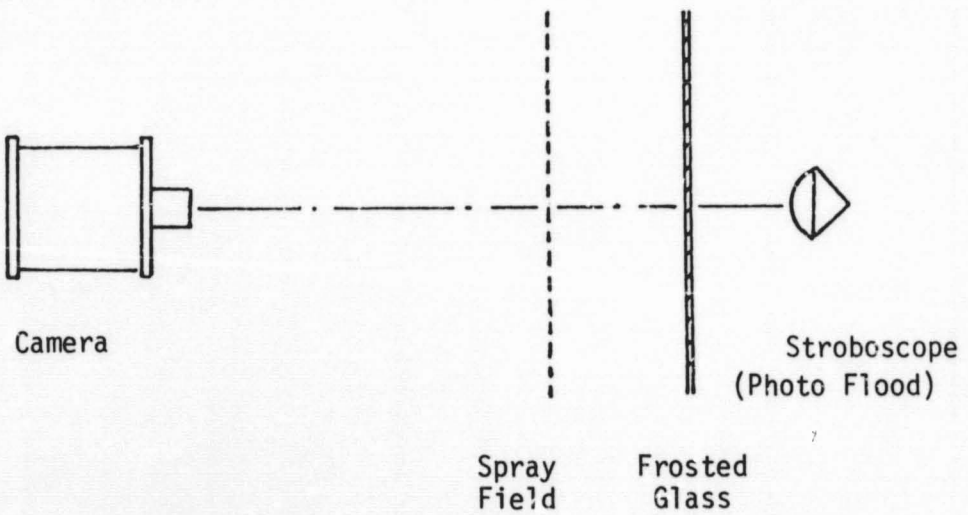

(b) Stroboscopic Back-Lighting

Figure 9. Stop-Action Photographic Techniques

several different operating conditions for the standard x-doublet model (XD-M1). However, since none of the movie frames are reproduced in this report, all of the data associated with the taking of the movie sequences are summarized in Appendix C.

3.4 Flow Visualization Studies

Internal flow visualization studies were conducted using the 15.7-to-1.0 transparent scale model of the x-doublet, shown in Figure 10. A sketch of this model is included in Appendix A. Since only the internal flow characteristics of the model were to be studied, water was used in the test and the flow rate was adjusted to obtain similarity of Reynolds numbers between model and prototype. Streak lines of the flow were rendered visible by the injection of ink into the flow field.

3.5 Inlet Cross-Flow Studies

The sensitivity of the x-doublet to an inlet cross-flow was studied through use of the inlet cross-flow manifold shown in Figure 11. A sketch of the manifold is included in Appendix A. The model injector was bolted to the manifold. Flow entered the manifold from the plenum chamber through the hole near the left of the manifold as seen in Figure 11, and proceeded along the rectangular slot. Part of the flow could be allowed to bypass the injector and exit through the pipe attached to the manifold. The amount of cross-flow was regulated by a valve in the exit line. Cross-flow velocities of 23% of the injector exit velocity could be obtained with the injector operating at design conditions. The inlet orifices of the injector could be oriented at various angles to the cross-flow.

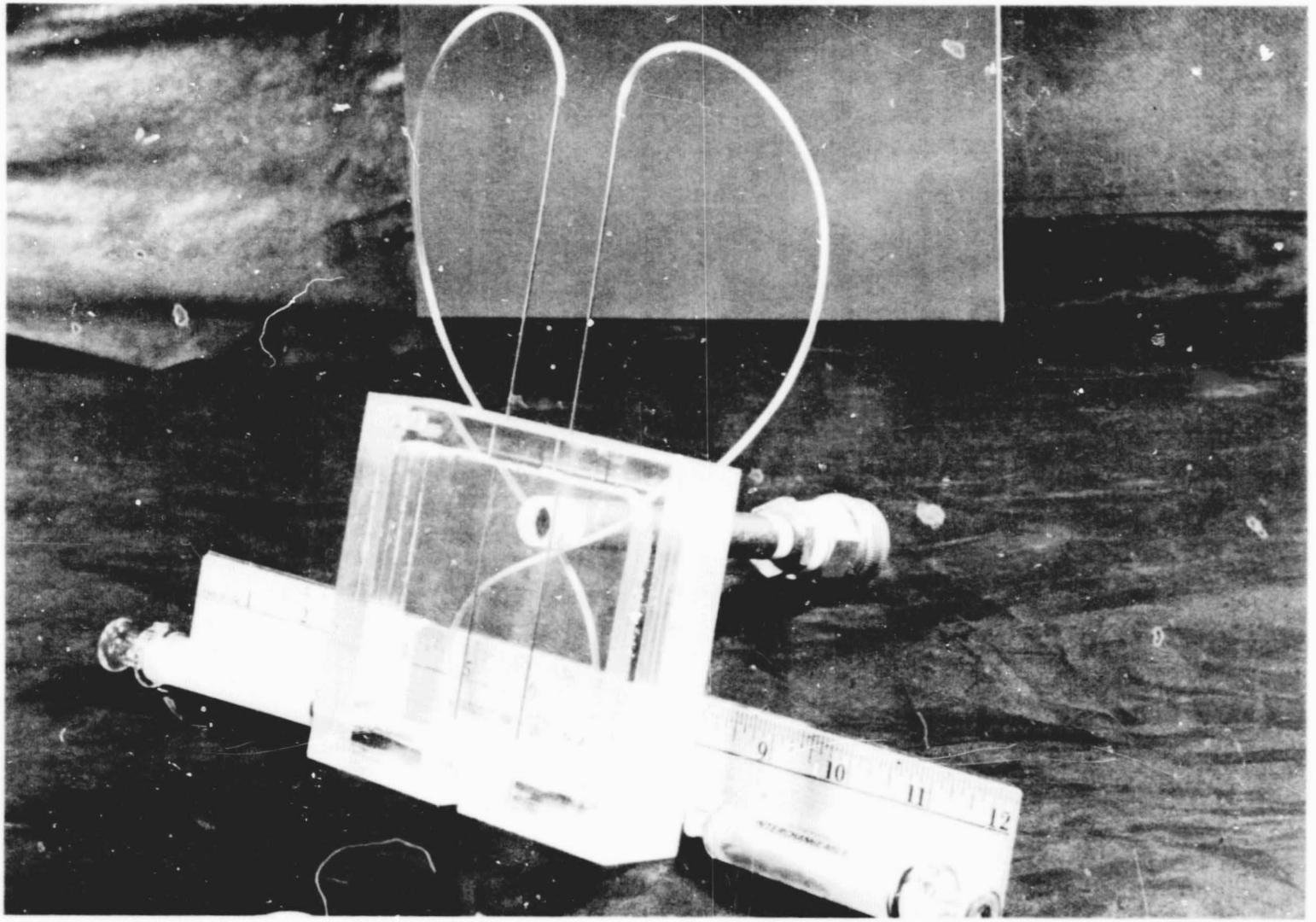

Figure 10. Flow Visualization Model for X-Doublet

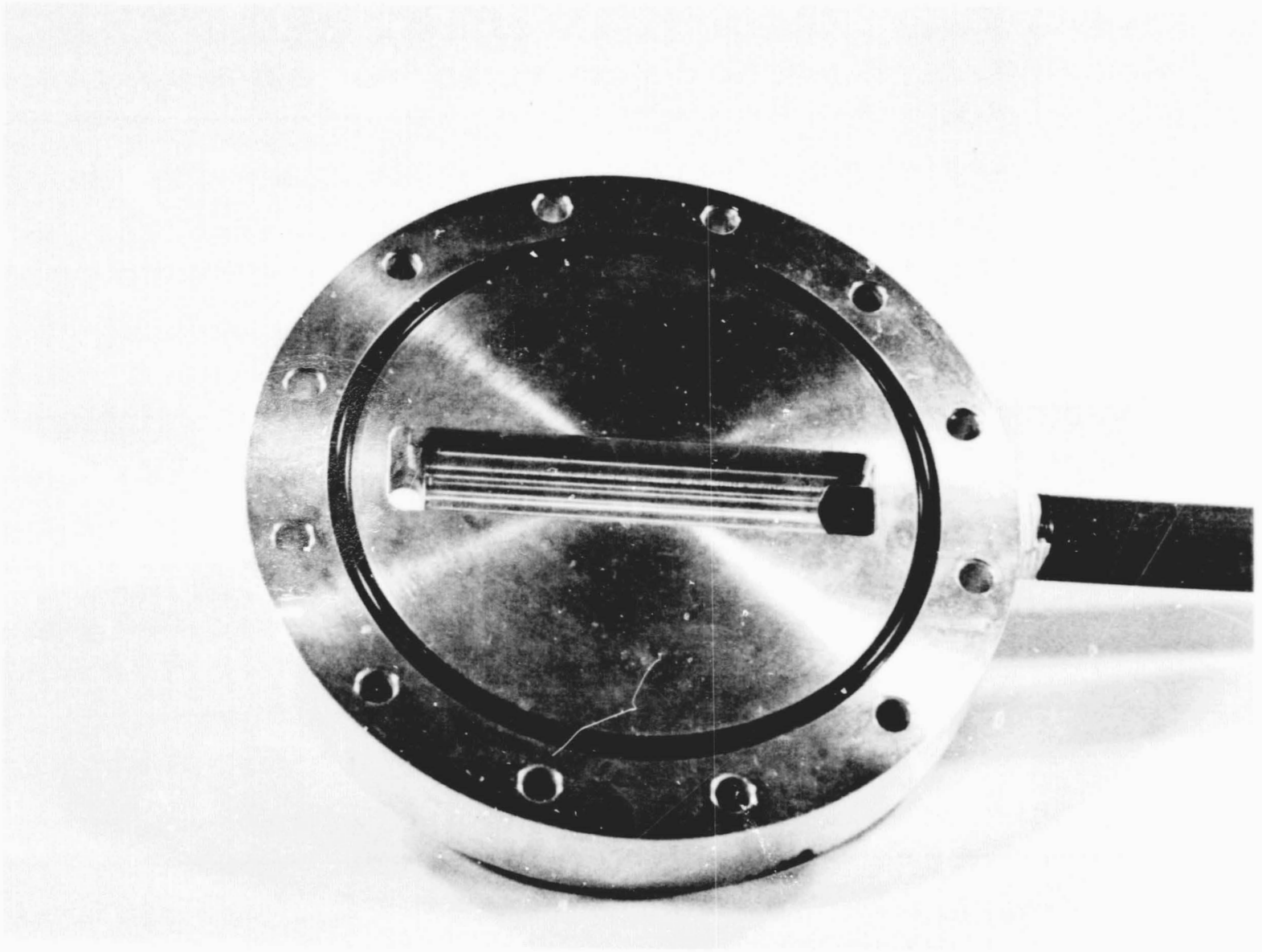

Figure 11. Inlet Cross-Flow Manifold

3.6 Mass Distribution in Spray Field

Mass distribution in the spray field generated by the x-doublet was investigated using the apparatus shown in Figure 12. The experimental set up actually used is depicted in Figure 8. As with other components of the experimental apparatus, a sketch of this device is also included in Appendix A. The mass distribution in the spray field was measured by collecting the outflow from the injector in a 1/8-inch wide collection slot positioned perpendicular to the spray fan. The collection slot could be translated parallel to the spray fan, thus allowing the mass distribution to be determined. Since the spray fan thickness was small compared with its width, measurements were not obtained in a direction normal to the face of the fan.

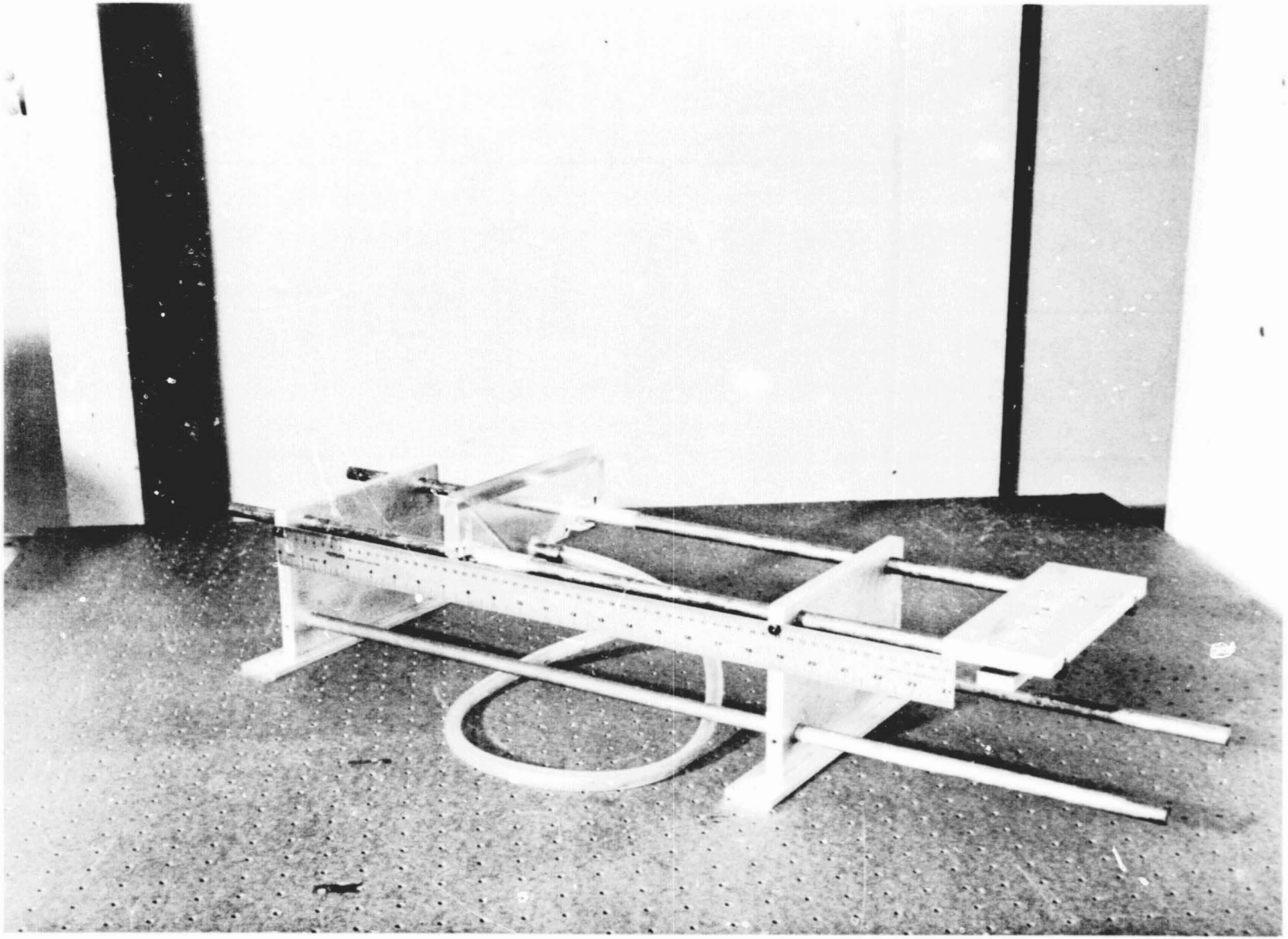

Figure 12. Apparatus Used for Measuring Mass Distribution in Injector Spray Field

4. RESULTS

4.1 Photographs of Prototype Injectors

Photographs of the atomized spray fields produced by both x-doublet and splash-plate prototype injectors are presented in Figures 13 and 14. The pertinent data associated with these photographs are summarized in Table 1. In this table, as well as subsequent tables, the photograph identification numbers refer to the photographic negative numbers tabulated in Appendix D. The photograph scale is the ratio of photographic dimensions to actual dimensions, hence in Figures 13 and 14 the photographs are 1.37 times actual size. The pressure drop is the difference in plenum chamber pressure, where the fluid velocity is negligible, and atmospheric pressure. All injectors tested were exhausted to ambient air at room conditions. Water was used as the working fluid in all prototype studies. Droplets which tended to collect on the face of the injectors during testing were removed by capillary tubes. These tubes are visible in some of the photographs, but they in no way interfered with the atomization process.

4.2 Photographs of X-Doublet Models

Photographic results obtained with the various x-doublet models tested are reproduced in Figures 14 through 22 with associated data tabulated in Table 2. Sketches of the various models are to be found in Appendix A. Model XD-M1 is the standard 7.81-to-1.0 scale model of the x-doublet prototype. Models XD-M2 through XD-M4 are models for which the various platelet thicknesses have been altered. Model XD-M5 is the standard model operating without an orifice plate. Model XD-M6 is a standard model

for which the edges of the outlet orifice were beveled. In model XD-M7 the spacing between inlet orifices was increased by 50% over that used in the standard design.

The atomized fluid illustrated in all figures except Figure 22 was a glycerol-water solution with a specific gravity of 1.085. In Figure 22 the specific gravity was 1.059. When water is used in the prototype, the first of the transfer equations (11) dictates that, for a model scale of 7.81-to-1.0, it is necessary to use a glycerol-water solution with a specific gravity of approximately 1.085 (34% glycerol) in the model in order to maintain similarity of the flows. For this case, the transfer ratios are

$$\frac{\ell_m}{\ell_p} = 7.8 \quad , \quad \frac{V_m}{V_p} = 0.336 \quad , \quad \frac{\Delta p_m}{\Delta p_p} = 0.122 \quad . \qquad (13)$$

If, however, it is assumed that liquid MMH at 200°F is the prototype fluid, then a solution with a specific gravity of 1.059 (24% glycerol) is appropriate. The transfer relations in this case are

$$\frac{\ell_m}{\ell_p} = 7.8 \quad , \quad \frac{V_m}{V_p} = 0.489 \quad , \quad \frac{\Delta p_m}{\Delta p_p} = 0.253. \quad . \qquad (14)$$

4.3 Photographs of Cross-Flow Studies

In Figure 23, photographs are presented for the standard injector (XD-M1), bolted to the cross-flow manifold, with and without cross-flow. The specific conditions for the test are summarized in Table 3. For each of the two orientations considered, the cross-flow velocity was approximately

23%. In establishing the cross-flow velocity, the following formula was used

$$\% \text{ Cross-flow Velocity} = \frac{(\text{Upstream Velocity} + \text{Downstream Velocity})/2}{\text{Average Exit Velocity from Injector}} \times 100. \tag{15}$$

Using the manifold and injector dimensions given in Appendix A, equation (15) becomes

$$\% \text{ Cross-flow Velocity} = 6.4 \left(\frac{2Q_T - Q_I}{Q_I} \right) , \tag{15a}$$

where Q represents a volumetric flow rate and the subscripts T and I refer to the total and injector volumetric flow rates, respectively.

4.4 Photographic Comparison of Model and Prototype

In Figure 24, photographs are presented which allow direct comparisons to be made between model and prototype. For example, the model pressure drop associated with Figure 24.a is 2.44 psi which corresponds to a pressure drop of 20 psi in the prototype. Likewise, the photographic scale of 3.83 is 7.98 times larger than the scale of 0.48 used for the model photographs. The value 7.98 compares reasonably well with the correct value of 7.81.

4.5 V-Doublet Injector

A highly modified version of the x-doublet model injector, called a v-doublet (VD-M1) was constructed during the course of the study. A photograph of the model together with a shop drawing are included in

Table 1. Data for Prototype Photographs

Figure	Photograph	Injector	View	Specific Gravity	Photograph Scale	Pressure Drop (psi)	Flow Rate (gm/sec)
13.a	6	XD-P	Face	1.0	1.37	10	1.90
.b	27		Side			10	1.90
.c	7		Face			20	2.68
.d	28		Side			20	2.68
.e	8		Face			30	3.32
.f	29		Side			30	3.32
.g	9		Face			40	3.80
.h	30		Side			40	3.80
.i	10		Face			50	4.26
.j	31		Side			50	4.26
14.a	36	SP-P	Face	1.0	1.37	20	2.26
.b	41		Side			20	2.26
.c	38		Face			30	2.77
.d	43		Side			30	2.77
.e	39		Face			40	3.20
.f	44		Side			40	3.20

Table 2. Data for X-Doublet Model Photographs

Figure	Photograph	Injector	View	Specific Gravity	Photograph Scale	Pressure Drop (psi)	Flow Rate (gm/sec)
15.a	48B	XD-M1	Face	1.085	0.48	1.25	0.6
.b	49B					2.35	0.8
.c	50B					3.65	1.0
.d	51A					5.30	1.2
.e	52A					7.20	1.4
.f	53B					9.65	1.6
16.a	54	XD-M2	Face	1.085	0.48	2.35	0.8
.b	55A					3.75	1.0
.c	56					5.50	1.2
.d	57					7.50	1.4
17.a	72	XD-M3	Face	1.085	0.48	1.95	0.8
.b	73					3.20	1.0
.c	74					4.50	1.2
.d	75A					6.30	1.4
18.a	62	XD-M4	Face	1.085	0.48	2.05	0.8
.b	63					3.45	1.0
.c	64					4.95	1.2
.d	65					6.75	1.4

Table 2. (continued)

Figure	Photograph	Injector	View	Specific Gravity	Photograph Scale	Pressure Drop (psi)	Flow Rate (gal/min)
19.a	66	XD-M5	Face	1.085	0.48	1.45	0.8
.b	67					2.35	1.0
.c	68					3.45	1.2
.d	69					4.70	1.4
20.a	86	XD-M6	Face	1.085	0.48	0.70	0.6
.b	87					2.10	1.0
.c	88					4.50	1.4
21.a	94	XD-M7	Face	1.090	0.48	3.2	1.0
.b	99					3.2	1.0
.c	95					4.70	1.2
.d	97					6.60-8.80	1.4-1.6
22.a	77	XD-M1	Face	1.059	0.48	1.30	0.6
.b	78A					3.65	1.0
.c	79B					7.20	1.4

Table 3. Data for Cross-Flow Photographs

Figure	Photograph	Injector	View	Specific Gravity	Photograph Scale	Pressure* Drop (psi)	Total Flow Rate (gal/min)	Injector Flow Rate (gal/min)	Injector** Orientation in Channel
23.a	81B	XD-M1	Face	1.059	0.48	3.20	2.00	0.87	Perpendicular
.b	82RB					2.65	0.87	0.87	"
.c	83					3.25	2.00	0.88	Parallel
.d	84					2.75	0.88	0.88	"

* Pressure drop measured between plenum and ambient air, i.e., across entire manifold arrangement.

** Perpendicular:

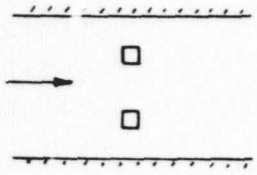

Parallel:

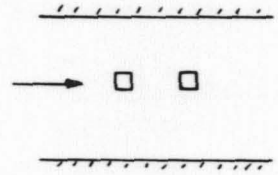

Table 4. Data for Comparison Photographs of Model and Prototype

Figure	Photograph	Injector	View	Specific Gravity	Photograph Scale	Pressure Drop (psi)	Flow Rate
24.a	89	XD-M1	Face	1.085	0.48	2.44	0.82 gal/min
.b	7	XD-P		1.0	3.83	20	2.68 gm/sec
.c	90	XD-M1		1.085	0.48	3.66	1.00 gal/min
.d	8	XD-P		1.0	3.83	30	3.32 gm/sec
.e	91	XD-M1		1.085	0.48	4.88	1.14 gal/min
.f	9	XD-P		1.0	3.83	40	3.80 gm/sec
.g	92	XD-M1		1.085	0.48	6.10	1.28 gal/min
.h	10	XD-P		1.0	3.83	50	4.26 gm/sec

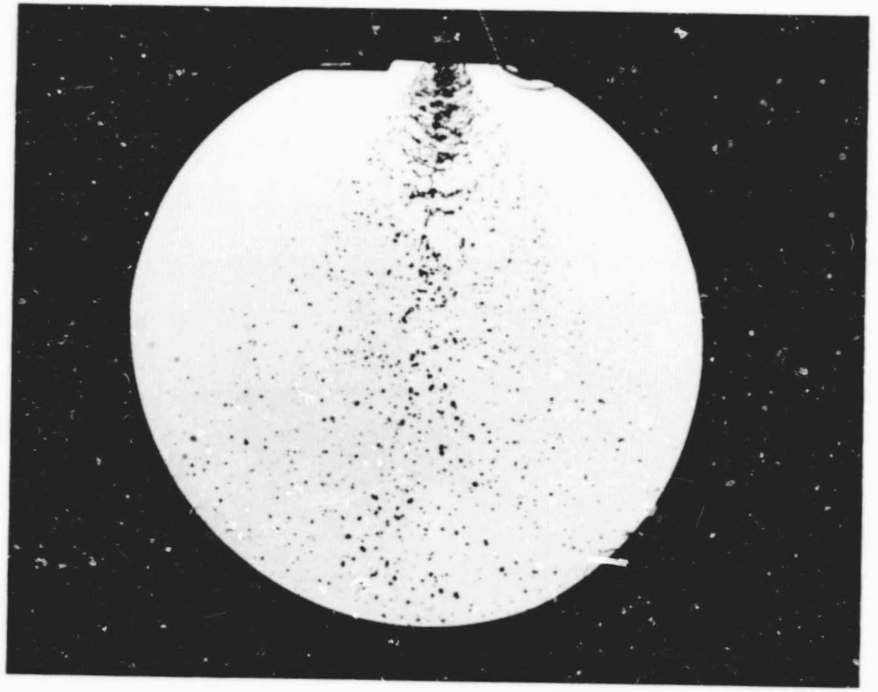

13.a X-Doublet Prototype, Face
S.G. = 1.0, 10 psi, 1.90 gm/sec

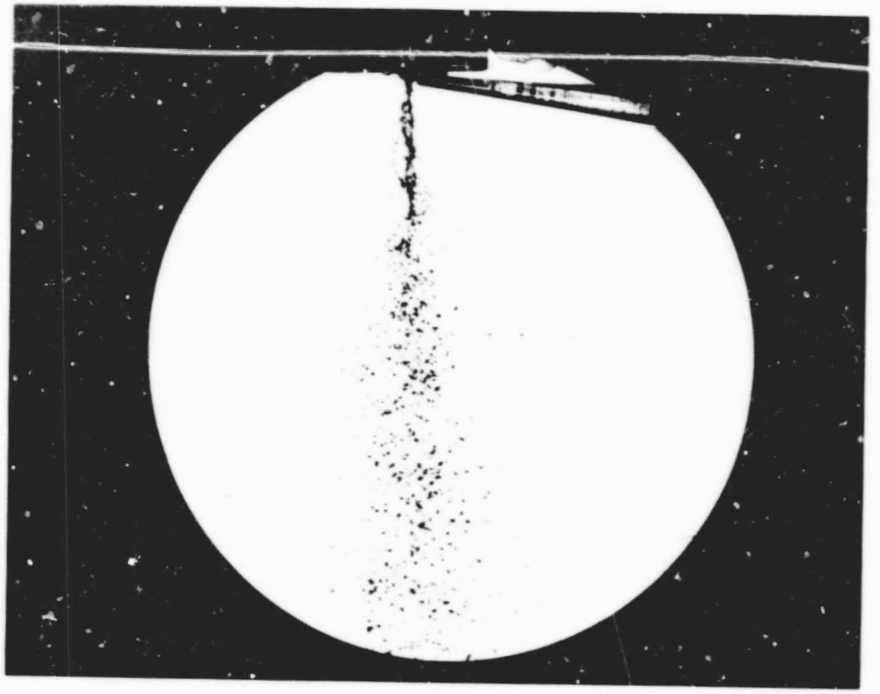

13.b X-Doublet Prototype, Side
S.G. = 1.0, 10 psi, 1.90 gm/sec

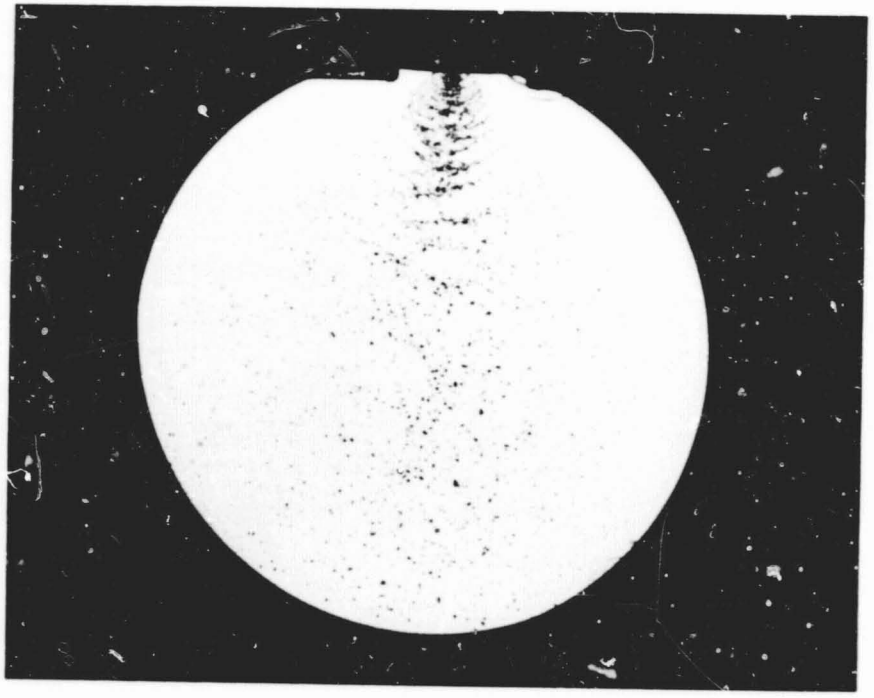

13.c X-Doublet Prototype, Face
S.G. = 1.0, 20 psi, 2.68 gm/sec.

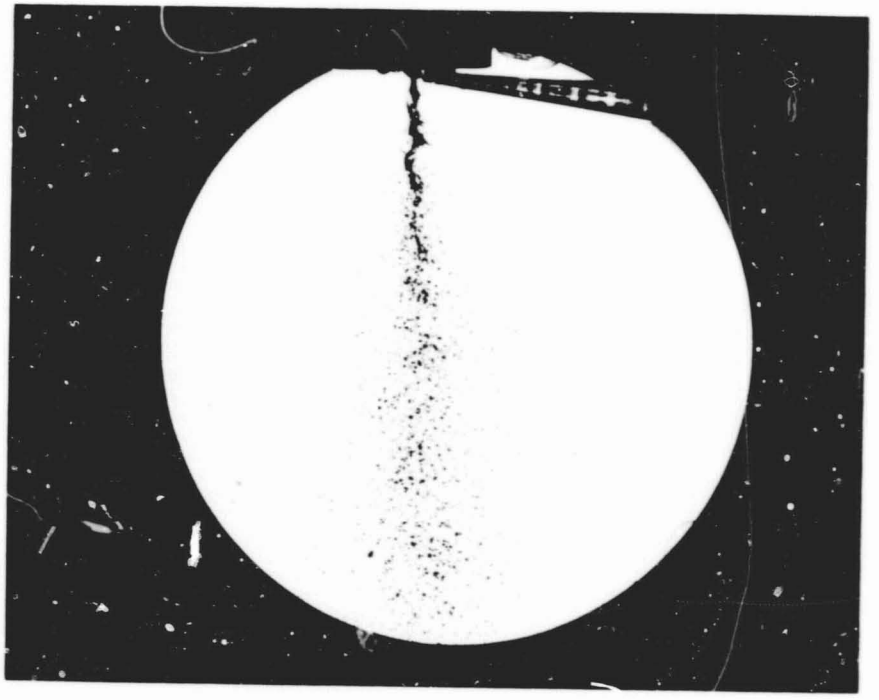

13.d X-Doublet Prototype, Side
S.G. = 1.0, 20 psi, 2.68 gm/sec.

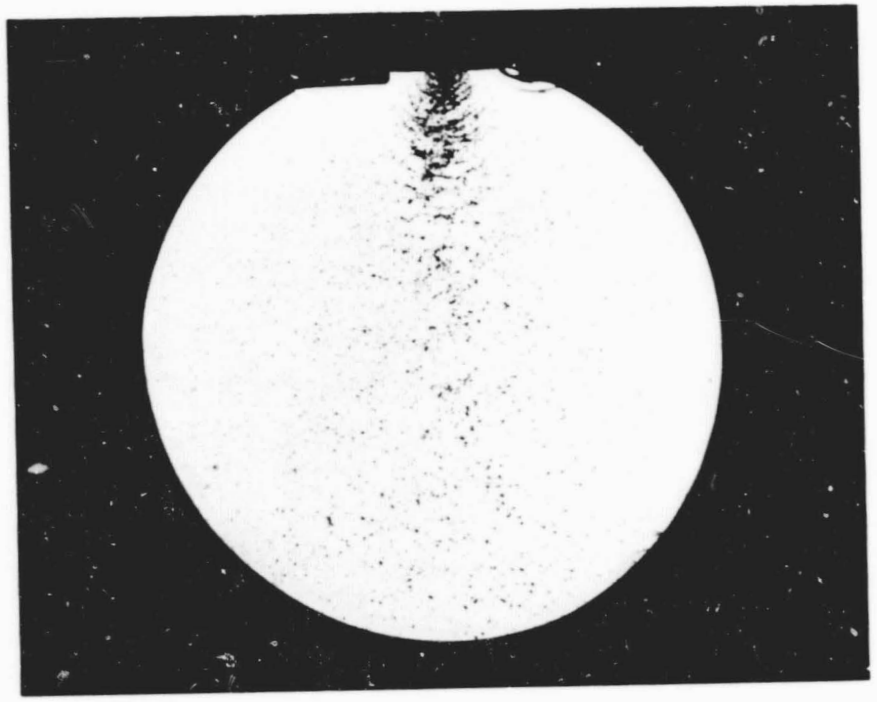

13.e X-Doublet Prototype, Face
S.G. = 1.0, 30 psi, 3.32 gm/sec.

13.f X-Doublet Prototype, Side
S.G. = 1.0, 30 psi, 3.32 gm/sec.

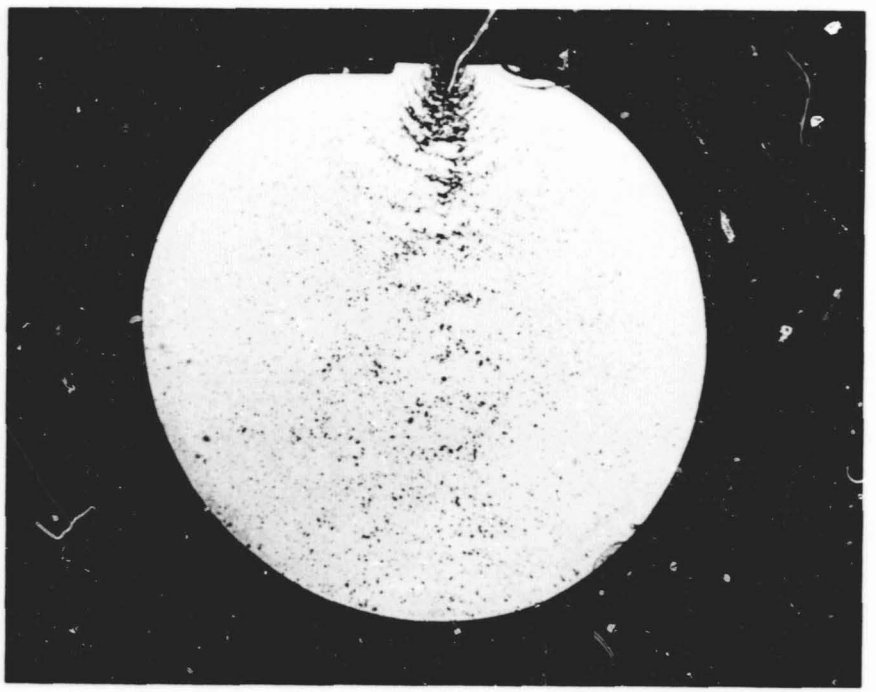

13.g X-Doublet Prototype, Face
S.G. = 1.0, 40 psi, 3.80 gm/sec.

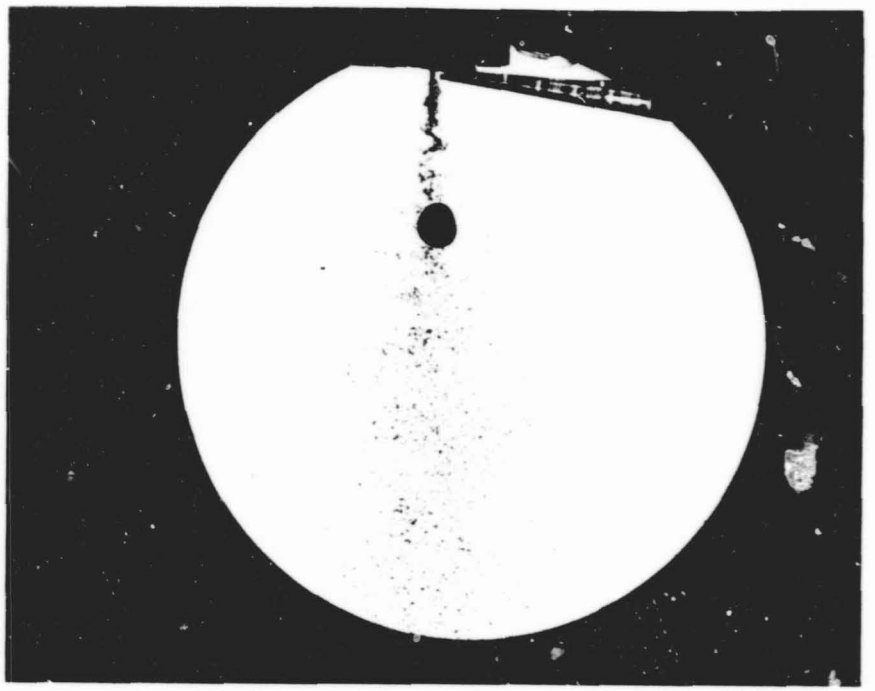

13.h X-Doublet Prototype, Side
S.G. = 1.0, 40 psi, 3.80 gm/sec.

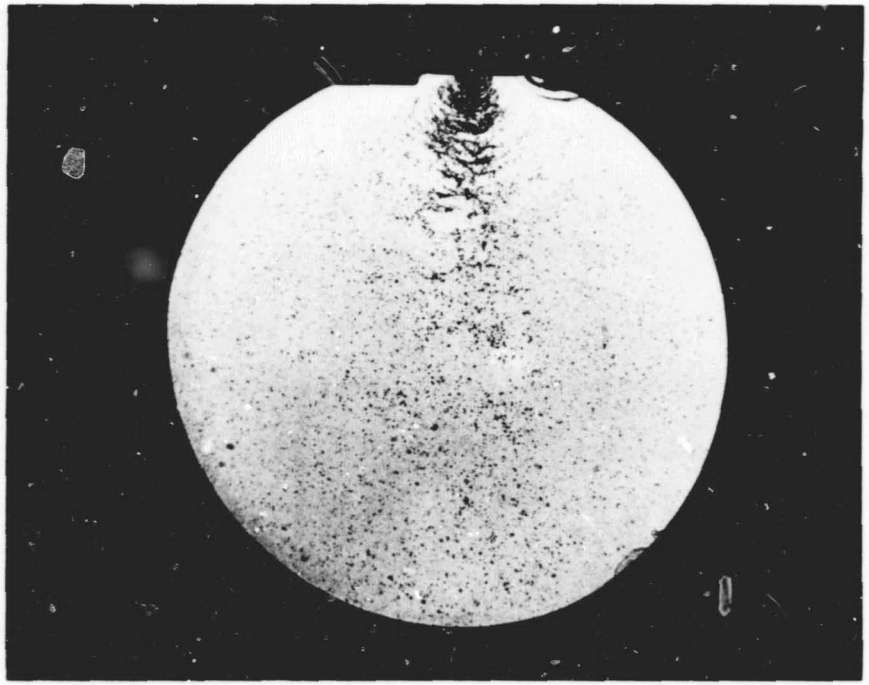

13.i X-Doublet Prototype, Face
S.G. = 1.0, 50 psi, 4.26 gm/sec.

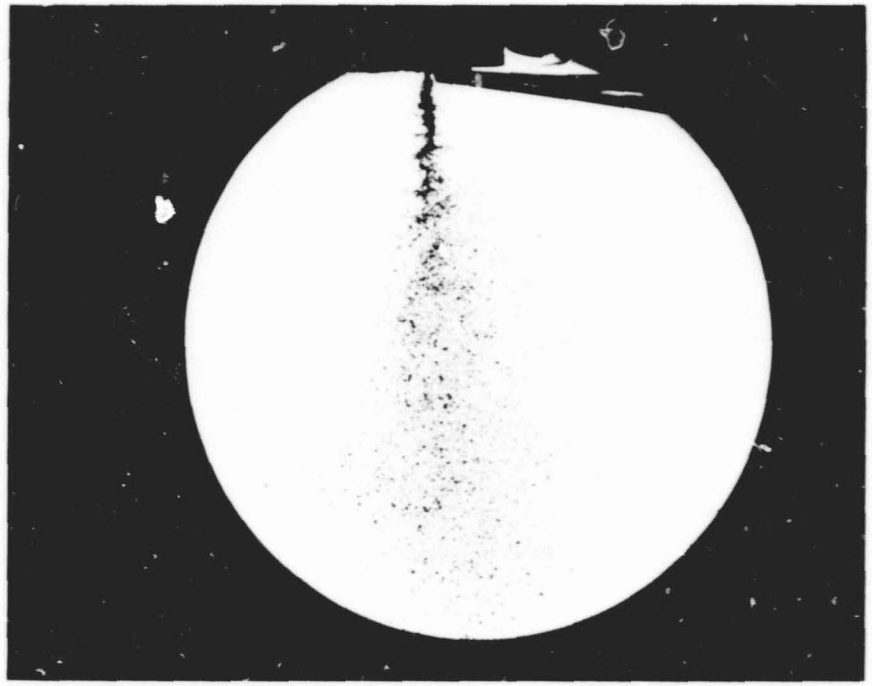

13.j X-Doublet Prototype, Side
S.G. = 1.0, 50 psi, 4.26 gm/sec.

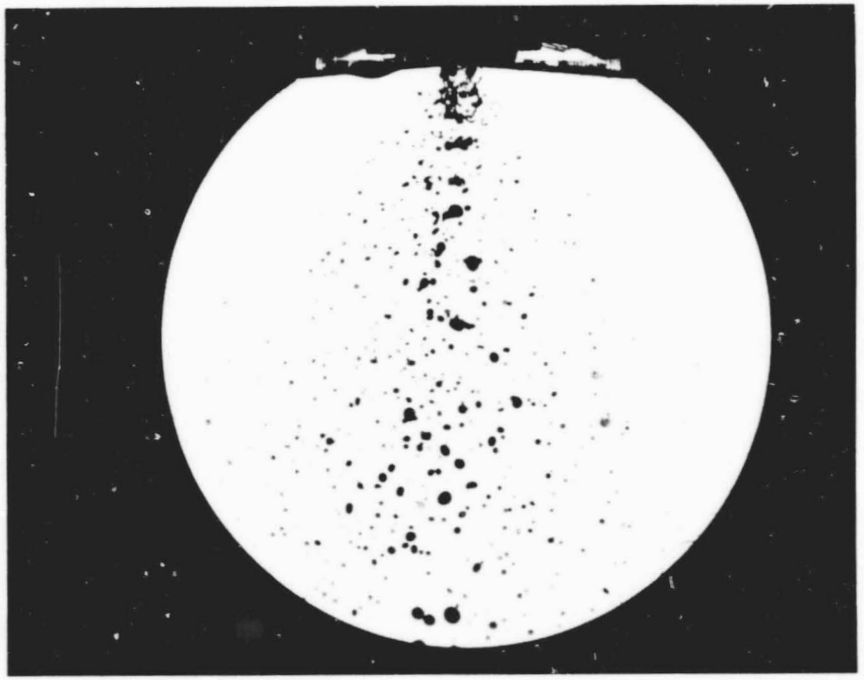

14.a Splash-Plate Prototype, Face
S.G. = 1.0, 20 psi, 2.26 gm/sec.

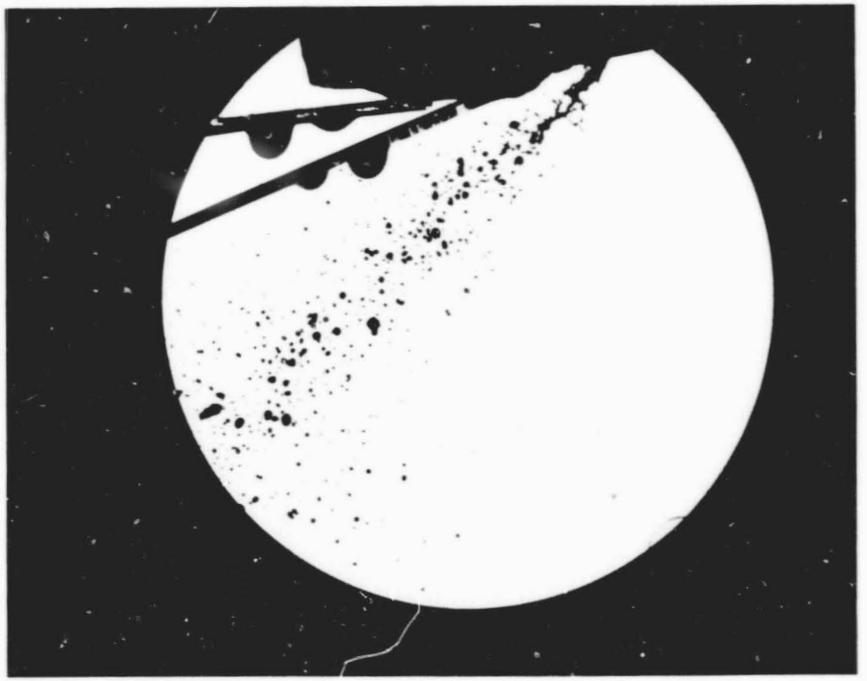

14.b Splash-Plate Prototype, Side
S.G. = 1.0, 20 psi, 2.26 gm/sec.

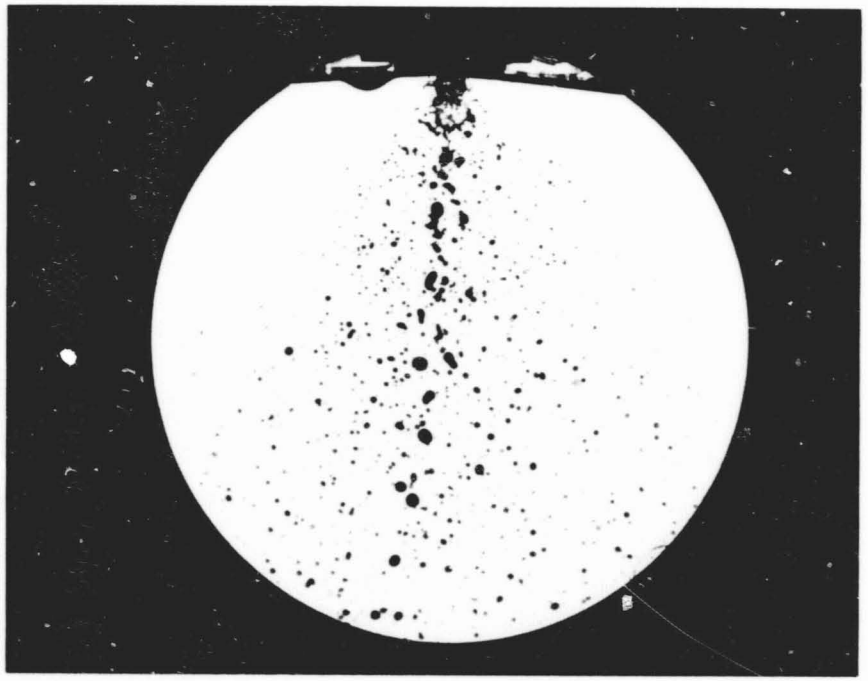

14.c Splash-Plate Prototype, Face
S.G. = 1.0, 30 psi, 2.77 gm/sec.

14.d Splash-Plate Prototype, Side
S.G. = 1.0, 30 psi, 2.77 gm/sec.

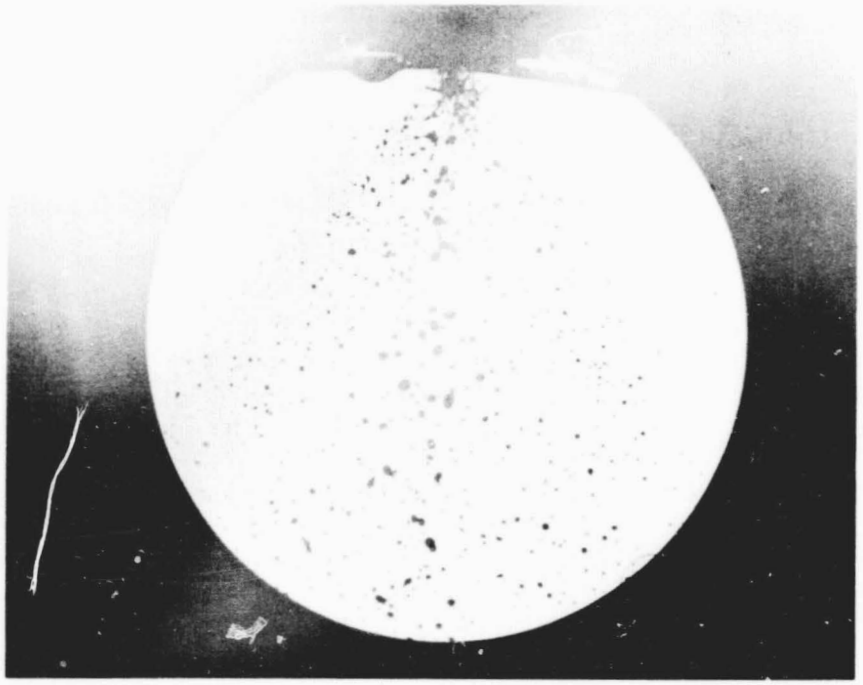

14.e Splash-Plate Prototype, Face
S.G. = 1.0, 40 psi, 3.20 gm/sec.

14.f Splash-Plate Prototype, Side
S.G. = 1.0, 40 psi, 3.20 gm/sec.

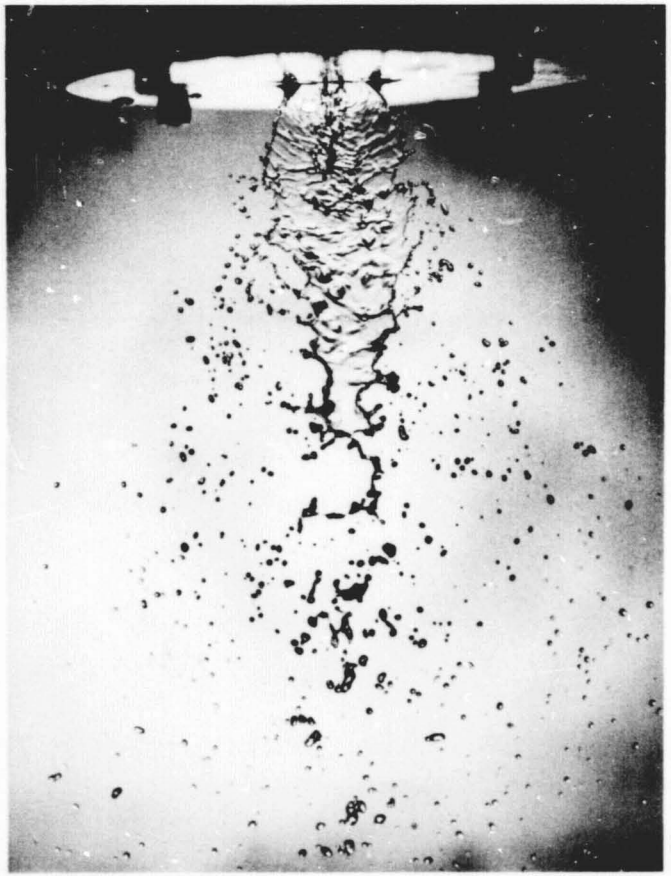

15.a Model XD-M1
S.G.=1.085, 1.25 psi, 0.6 gal/min.

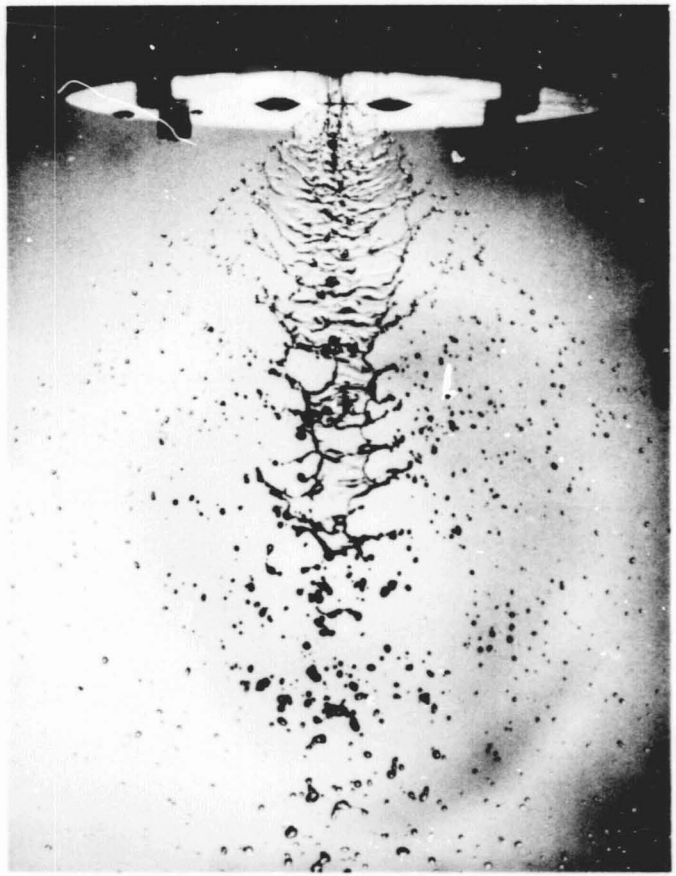

15.b Model XD-M1
S.G.=1.085, 2.35 psi, 0.8 gal/min.

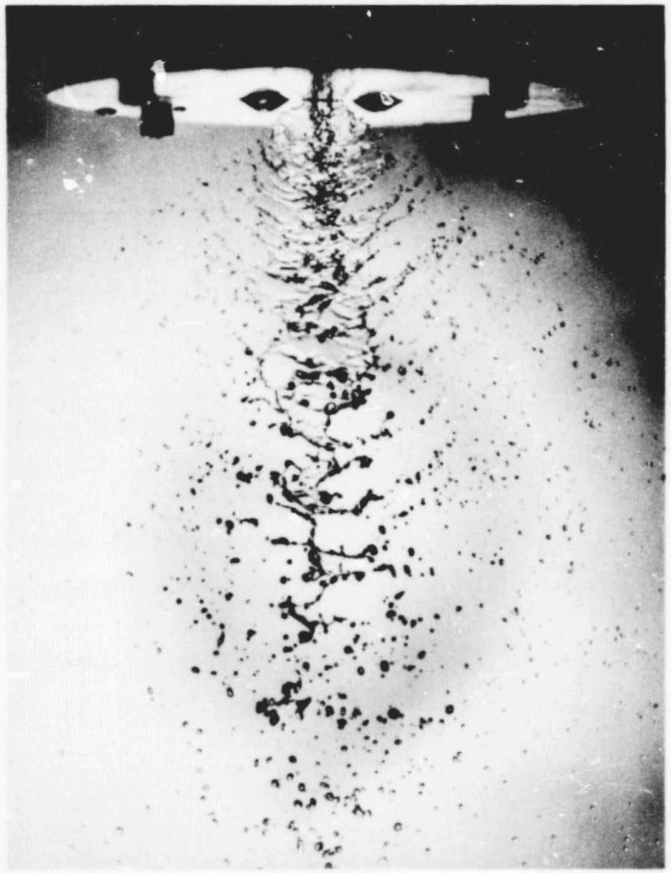

15.c Model XD-M1
S.G.=1.085, 3.65 psi, 1.0 gal/min.

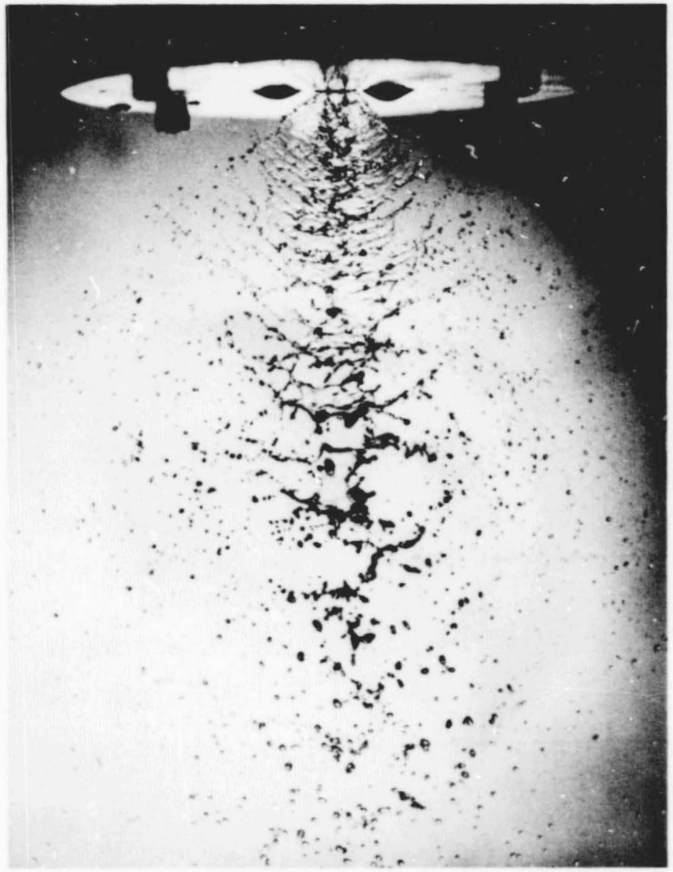

15.d Model XD-M1
S.G.=1.085, 5.3 psi, 1.2 gal/min.

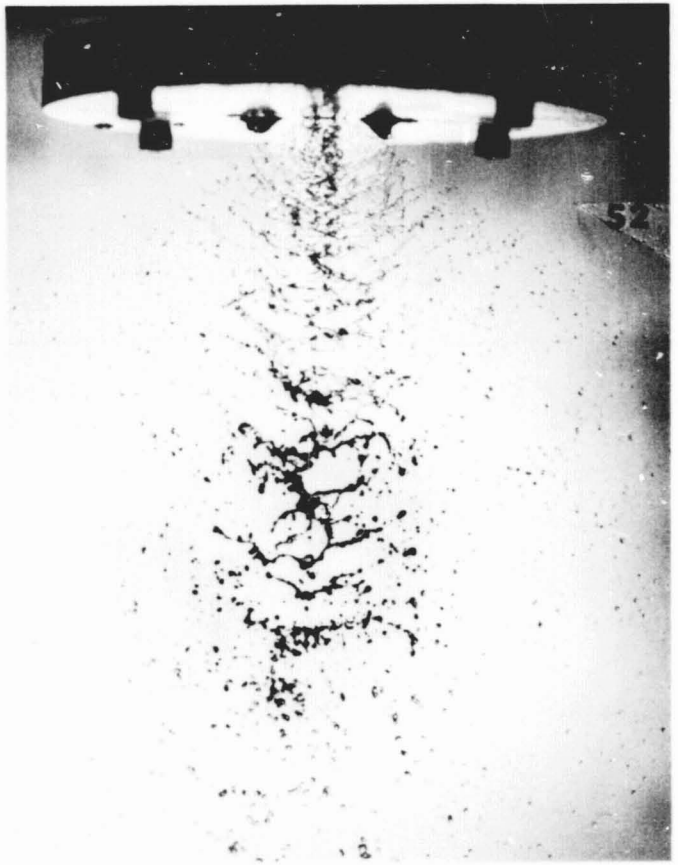

15.e Model XD-M1
S.G.=1.085, 7.20 psi, 1.4 gal/min.

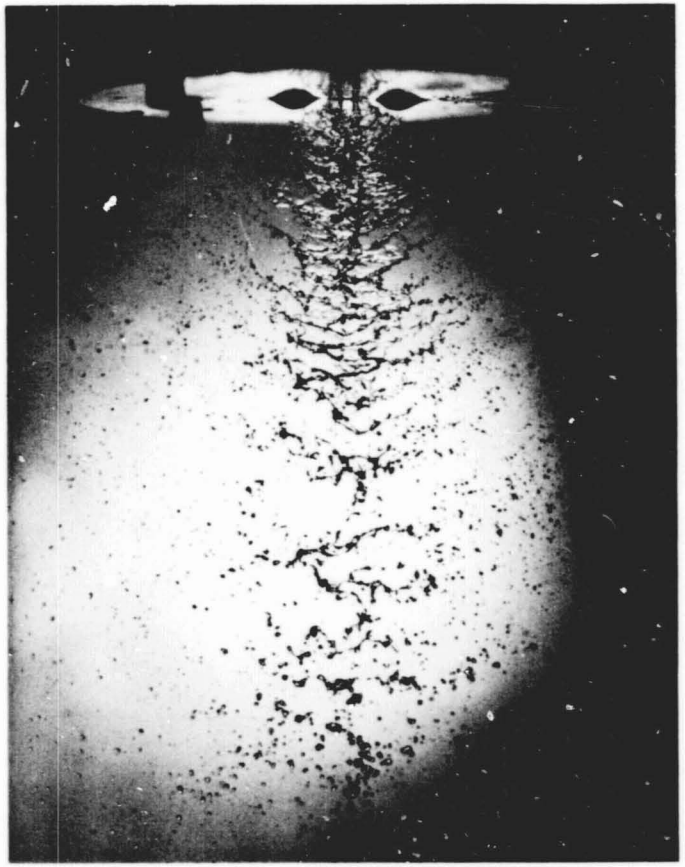

15.f Model XD-M1
S.G.=1.085, 9.65 psi, 1.6 gal/min.

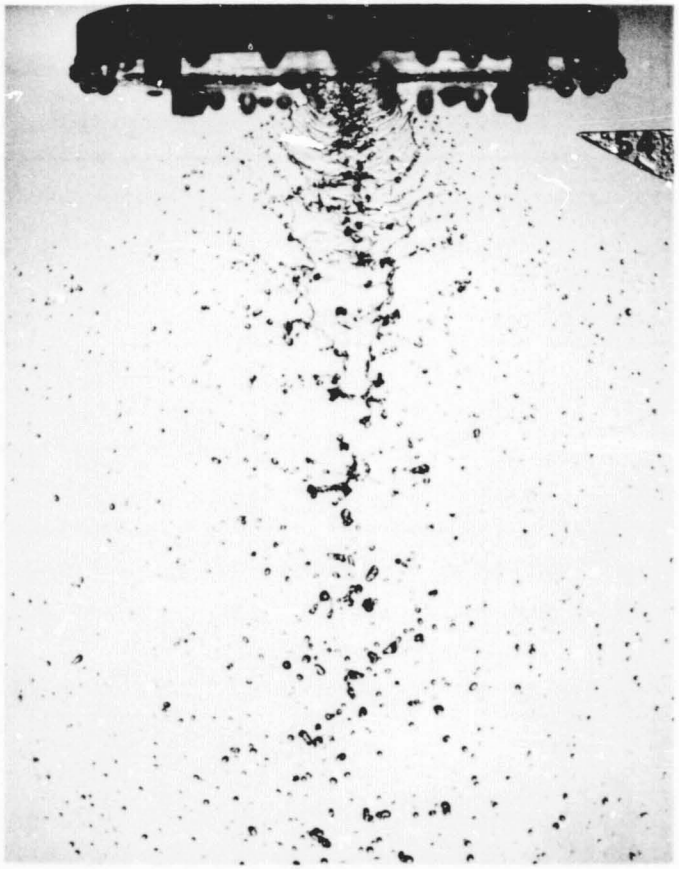

16.a Model XD-M2
S.G.= 1.085, 2.35 psi, 0.8 gal/min.

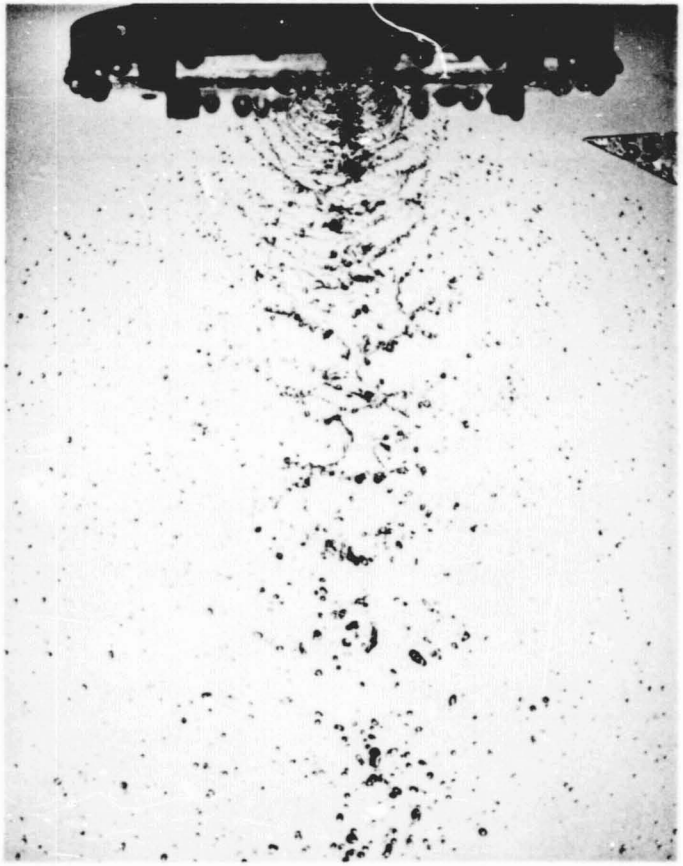

16.b Model XD-M2
S.G.=1.085, 3.75 psi, 1.0 gal/min.

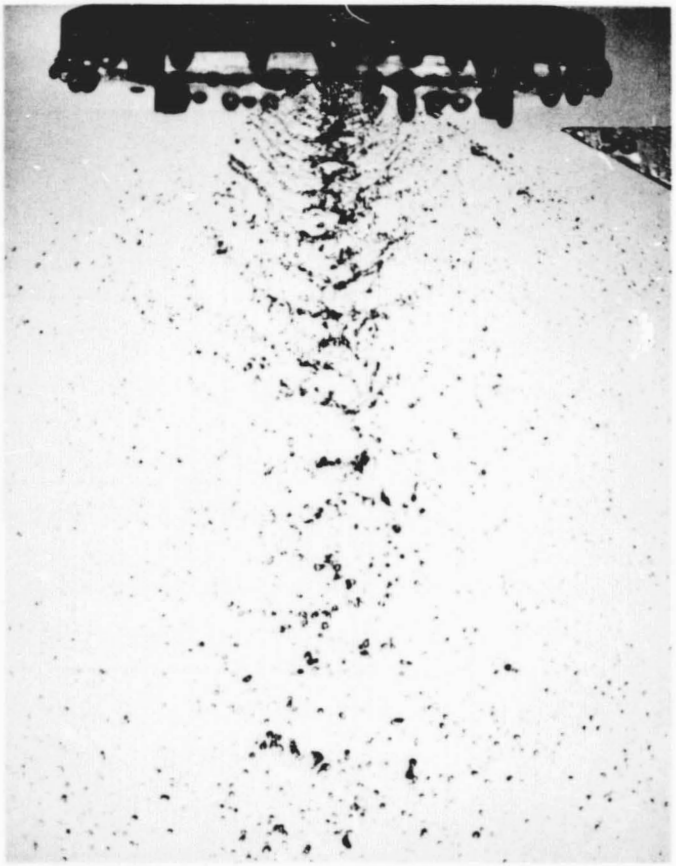

16.c Model XD-M2
S.G.=1.085, 5.50 psi, 1.2 gal/min.

16.d Model XD-M2
S.G.=1.085, 7.50 psi, 1.4 gal/min.

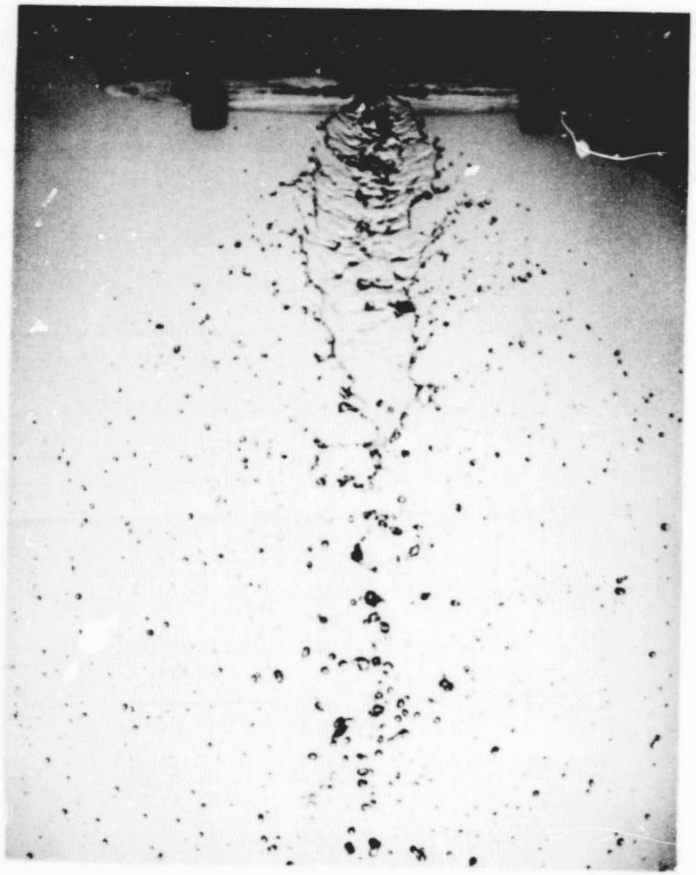

17.a Model XD-M3
S.G.=1.085, 1.95 psi, 0.8 gal/min.

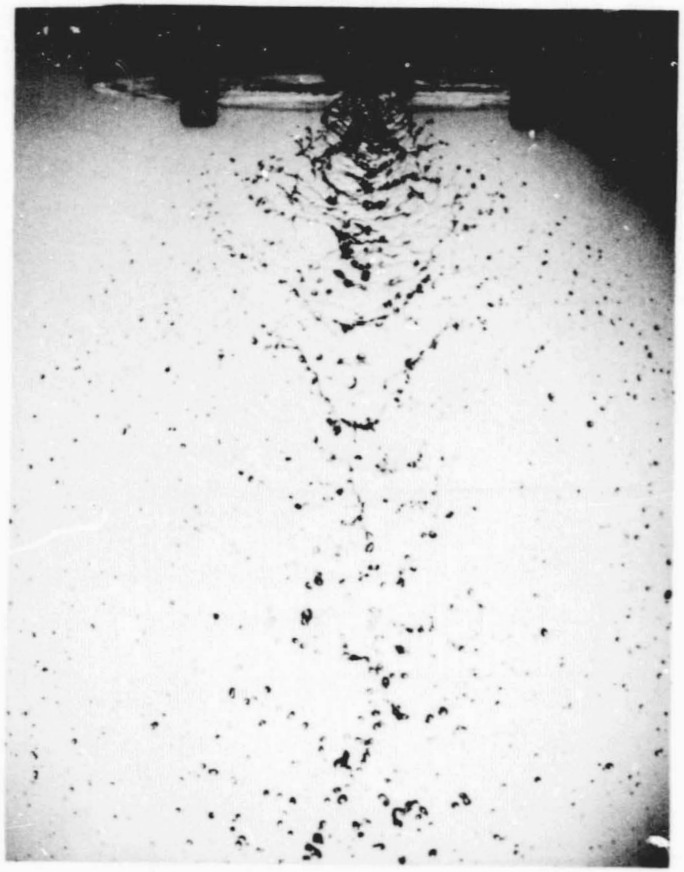

17.b Model XD-M3
S.G.=1.085, 3.20 psi, 1.0 gal/min.

17.c Model XD-M3
S.G.=1.085, 4.50 psi, 1.2 gal/min.

17.d Model XD-M3
S.G.=1.085, 6.30 psi, 1.4 gal/min.

18.a Model XD-M4
S.G.=1.085, 2.05 psi, 0.8 gal/min.

18.b Model XD-M4
S.G.=1.085, 3.45 psi, 1.0 gal/min.

18.c Model XD-M4
S.G.=1.085, 4.95 psi, 1.2 gal/min.

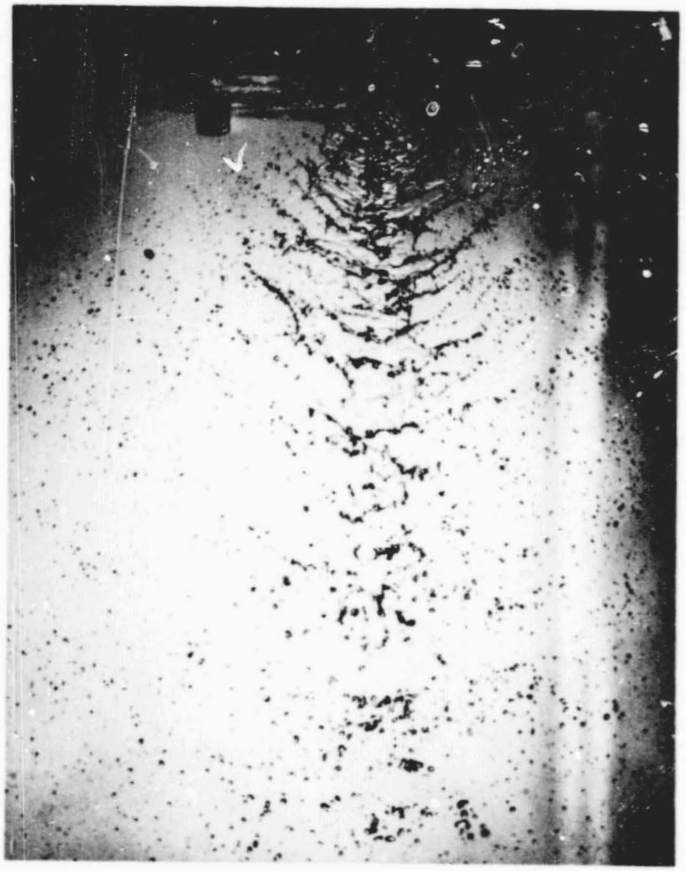

18.d Model XD-M4
S.G.=1.085, 6.75 psi, 1.4 gal/min.

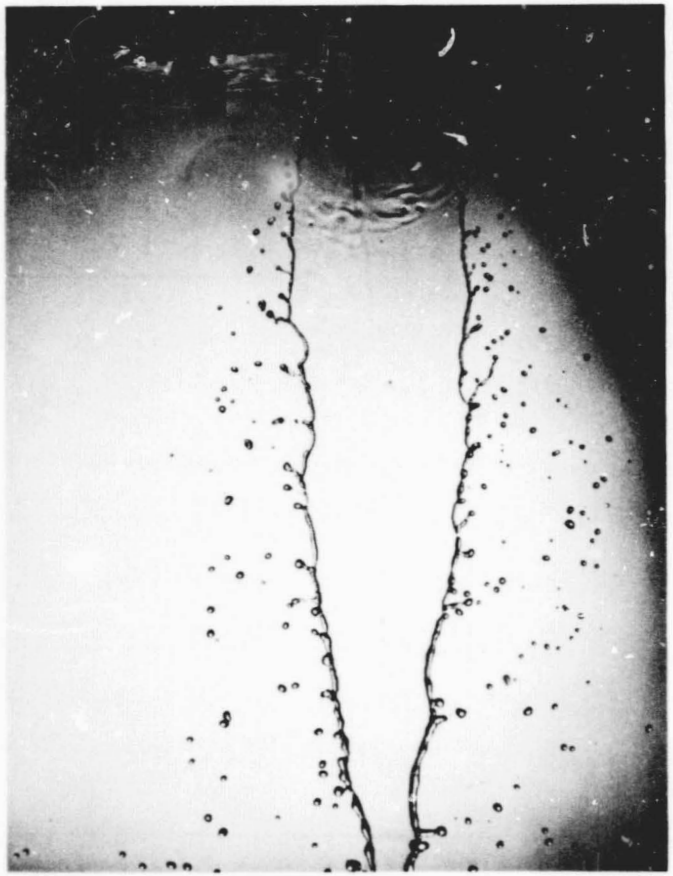

19.a Model XD-M5
S.G.=1.085, 1.45 psi, 0.8 gal/min.

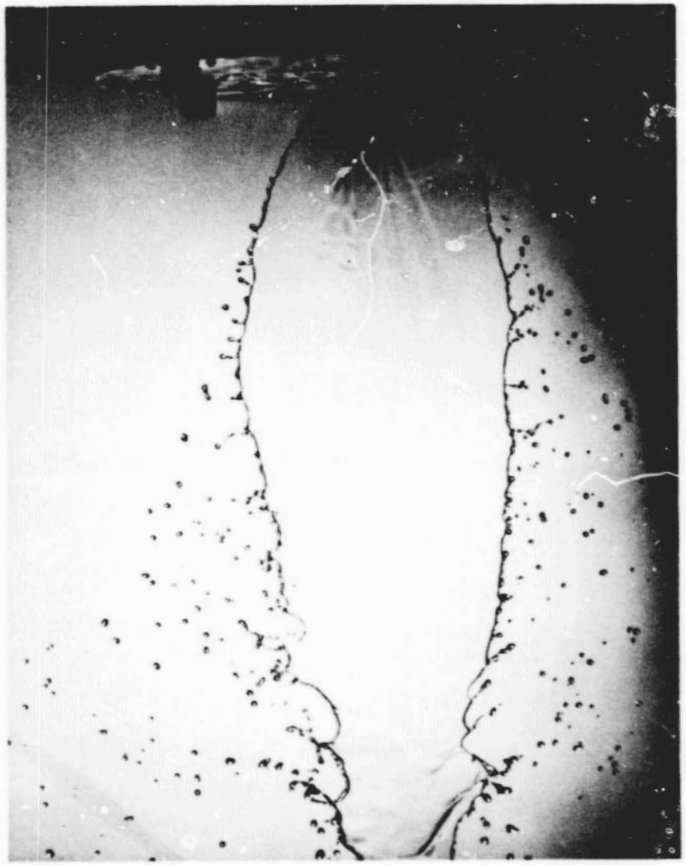

19.b Model XD-M5
S.G.=1.085, 2.35 psi, 1.0 gal/min.

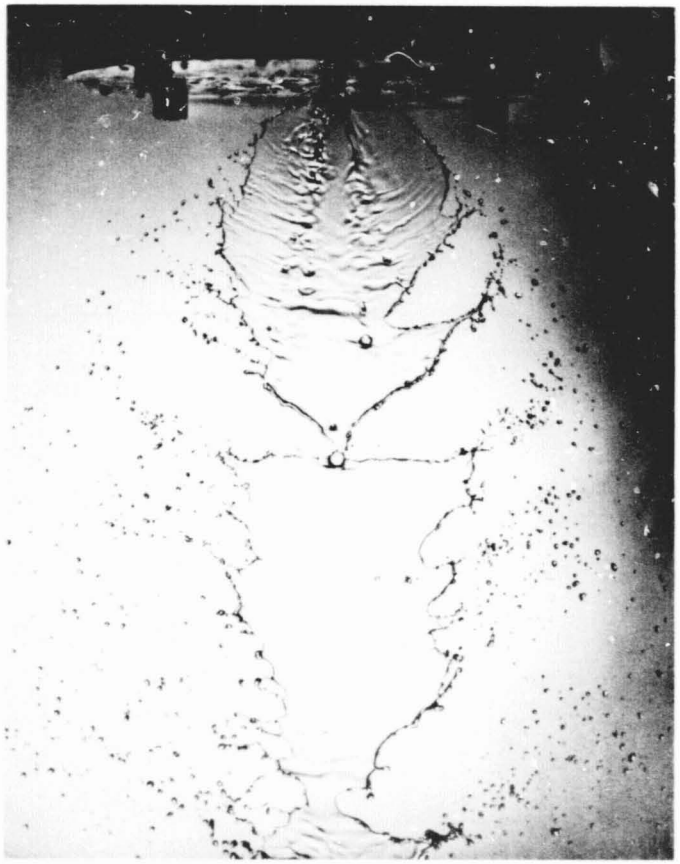

19.c Model XD-M5
S.G.=1.085, 3.45 psi, 1.2 gal/min.

19.d Model XD-M5
S.G.=1.085, 4.70 psi, 1.4 gal/min.

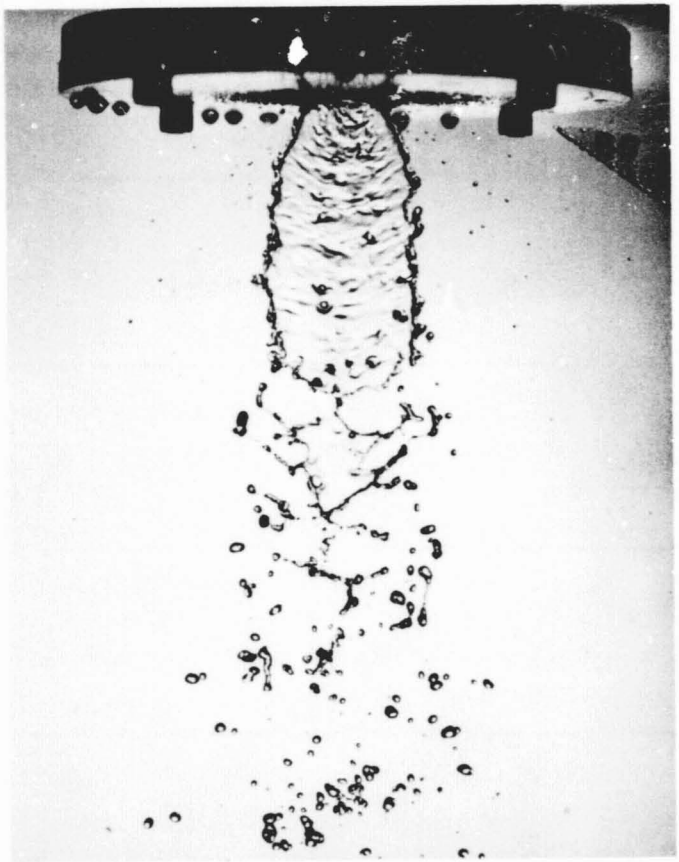

20.a Model XD-M6
S.G.=1.085, 0.70 psi, 0.6 gal/min.

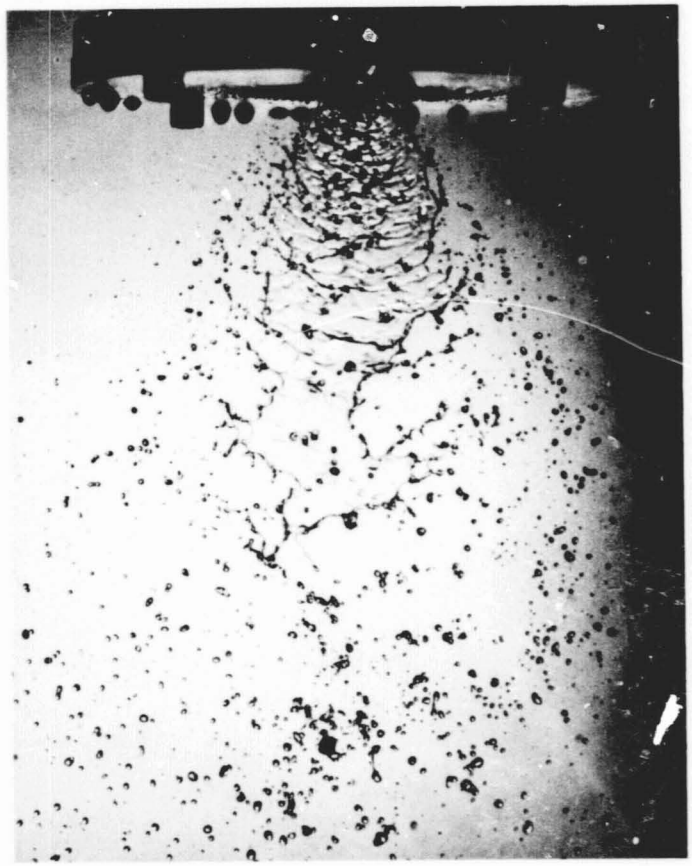

20.b Model XD-M6
S.G.=1.085, 2.10 psi, 1.0 gal/min.

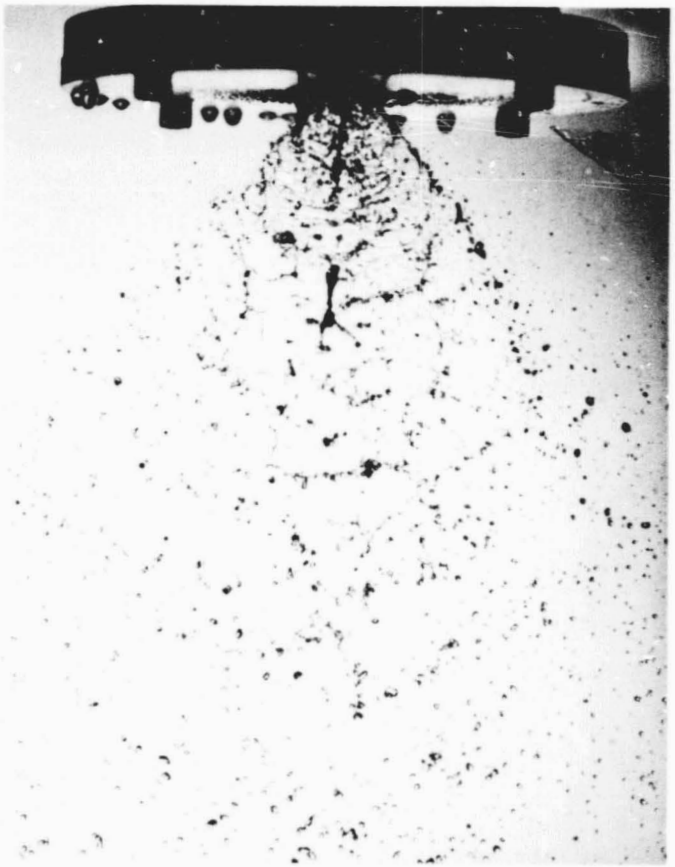

20.c Model XD-M6
S.G.= 1.085, 4.50 psi, 1.4 gal/min.

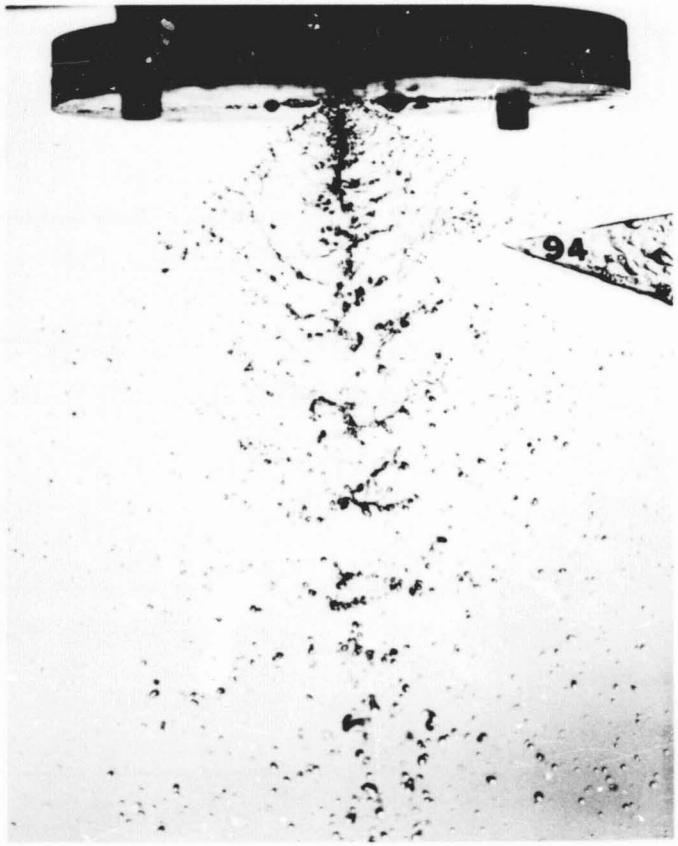

Figure 21.a XD-M7
S.G.=1.090, 3.20 psi, 1.0 gal/min.

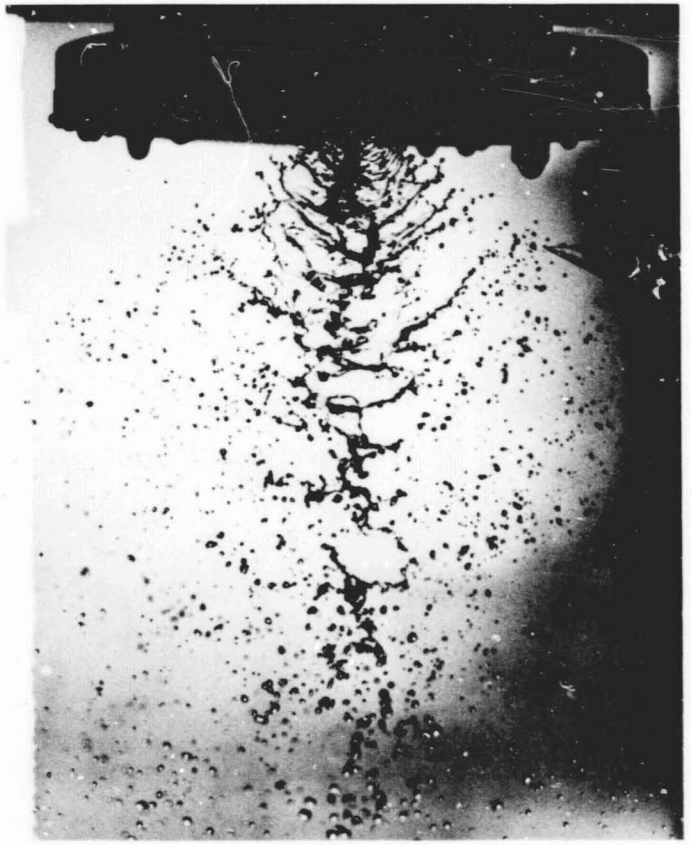

Figure 21.b XD-M7
S.G.=1.090, 3.20 psi, 1.0 gal/min.

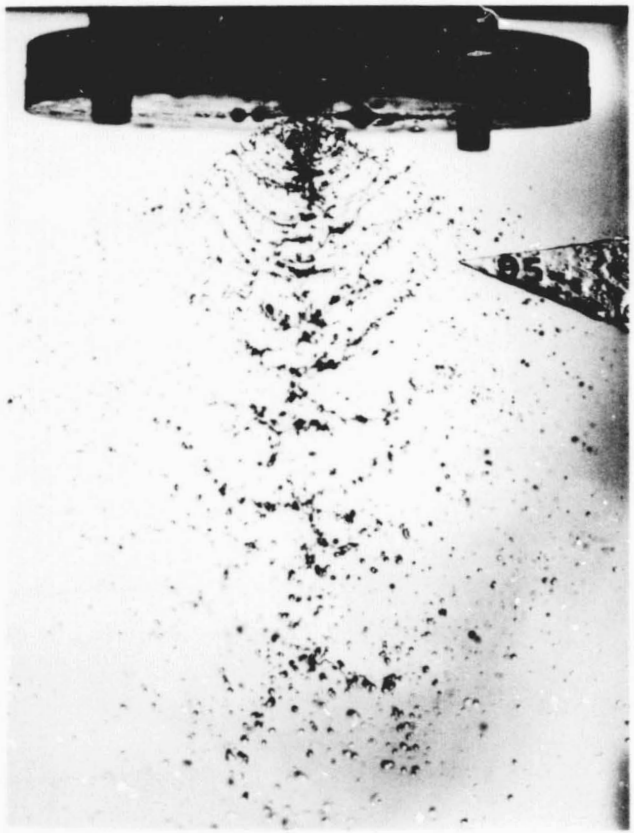

Figure 21.c XD-M7
S.G.=1.090, 4.70 psi, 1.2 gal/min.

Figure 21.d XD-M7
S.G.=1.090, 6.6-8.8 psi,
1.4-1.6 gal/min.

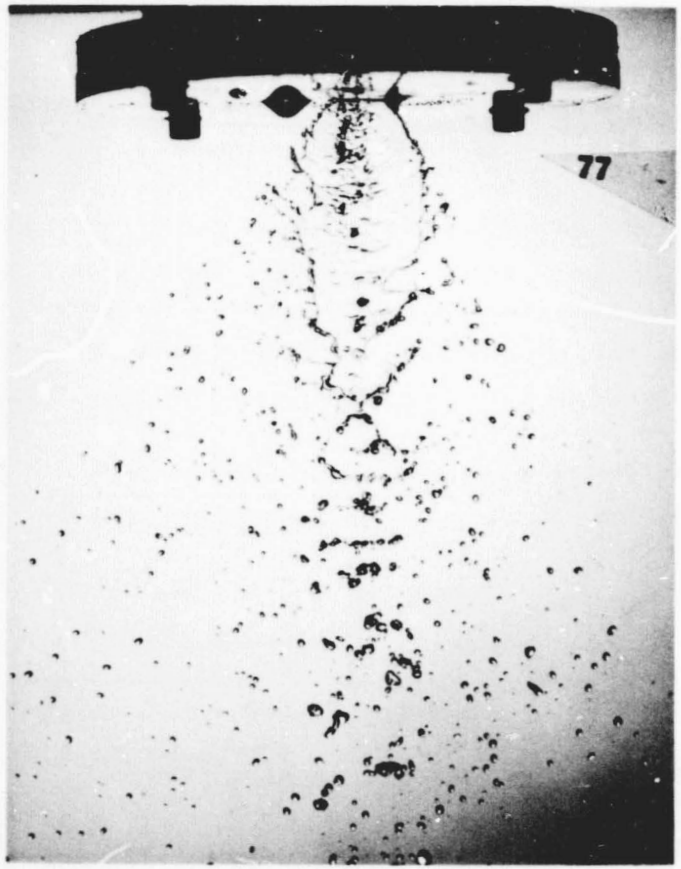

22.a Model XD-M1
S.G.=1.059, 1.30 psi, 0.6 gal/min.

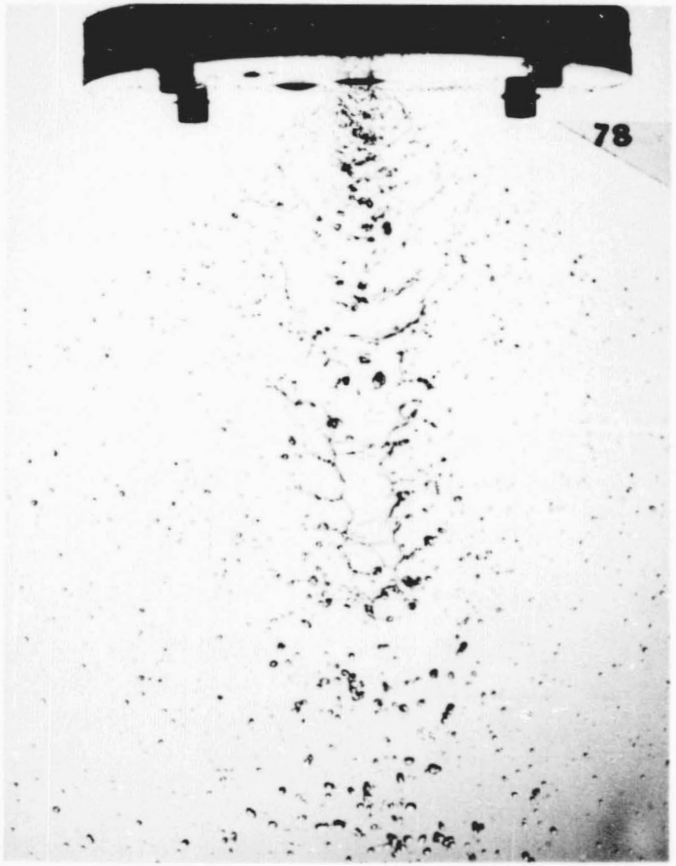

22.b Model XD-M1
S.G.-1.059, 3.65 psi, 1.0 gal/min.

22.c Model XD-M1
S.G.=1.059, 7.20 psi, 1.4 gal/min.

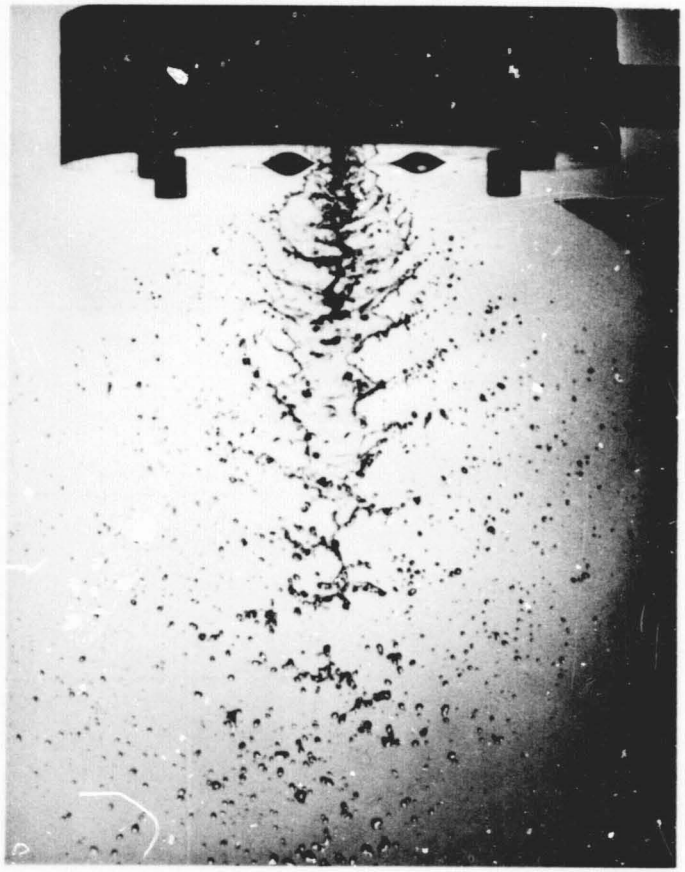

23.a Model XD-M1, 23% Cross Flow Velocity
S.G.=1.059, perpendicular

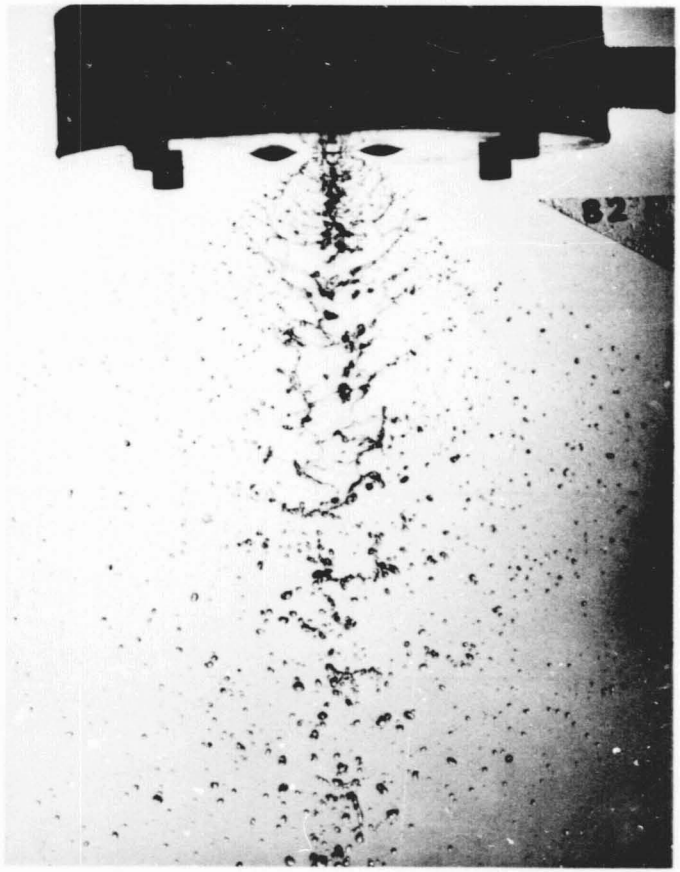

23.b Model XD-M1, No Cross Flow
S.G.=1.059, perpendicular

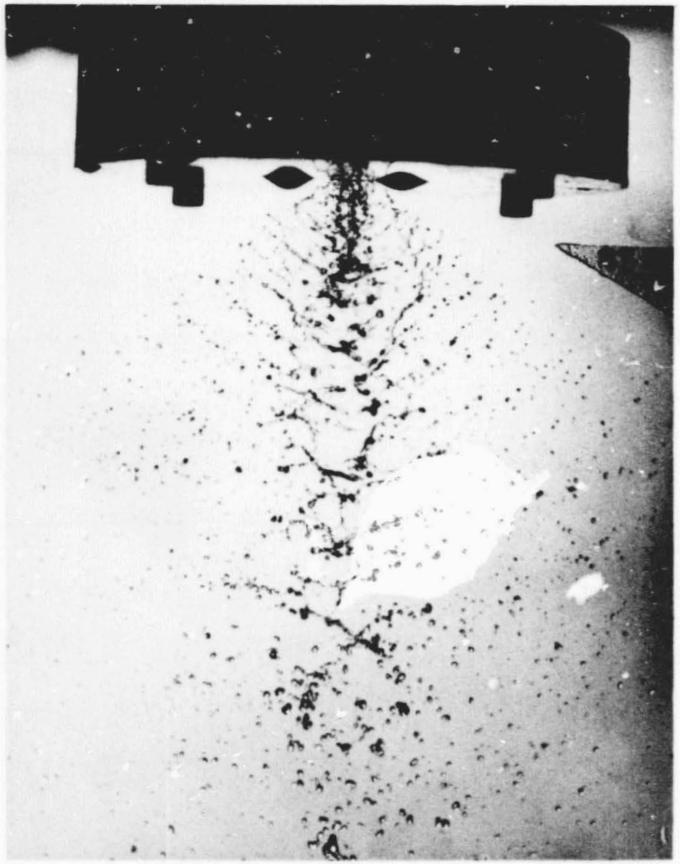

23.c Model XD-M1, 23% Cross-Flow Velocity
S.G.=1.059, parallel

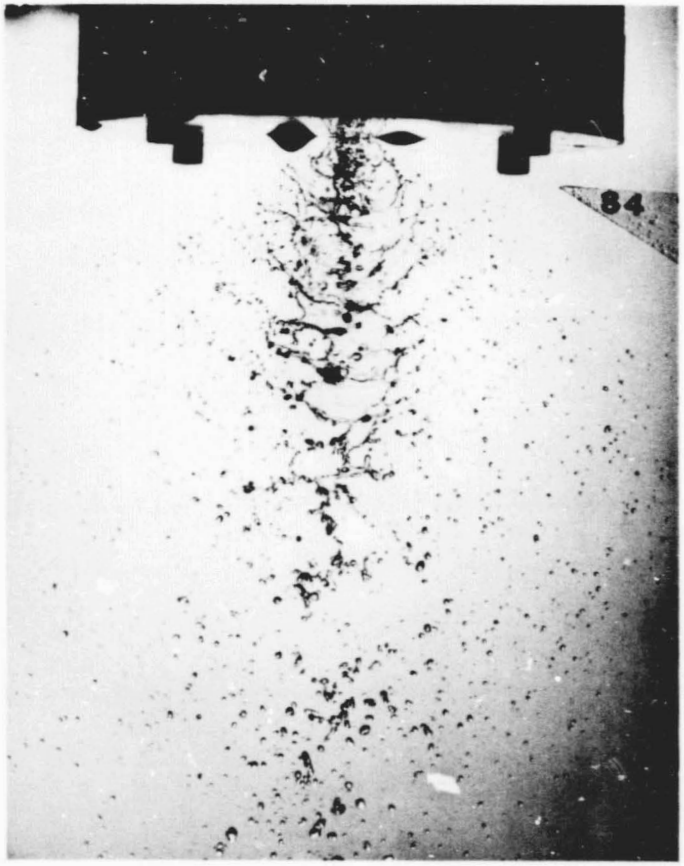

23.d Model XD-M1, No Cross-Flow
S.G.=1.059, parallel

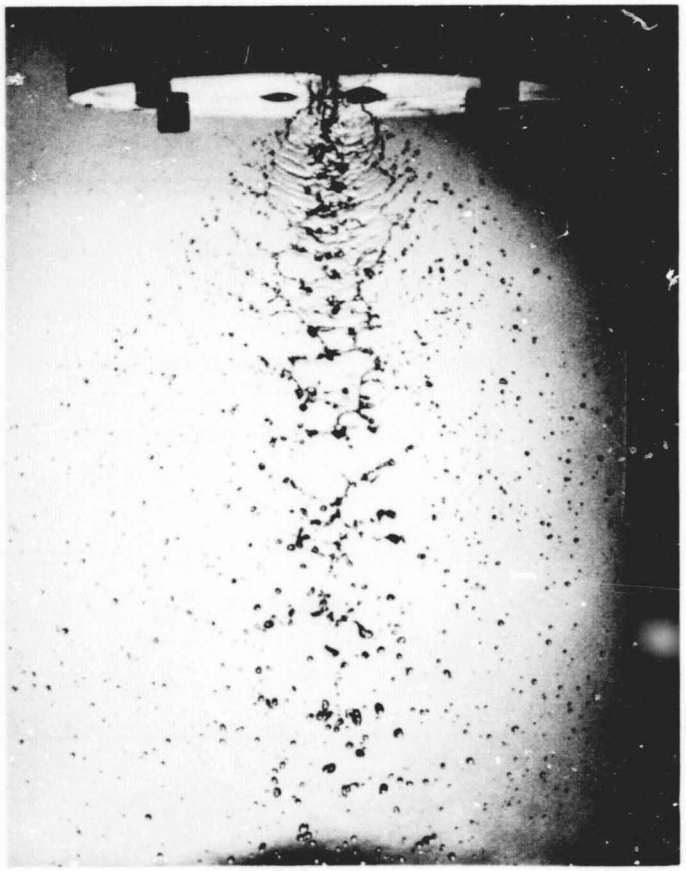

24.a Model XD-M1, Scale = 0.48
S.G.=1.085, 2.44 psi, 0.82 gal/min.

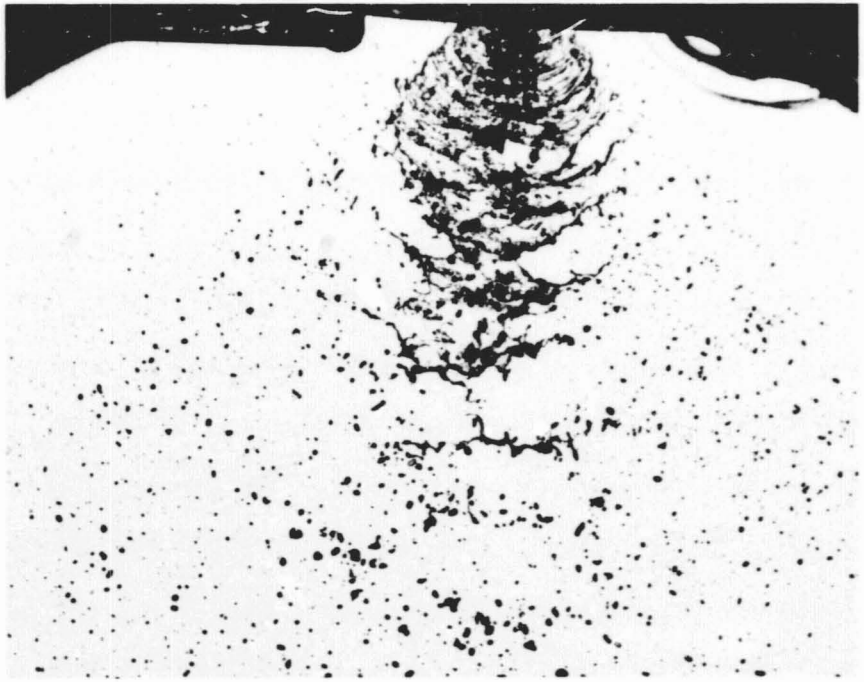

24.b X-Doublet Prototype, Scale = 3.83
S.G.=1.0, 20 psi, 2.68 gm/sec.

24.c Model XD-M1, Scale = 0.48
S.G.=1.085, 3.66 psi, 1.00 gal/min.

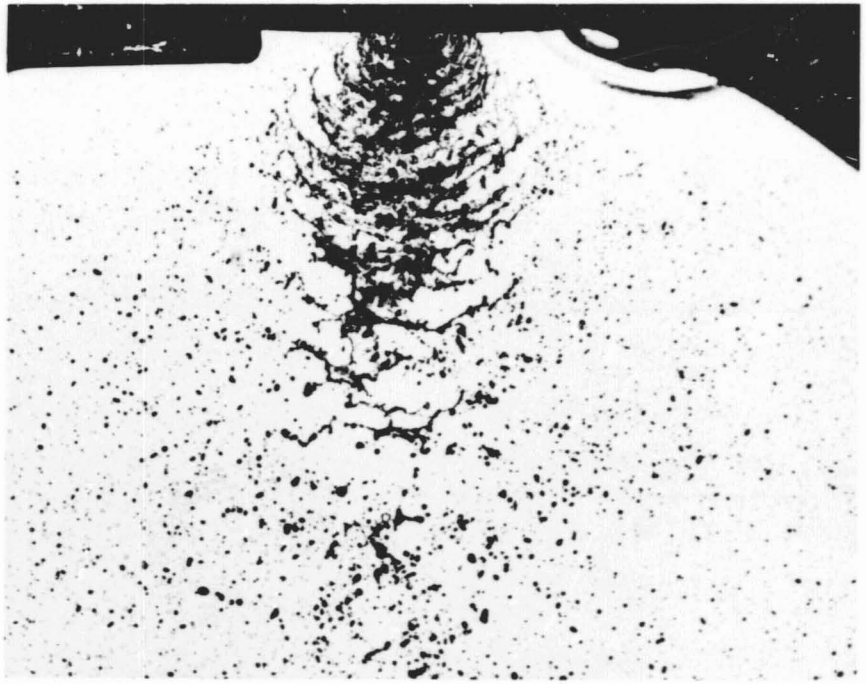

24.d X-Doublet Prototype, Scale = 3.83
S.G.=1.0, 30 psi, 3.32 gm/sec.

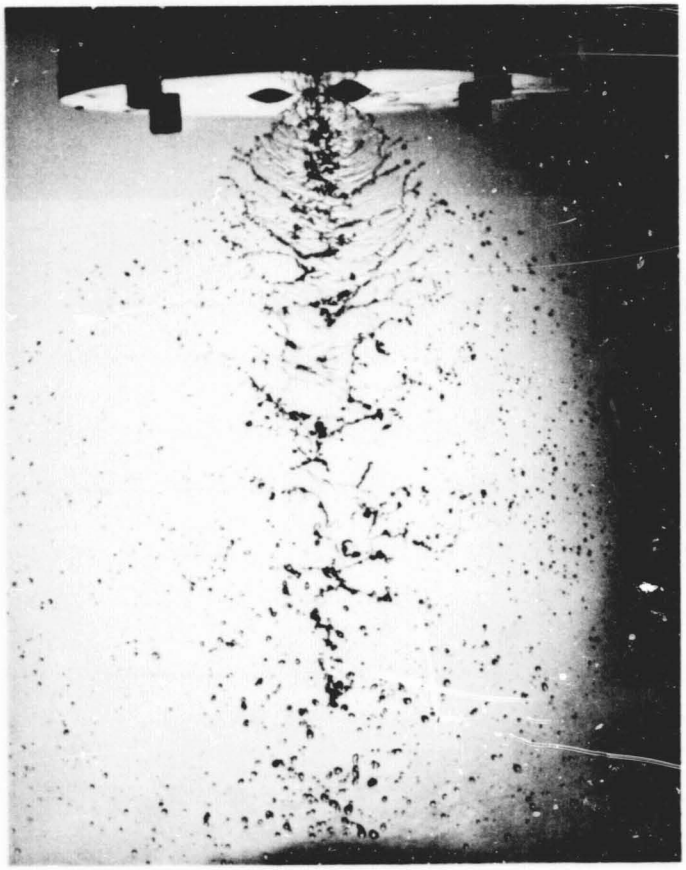

24.e Model XD-M1, Scale = 0.48
S.G.=1.085, 4.88 psi, 1.14 gal/min.

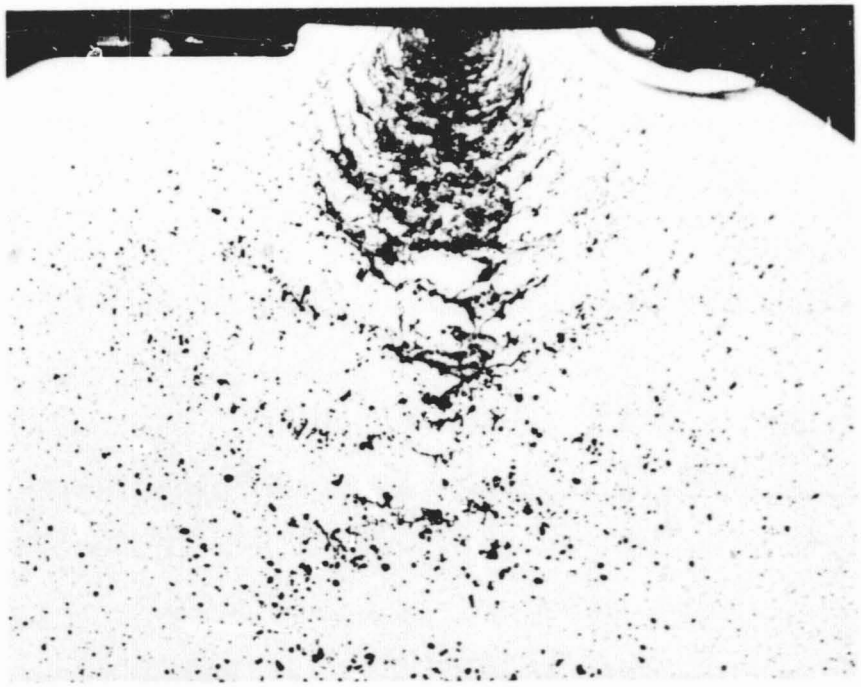

24.f X-Doublet Prototype, Scale = 3.83
S.G.=1.0, 40 psi, 3.80 gm/sec.

24.g Model XD-M1, Scale = 0.48
S.G.=1.085, 6.10 psi, 1.28 gal/min.

24.h X-Doublet Prototype, Scale = 3.83
S.G.=1.0, 50 psi, 4.26 gm/sec.

Appendix A. The relatively large flow rate required for this injector was not attainable without modifying the experimental facility. Accordingly, no photographs of the atomization characteristics of this injector were obtained.

4.6 Quantitative Information Obtained from Tests

Although most of the results of this study were qualitative in nature, a certain amount of quantitative information was obtained. Measurements of the flow rate versus overall pressure drop were made for all the injectors tested during the program. The results obtained with the prototype injectors using water are plotted Figure 25. Similar results for the standard x-doublet model using a glycerol-water solution with a specific gravity of 1.085 (34% glycerol) are plotted in Figure 26. Flow rate versus pressure drop data for the remainder of the injectors tested are presented in Figure 27. Measurements of flow rate versus pressure drop were also made for the standard x-doublet (XD-M1) using a glycerol-water solution of specific gravity 1.059 (24% glycerol) in order to more closely model the properties of liquid MMH at 200°F. The data obtained are virtually indistinguishable from the data of Figure 27 and are, consequently, not plotted.

An injector discharge coefficient C_d can be defined by the equation

$$Q = C_d A \sqrt{2\Delta p/\rho} \quad . \tag{16}$$

where Q is the volumetric flow rate, A the minimum flow cross-sectional area, Δp the pressure drop, and ρ the density. Using (16), together with Figures 25 and 26, coefficients for the x-doublet prototype and model were found

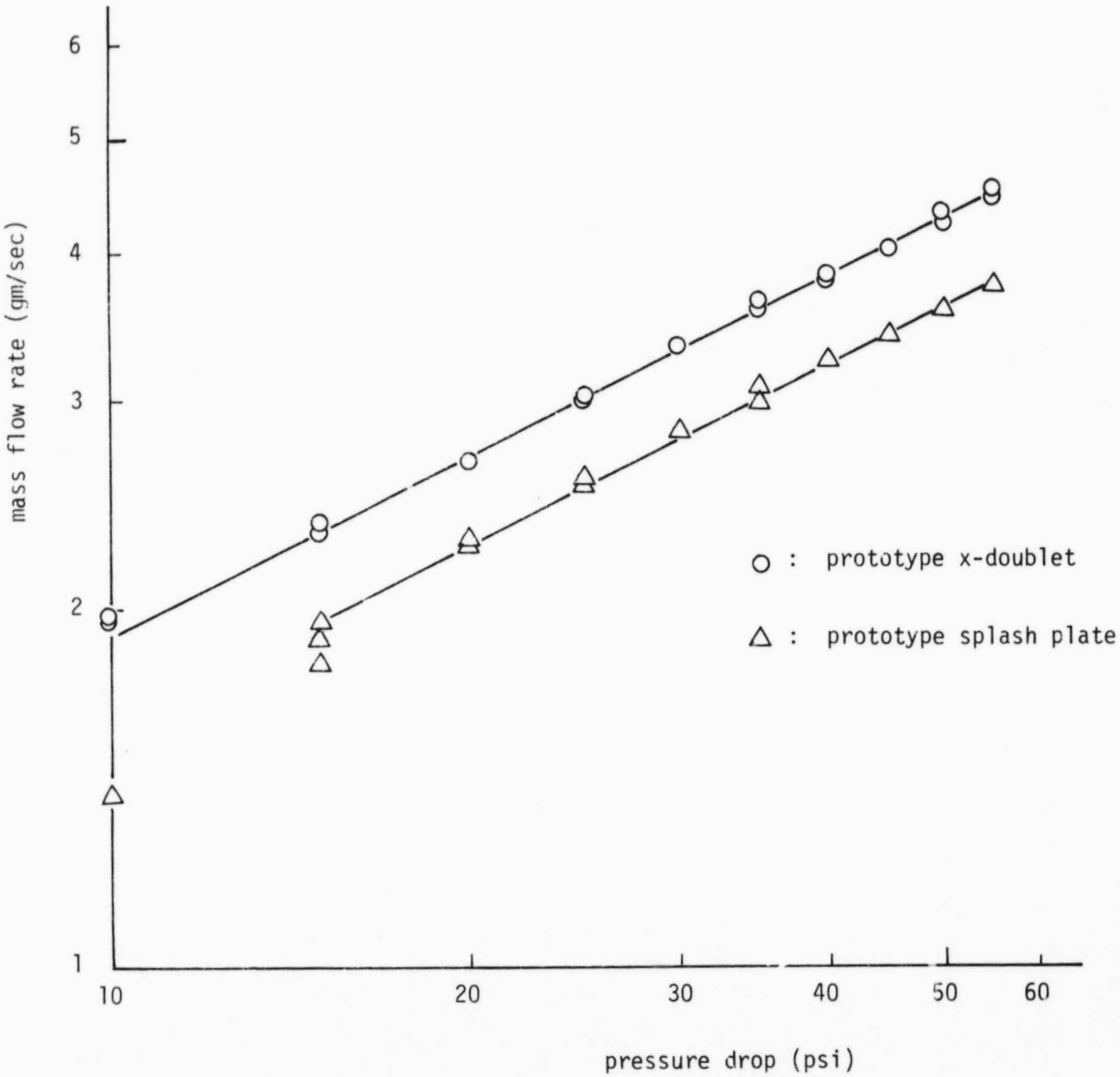

Figure 25. Mass Flow Rate Versus Pressure Drop for Water-Flow Tests of Prototype Injectors

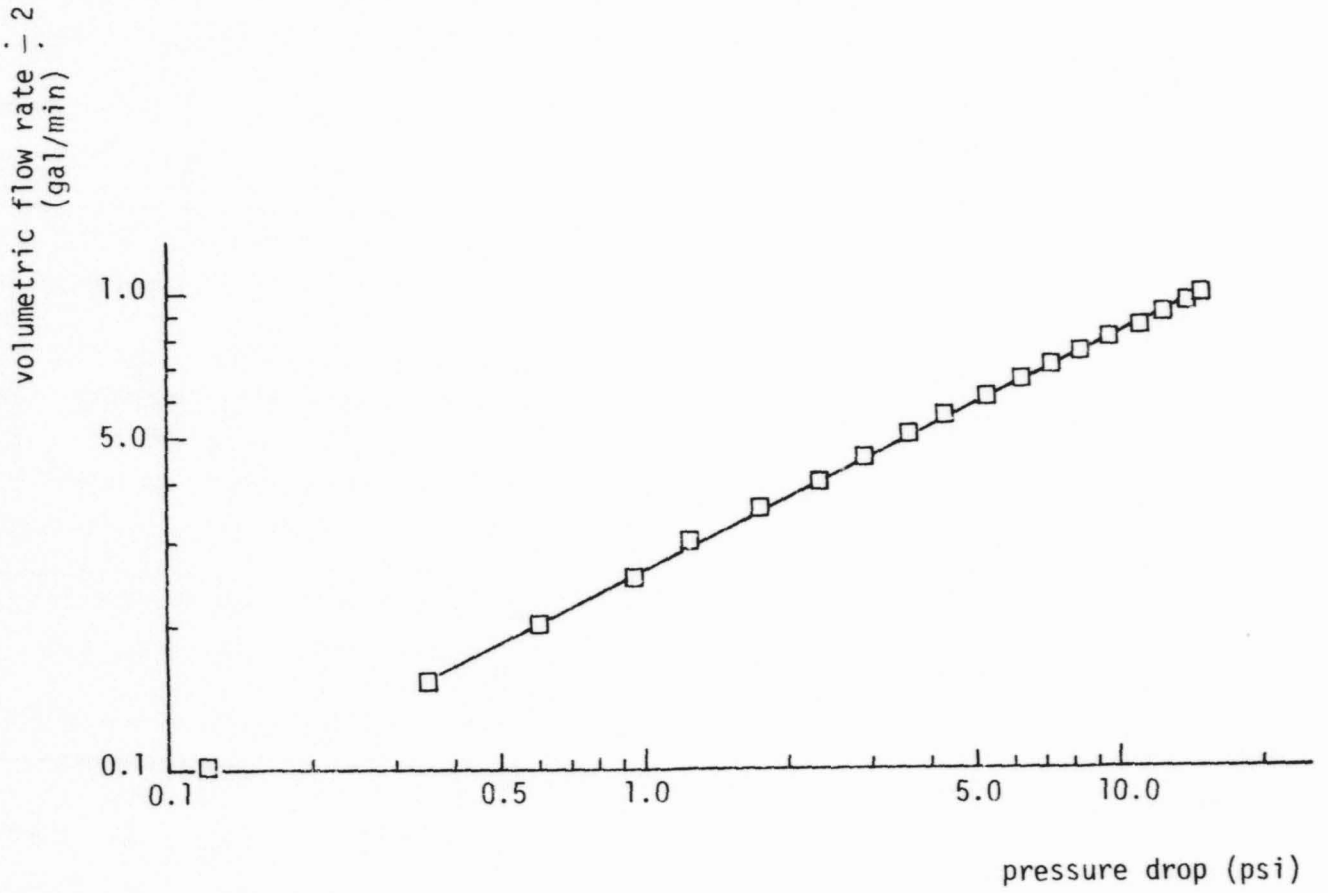

Figure 26. Volumetric Flow Rate Versus Pressure Drop for Standard X-Doublet Model (XD-M1) (Glycerol-Water Solution with S.G. = 1.085)

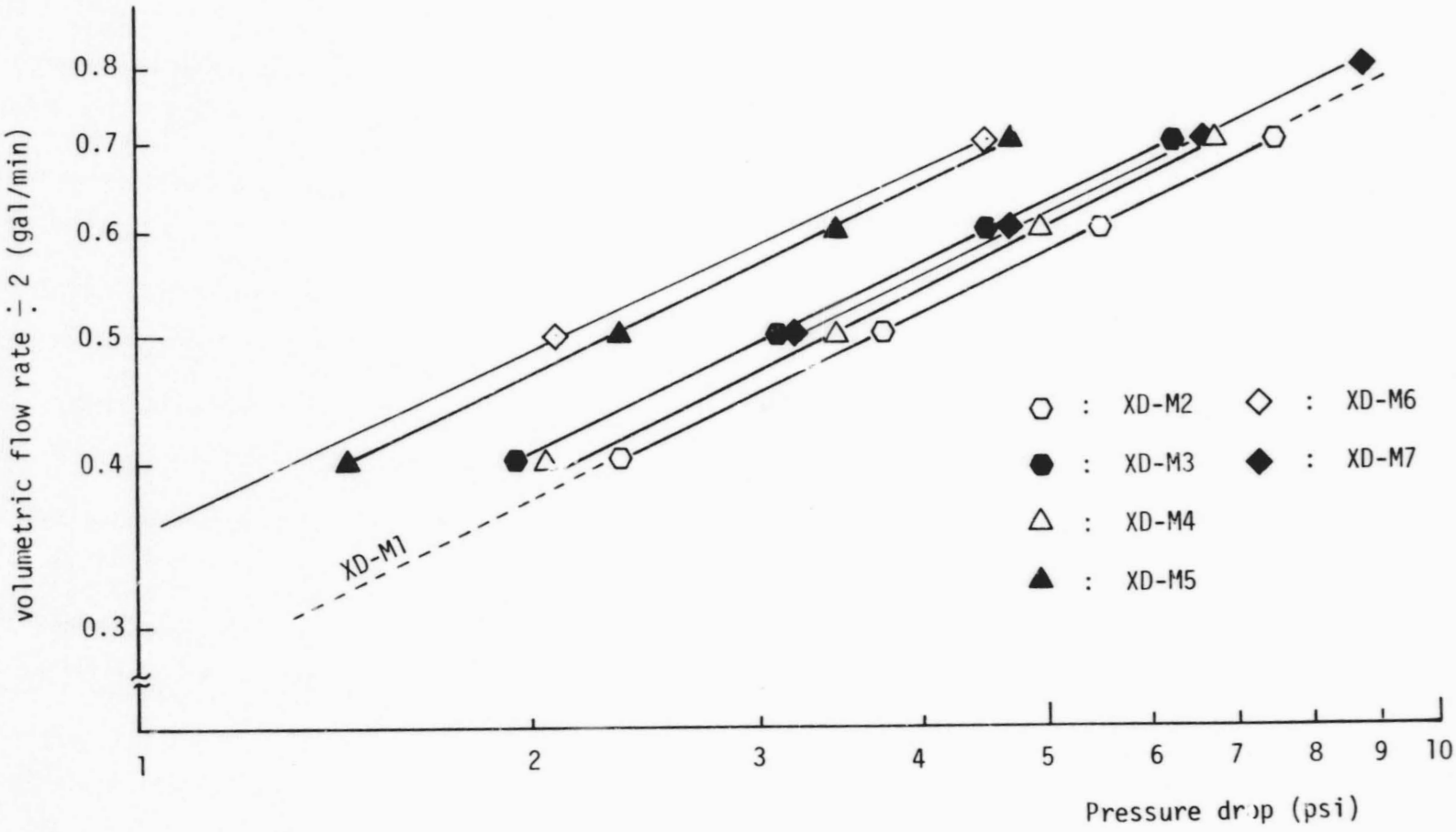

Figure 27. Volumetric Flow Rate Versus Pressure Drop for X-Doublet Models (Glycerol-Water Solution with S.G. = 1.085)

to be virtually constant over the range of conditions investigated and given by

$$(C_d)_{\text{prototype}} = 0.63 \quad , \quad (C_d)_{\text{model}} = 0.59 \quad . \qquad (17)$$

Also, the slopes of all the curves in Figures 25 through 27 were found to be equal to one-half, in accordance with Equation (16). All data upon which Figures 25 through 27 are based is tabulated in Appendix D.

From careful considerations of enlarged photographs, it was possible to measure the total included angle of the spray field for both the x-doublet model and prototype. The results of this investigation are tabulated in Appendix D and presented graphically in Figure 28. In Figure 28, the pressure drop Δp is nondimensionalized with respect to the surface tension and a characteristic length, taken to be the minimum dimension of the injector exit.

The initial length of the fluid sheet ℓ_i prior to complete breakup was also measured from photographs of the spray field. These measurements are included in Appendix D and form the basis for Figure 29. Although measurements of this type tend to be somewhat subjective, a reasonably consistent behavior is descernible from Figure 29.

The mass distribution in the spray fan generated by the standard x-doublet model was measured by collecting the efflux in a 1/8-inch wide collection slit placed perpendicular to the spray fan. In this way, the mass distribution plotted in Figure 30 was determined. In Figure 30, $\dot{m}$ represents the mass collected per unit time in the collection slit, $\dot{M}$ is the total mass flow per unit time from the injector, x is the distance

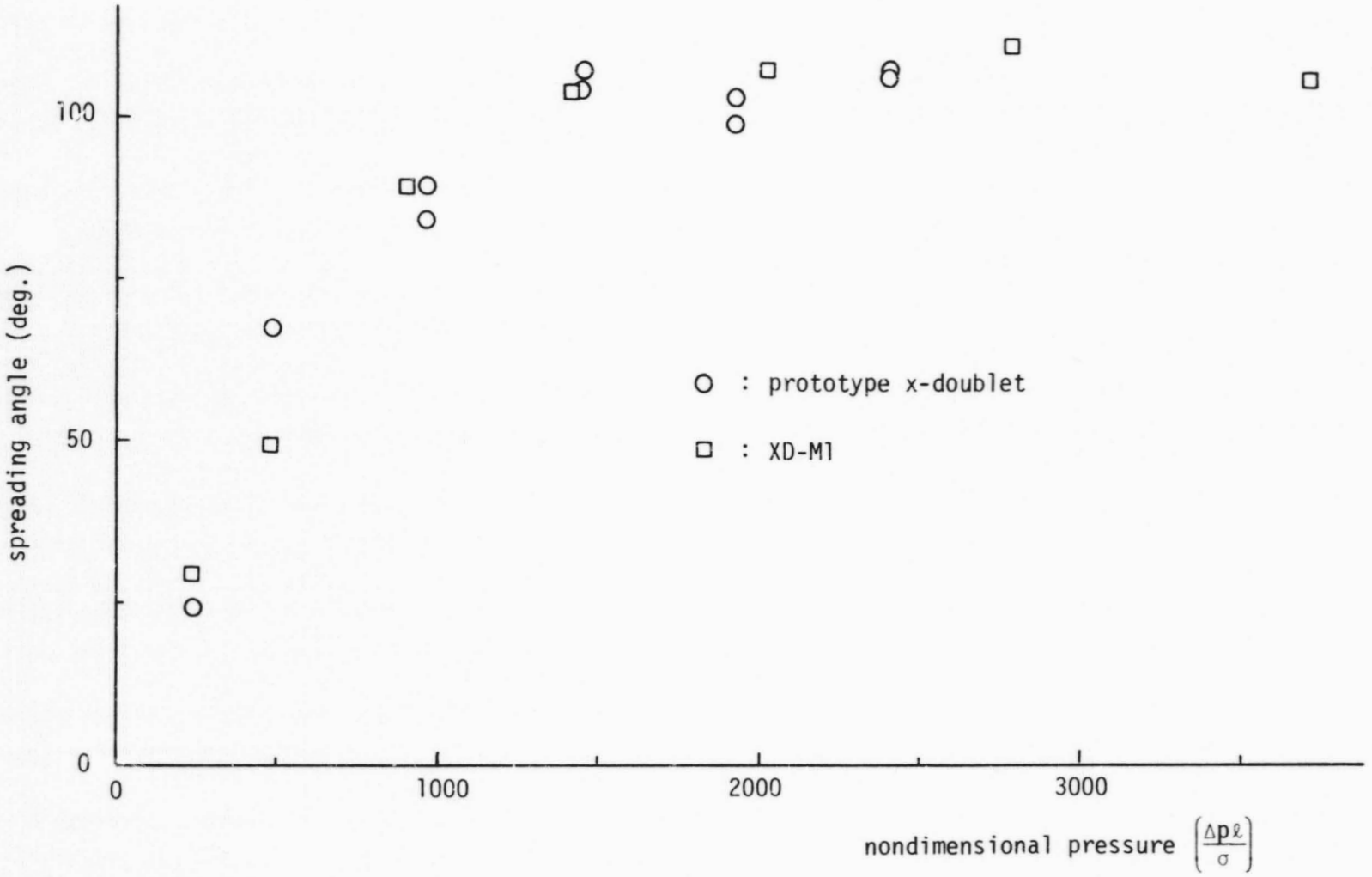

Figure 28. Total Included Spreading Angle of the Atomized Spray Field Versus Nondimensional Pressure. (S.G. = 1.0 for prototype, = 1.085 for XD-M1)

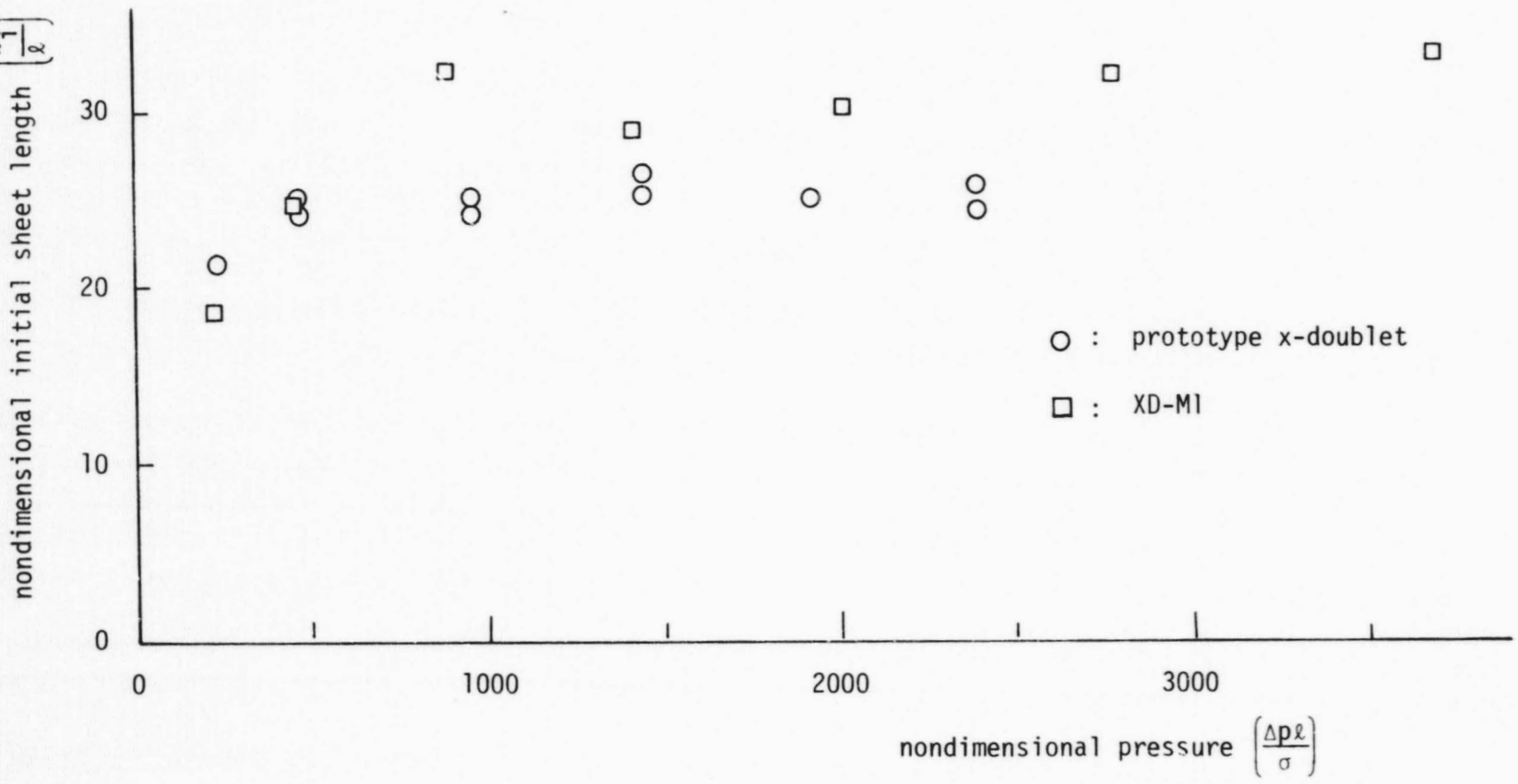

Figure 29. Initial Sheet Length Versus Nondimensional Pressure.
(S.G. = 1.0 for prototype = 1.085 for XD-M1)

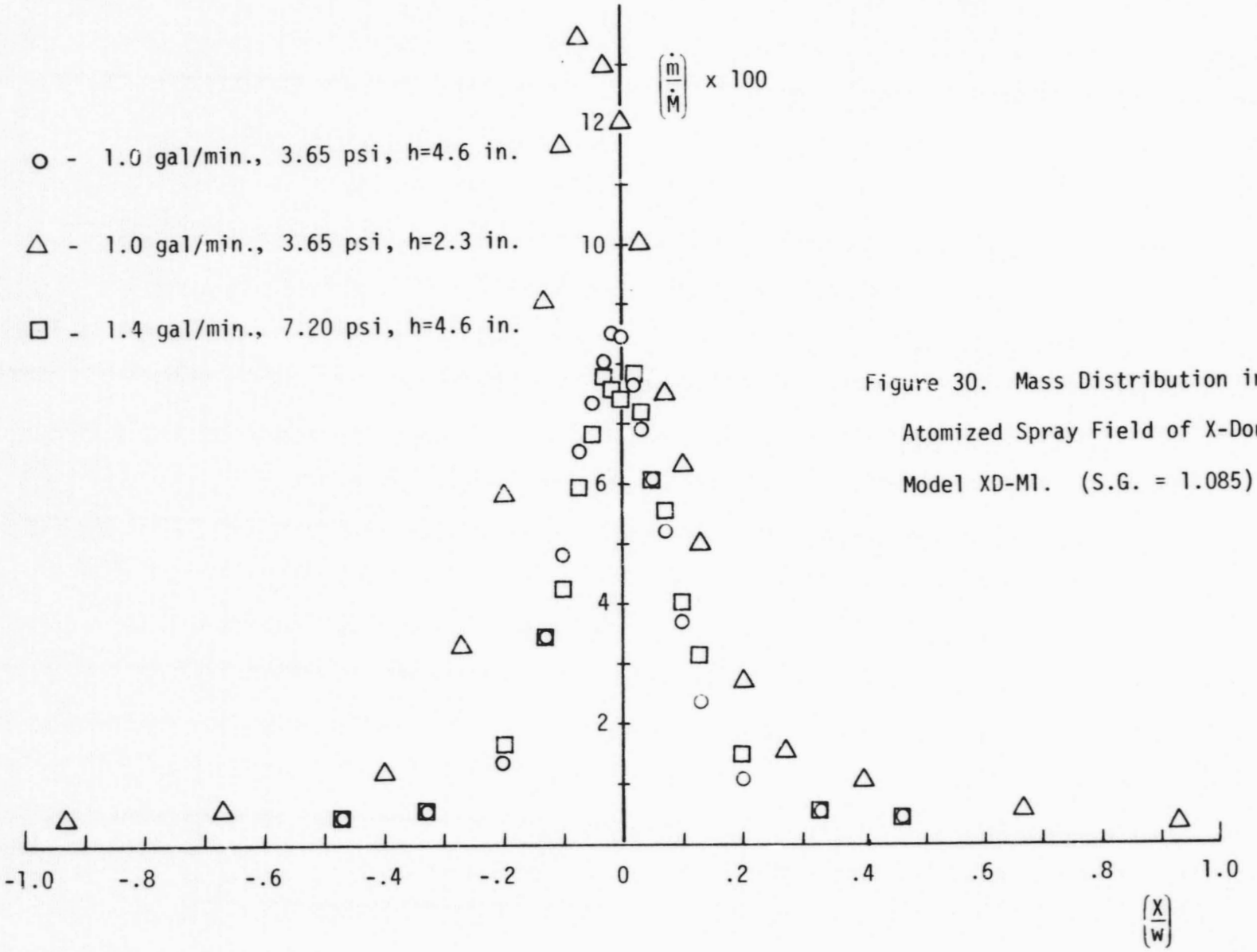

Figure 30. Mass Distribution in Atomized Spray Field of X-Doublet Model XD-M1. (S.G. = 1.085)

from the centerline of the injector to the centerline of the collection slit, w is one-half the width of the spray field at the location where the measurements were made, and h is the distance from the face of the injector to the collection slit. Since the spray fan was essentially two-dimensional, it was deemed sufficient to measure the mass distribution across the face of the spray fan, only.

4.7 Comparison of Model to Prototype

If the information contained in Figures 25, 26, 28, and 29 is studied carefully, the following conclusions can be drawn with regard to the x-doublet prototype and the standard model (XD-M1):

1. The dependence of flow rate on pressure drop is identical for both model and prototype.
2. The discharge coefficients for model and prototype agree within 10%.
3. Fan spreading angles for both model and prototype are closely correlatable.
4. Initial sheet length before complete atomization is reasonably constant from model to prototype.

In addition to the above items, the photographs reproduced in Figure 24 exhibit reasonable similarity between model and prototype atomization. When comparing photographs, it should be borne in mind that the model photographs are shadowgraphs while the prototype was photographed using back-lighting. Consequently, the depth of field is considerably greater for the prototypes than for the models and a greater number of droplets

are visible in the photographs of the prototype.

At this stage, the evidence tends to verify the modeling procedure. In order to provide a definitive verification, however, it would be necessary to measure droplet sizes and distributions, a procedure not attempted during the course of the reported study.

4.8 Visualization of Internal Flow

As mentioned previously, a 15.7-to-1.0 scale model of the x-doublet was constructed from transparent acrylic plastic in order to provide a means for visualization of the internal flow. Since only the internal flow was to be modeled, water was used in the tests. Similarity of Reynolds numbers could be maintained between model and prototype which was sufficient for the modeling of the internal flow. Ink was injected into the flow through small tubes in order to make the streak lines of the flow visible. The photographs thus obtained are collected in Figure 31. Figures 31.a and 31.b show general streak lines for typical flow conditions. Figures 31.b and 31.c illustrate the corner blockage effect. Figures 31.d and 31.e show the blockage which occurs between the inlet orifices. The remainder of the photographs in Figure 31 show typical overall flow conditions. The many small bubbles apparent in the photographs were air bubbles which collected on the inside wall of the model. The bubbles had no noticeable effect on the flow.

Two effects are immediately apparent upon consideration of the photographs. First, it is apparent that the two inlet flow streams are considerably constricted prior to exiting from the injector. Secondly, it can be observed that the two internal flow streams intersect at an angle of

approximately 145°. It was this latter effect which prompted the construction of model XD-M7 in which the inlet orifice spacing was increased by 50%. It was thought that the increased spacing would cause the intersection angle to be nearer 180° which would, in turn, result in a more uniform external spray field.

4.9 High Speed Movies

High speed movies (4000 frames/sec.) were obtained for several flow conditions with the x-doublet model XD-M1. The films were submitted to NASA representatives at the conclusion of the injector study program. However, since it was not possible to effectively reproduce prints of the films for this report, all information concerning the taking of the movies is presented in Appendix C.

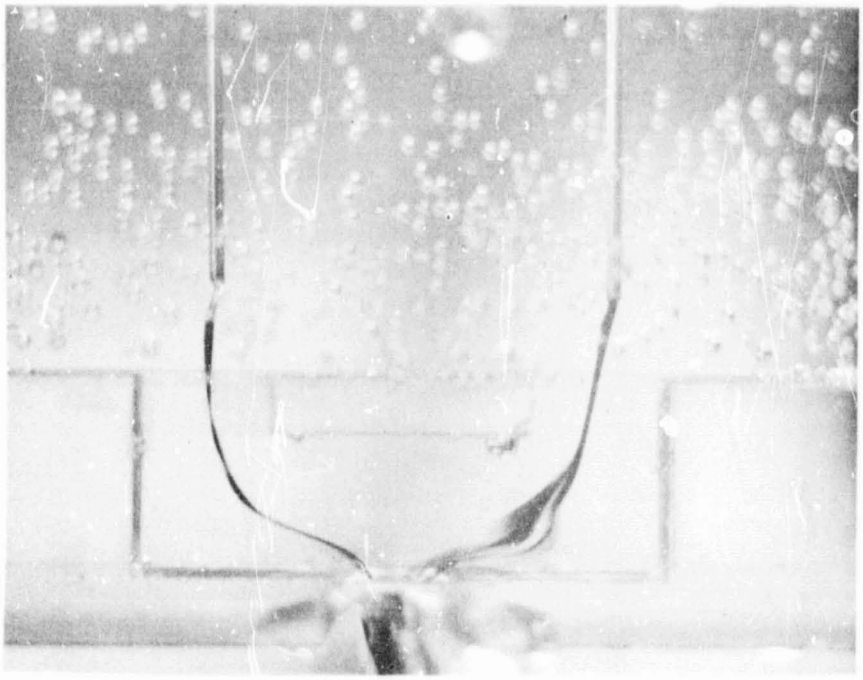

Figure 31.a Streak Lines (1.0 gal/min)

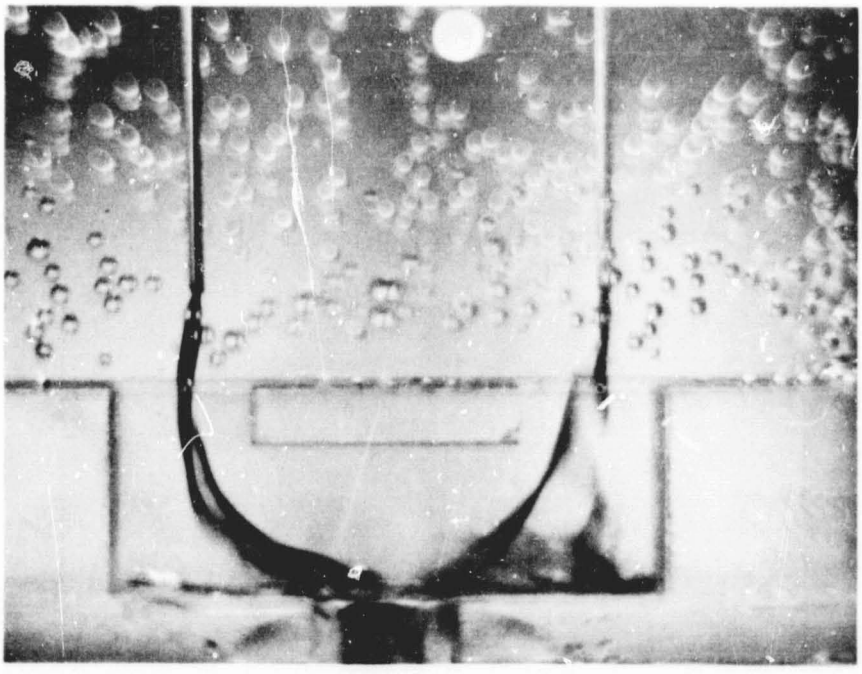

Figure 31.b Streak Lines (2.0 gal/min)

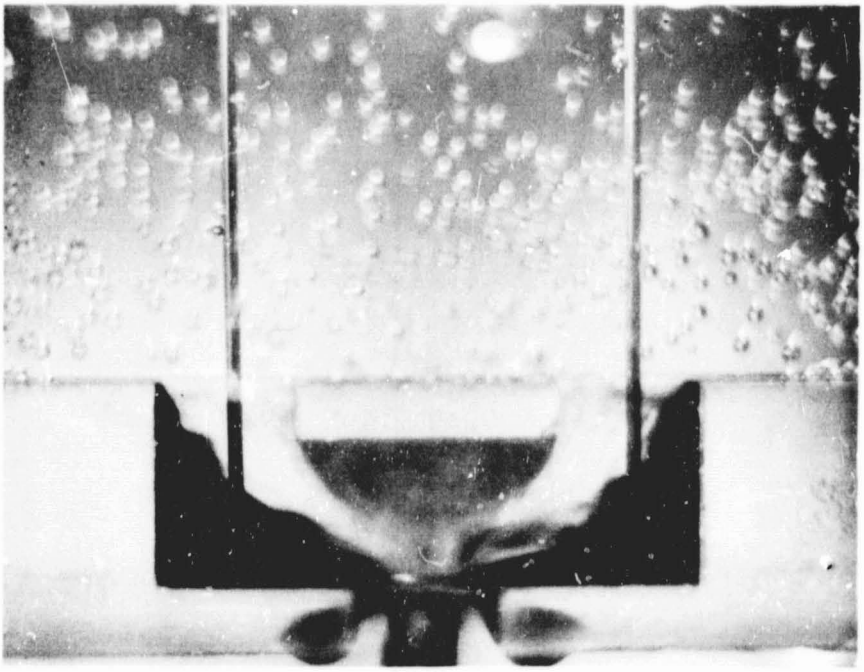

Figure 31.c Corner Blockage Effect (1.0 gal/min)

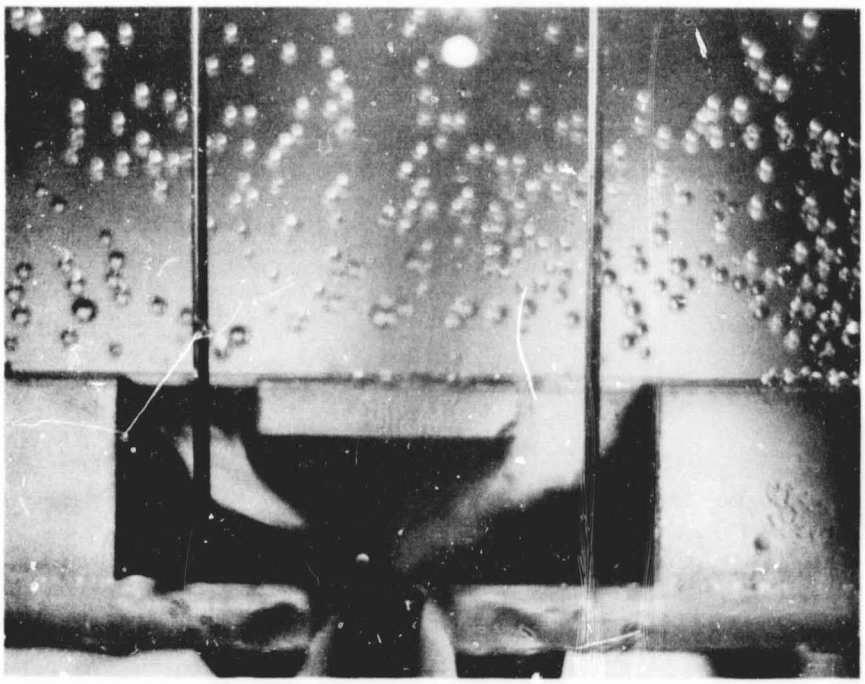

Figure 31.d Corner Blockage Effect (2.0 gal/min)

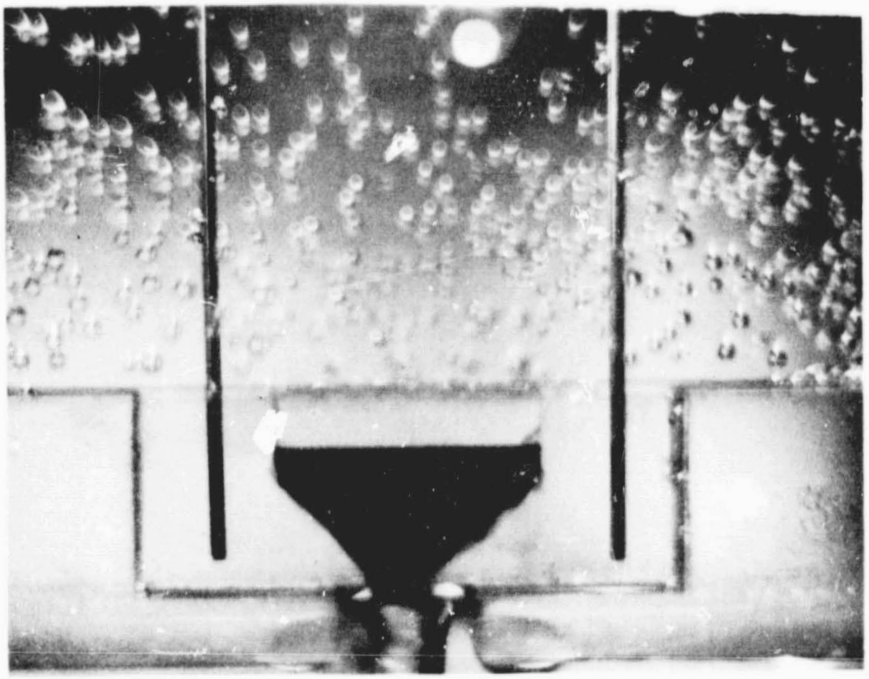

Figure 31.e Central Blockage Effect (1.0 gal/min)

Figure 31.f Central Blockage Effect (2.0 gal/min)

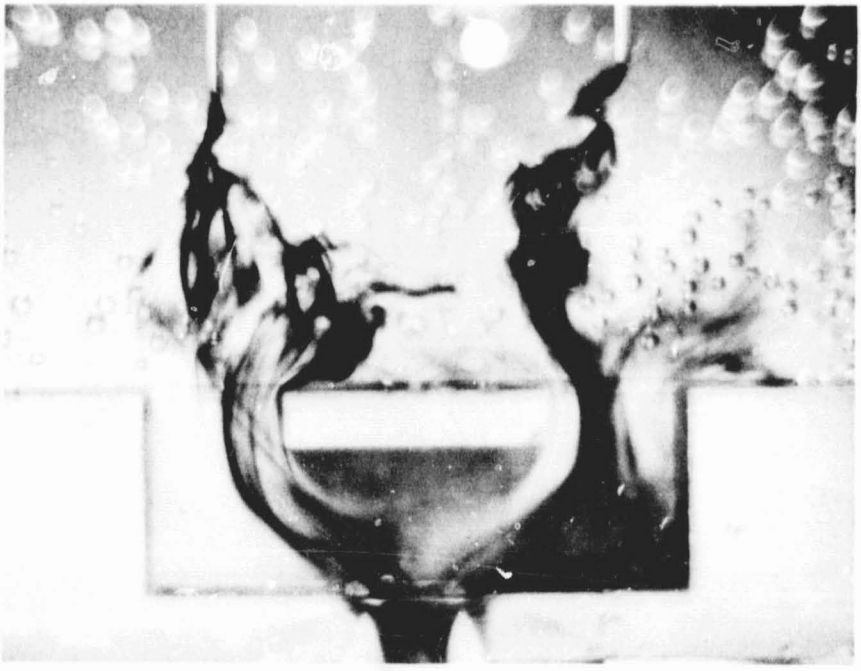

Figure 31.g General Aspects of Flow (2.0 gal/min)

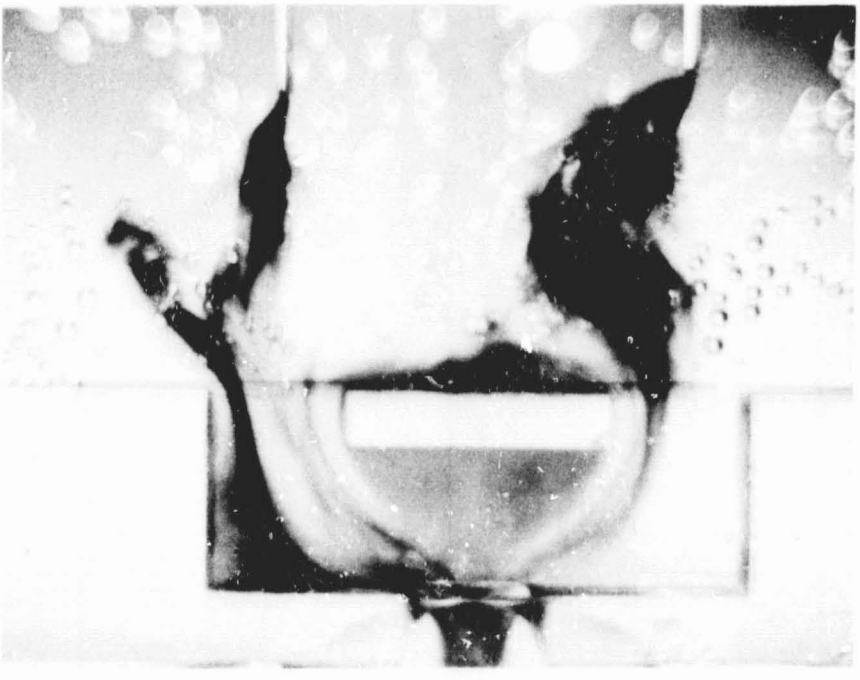

Figure 31.g (continued)

Figure 31.g (continued)

5. DISCUSSION

In the previous section, representative photographs along with measured data obtained during the course of the study were presented. It is now desired to offer some observations of a general nature regarding the results of Section 4 as well as to emphasize other important results of previous sections.

In Section 2 a theory was developed upon which model atomization studies could be based. Using this theory as a guide, an experimental program was conducted which provided the results described in Section 4. The information contained in Figures 24 through 29 indicates reasonable agreement between model and prototype behavior and confirms, in a general sense, the modeling criteria developed in Section 2. This agreement allows one to deduce, with confidence, the behavior of a prototype injector from model experiments.

Although reasonable confidence has been established for the methods employed in the model studies, there is one additional item which, if determined, could establish complete confidence in the method. This would consist of a comparison of droplet sizes and distributions produced by models and prototypes operating under dynamically similar conditions. Measurements of these quantities could be obtained directly from the photographic negatives produced during the current study.

Photographs of the x-doublet prototype showed that the spray fan produced was similar to that produced by two impinging free jets. The mass distribution in the spray was not uniform, but tended to have a higher concentration along the centerline of the spray fan. Mean droplet size

appeared to decrease with an increase in flow rate through the injector. The flow rate versus pressure drop behavior was comparable to that of a sharp edged orifice.

From photographs, it was observed that the splash-plate prototype injector produced much larger diameter droplets than did the x-doublet. From this as well as other observations based on actual combustion data, it was decided to omit the splash-plate from further consideration and concentrate on the x-doublet injector concept.

From the experiments performed with x-doublet models with altered platelet thicknesses, it was observed that the discharge coefficient for the injector could be controlled to a limited extent without seriously affecting the atomization characteristics of the injector. These observations are evident upon consideration of Figures 16, 17, 18, and 27.

Figure 19 illustrates the adverse effect that the omission of the orifice plate has on atomization. Figure 20 illustrates the effect of beveling the outlet edge of the metering element. This alteration results in the production of an initial sheet of liquid of somewhat greater extent than that produced by the standard injector. However, once atomized, the resulting spray seems to be composed of more numerous, smaller droplets. The beveling of the outlet edge of the metering element could be construed as an approximation to the effect of errosion at this location. An increase of 50% in the spacing of the inlet orifices results in a greater initial spreading angle and a shorter initial sheet length as well as better and more uniform atomization. It is suggested that this altered design be studied in more detail in order to assess the magnitude of the apparent improvements in operating conditions.

Figure 22 consists of photographs taken of the standard x-doublet model operating with a glycerol-water solution of specific gravity 1.059. This condition models the prototype behavior when liquid MMH at 200°F is the working fluid. The change of fluid produced no noticeable effect in the model study as compared with the standard x-doublet model operated with a glycerol-water solution of specific gravity 1.085.

Three high speed movies (4000 frames per second) were taken of the standard x-doublet model operating at different flow rates. One movie was taken of the model when operating with a glycerol-water solution of specific gravity 1.059 instead of the standard value of 1.085. It was not possible to reproduce sufficiently good photographs from the movie frames for inclusion in this report. Hence, pertinent information concerning the movies is relegated to Appendix C. Upon studying the movies, it was, however, possible to verify several features of the flow field. The dynamics of the atomization process appeared to correspond qualitatively with the illustration used in Figure 3. No unusual oscillations were apparent. The change in specific gravity from 1.085 to 1.059 had no noticeable effect. Most of the mass in the spray field appeared to be concentrated in a narrow region around the centerline of the spray fan.

The distribution of mass within the spray field generated by the standard x-doublet model was measured and is presented in normalized form in Figure 30. The fundamental result apparent in this figure is that the substantial portion of the spray is contained in the central portion of the spray fan. The width of this central portion is approximately 20% of the total width of the spray fan. This result is in qualitative agreement with the observations made from the photographic studies.

Inlet cross-flow studies were conducted for the x-doublet with an inlet cross-velocity equal to 23% of the injector mean exit velocity when operating at a flow rate corresponding to a scaled pressure drop of 30 psi. The cross-velocity was directed both parallel and perpendicular to a line joining the two inlet orifices. The cross-velocity had no apparent effect on the atomization characteristics of the injector.

The internal flow visualization studies which resulted in the photographs presented in Figure 31 have been adequately discussed in Section 4.

A model of a highly modified version of the x-doublet, called the V-doublet, was constructed during the course of the experimental program. Information concerning this injector is contained in Appendix A. Flow rate versus pressure drop information for this design is contained in Figure A.13 in Appendix A. The relatively large flow rate required for efficient atomization precluded the testing of this model in the existing experimental setup.

Finally, the effect of inlet orifice blockage was investigated in a preliminary manner for the x-doublet. Results of these studies are contained in Appendix E. It was generally found that complete blockage of an inlet orifice caused "tilting" of the spray fan with only minor degradation of the quality of atomization. Partial blockage of an inlet orifice (if accomplished in the manner illustrated in Appendix E) was found to cause a "skewing" of the mass distribution in the spray fan with, again, only minor degradation of the quality of atomization.

BIBLIOGRAPHY

Surveys of Atomization Phenomena

1. Brodkey, R.S., The Phenomena of Fluid Motions, Addisen-Wesley Pub. Co., Chap. 17, 1967.

2. Harrje, D.T., Ed., "Liquid Propellant Rocket Combustion Instability," NASA SP-194, 1972.

3. Lapple, C.E., Henry, J.P., and Blake, D.E., "Atomization - A Survey and Critique of the Literature," Stanford Res. Inst., Special Tech. Rept. No. 6, PAU 4900, 1966.

4. Putnam, A.A., et. al., "Injection and Combustion of Liquid Fuels," WADC Tech. Rept. 56-344, 1957.

5. Zajac, L.J., "Correlation of Spray Dropsize Distribution and Injector Variables," Rept. R-8455, Rocketdyne Corp., Canoga Park, California, Contract NAS7-726.

Fundamental References on Atomization Phenomena

6. Dombrowski, N. and Fraser, R., "A Photographic Investigation into the Disintegration of Liquid Sheets," British Chemical Engr., v. 247, A-924, p. 101, Sept. 1954.

7. Dombrowski, N. and Hooper, P., "A Study of the Sprays Formed by Impinging Jets in Laminar and Turbulent Flow," J. Fluid Mech., v. 18, part 3, pp. 392-400, 1964.

8. Dombrowski, N. and Johns, W.R., "The Aerodynamic Instability and Disintegration of Viscous Liquid Sheets," Chem. Engr. Sci., v. 18, pp. 203-214, 1963.

9. Hagerty, W.W. and Shea, J., "A Study of the Stability of Plane Fluid Sheets," Appl. Mech., p. 510, Dec. 1955.

10. Hasson, D. and Peck, R.E., "Thickness Distribution in a Sheet Formed by Impinging Jets," A.I. Ch. E.J., v. 10, no. 5, pp. 752-759, Sept. 1964.

11. Heidmann, M.R., Priem, R., and Humphrey, J., "A Study of Sprays Formed by Two Impinging Jets," NACA TN 3835, March 1957.

12. LeClerc, A., "Deflection of a Liquid Jet by a Perpendicular Boundary," M.S. Thesis, U. of Iowa, 1948.

13. Mayer, E., "Theory of Liquid Atomization in High Velocity Gas Streams," ARS J., v.31, no. 12, pp. 1783-1785, Dec. 1961.

14. Popov, M., "Model Experiments on Atomization of Liquids," NASA Tech. Trans. F-65, July 1961.

15. Rayleigh, Lord (J.W. Strutt), "On the Instability of Jets," Proc. London Math. Soc., v. 10, p. 4, 1878.

16. Rayleigh, Lord (J.W. Strutt), "On the Stability of a Cylinder of Viscous Liquid under Capillary Force," Phil. Mag., v. 37, p. 153, 1892.

17. Squire, H.B. "Investigation of the Instability of a Moving Liquid Film," Brit. J. Appl. Phys., v. 4, pp. 167-169, June 1953.

18. Weber, C. "On the Breakdown of a Fluid Jet," Ninth Progress Rept., VII, Project MX-833, Sect. II, University of Colorado, Boulder, Colorado, 1931.

References Supplemental to Lapple Report (Ref. 3)

19. Adelberg, M., "Breakup Rate and Penetration of a Liquid Jet in a Gas Stream," AIAA J., v. 5, no. 8, pp. 1408-1415, 1967.

20. Bigelow, J.A., "Preliminary Tests of a Gas Turbine Combustor with an Air Atomizing Fuel Injector System," NAS-TM-X-52688, 1969.

21. Clark, C.J. and Dombrowski, N., "The Dynamics of the Rim of a Fan Spray Sheet," Chem. Engr. Sci., v. 26, pp. 1849-1952, 1971.

22. Dabora, E.K., "Production of Monodisperse Sprays," Rev. of Sci. Inst., v. 38, no. 4, 502-506, 1967.

23. Dombrowski, N. and Hasson, D., "The Flow Characteristics of Swirl (Centrifugal) Spray Pressure Nozzles with Low Viscosity Liquids," A.I. Ch. E.J., v. 15, no. 4, p. 604-611, 1969.

24. Dombrowski, N. and Wolfsohn, D.L., "A Note on the Photography of Particles by Scattered Light at Low Levels of Intensity," Chem. Engr. Sci., v. 27, pp. 1181-1183, 1972.

25. Drummond, A.M., "On Atomization and Linearized Free-Surface Instability on Rotating Bodies," Avail: NTIS HC, 1972.

26. Dunskii, V.F., "Method of Determining the Droplet Size Distribution in the Atomization of Liquids," Avail: CFSTI CSCL 14/2, 1968.

27. Gal-Or, B., Klinzing, E., and Tavlarides, L.L., "Bubble and Drop Phenomena," Ind. and Engr. Chem., v. 61, no. 2, 1969.

28. Goldschmidt, V.W. and Householder, M.K., "The Hot Wire Anemometer as an Aerosol Droplet Size Sampler," J. Atmospheric Environ., v. 3, no. 6, 1969.

29. Gooderum, P.B. and Bushnell, D.M., "Atomization, Drop Size, and Penetration for Cross-Stream Water Injection at High-Altitude Reentry Conditions with Application to the RAM C-1 and C-3 Flights," NASA-TN-D-6747, 1972.

30. Grandzol, R.J. and Tallmadge, J.A., "Water Jet Atomization of Molten Steel," A.I. Ch. E.J., v. 19, no. 6, 1149-1158, 1973.

31. Gulkov, S.A., "Theory and Design of Ejection Type Atomizer," Avail: CFSTI, 1969.

32. Haynes, L.G., Himmelblau, D.N., and Schechter, R.S., "Effect of Plate Wettability on Droplet Formation," Ind. and Engr. Chem., Proc. Designs Devel., v. 7, pp. 508-511, 1968.

33 Heidmann, M.F. and Groeneweg, J.F., "Analysis of the Dynamic Reponse of Liquid Jet Atomization to Acoustin Oscillations," NASA-TN-D-5339, 1969.

34. Karam, H.J. and Bellinger, J.C., "Deformation and Breakup of Liquid Droplets in a Simple Shear Field," Ind. and Engr. Chem. Fund., v. I, pp. 576-581, 1968.

35. Kim, K.Y. and Marshall, W.R. Jr., "Drop-Size Distributions from Pneumatic Atomizers," A.I. Ch. E.J., v. 17, no. 3, pp. 575-584, 1971.

36. Kulagin, L.V., "Combustion of Heavy Liquid Fuels, Russian translated to English, Avail: CFSTI CSCL 2 1/2, 1970.

37. Kunina, E.M., "On the Problem of the Atomization of a Liquid By a High Velocity Gas Stream," (ANL-TRANS-871) Avail: NTIS CSCL 20D, 1970.

38. Lefebvre, A.H. and Norster, E.R., "A Proposed Double Swirler Atomizer for Gas Turbine Fuel Injection," Avail: NTIS HC, 1972.

39. Masters, K., "Spray Drying," Ind. and Engr. Chem., v. 60, no. 10, 1968.

40. Meister, B.J. and Scheele, G.F., "Drop Formation from Cylindrical Jets in Immiscible Liquid Systems," A.I. Ch. E.J., v. 15, no. 5, pp. 700-706, 1969.

41. Nakano, Y. and Tien, C., "Application of Branching Process for Liquid Atomization," Ind. Engr. Chem., Fund., v. 9, pp. 98-100, 1970.

42. Narayanan, S., Basu, A., and Roy, N.K., "Prediction of Drop Diameter During Formation," Chem Engr. Sci., v. 25, pp. 1950-1951, 1970.

43. Phinney, R.E. and Humphries, W., "Stability of a Laminar Jet of Viscous Liquid - Influence of Nozzle Shape," A.I. Ch. E.J., v. 19, no. 3, pp. 655-657, 1973.

44. Rutland, D.F. and Jameson, G.J., "Droplet Production by the Disintegration of Rotating Liquid Jets," Chem Engr. Sci., v. 25, pp. 1301-1317, 1970.

45. Rutland, D.F. and Jameson, G.J., "Theoretical Prediction of the Sizes of Drops Formed in the Breakup of Capillary Jets," Chem. Engr. Sci. v. 25, pp. 1689-1698, 1970.

46. Wang, K-H and Tien, C., "Atomization and Drop Size of Polymer Solutions," Ind. and Engr. Chem. Proc. Des. Dev., v. 11, no. 2, pp. 169-178, 1972.

47. Woodmansee, D.E. and Hanraty, T.J., "Mechanism for the Removal of Droplets from a Liquid Surface by a Parallel Air Flow," Chem Engr. Sci., v. 24, pp. 299-307, 1969.

48. Zajac, L.J., "Droplet Breakup in Accelerating Gas Flows, Part I: Primary Atomization," NASA-CR-134478, Oct. 1973.

49. Zajac, L.J., "Droplet Breakup in Accelerating Gas Flows, Part II: Secondary Atomization," NASA-CR-134479, Oct. 1973.

Journals in Which Atomization Studies

Are Most Commonly Published

1. Advances in Chemical Engineering
2. A.I. Ch. E. Journal*
3. Canadian Journal of Chemical Engineering
4. Chemical Engineering Progress
5. Chemical Engineering Science*
6. Industrial and Engineering Chemistry*
7. Institute of Chemical Engineering Transactions
8. Journal of Applied Mechanics
9. Journal of Colloid and Interface Science
10. Journal of Fluid Mechanics*
11. Journal of Physical Chemistry
12. Nature
13. Philosophic Magazine
14. Physics of Fluids
15. Proceedings of the Royal Society

---

* Journals most frequently consulted.

Abstract Sources for Report of

Lapple, Henry, and Blake (Ref. 3)

1. Applied Mechanics Reviews (ASME)
2. Battelle Technical Review
3. Chemical Abstracts (ACS)
4. Dissertation Abstracts
5. International Aerospace Abstracts (AIAA)
6. Physics Abstracts: Science Abstracts, Sect. A (Inst. of Phy.)
7. Putnam, A.A., et.al., "Injection and Combustion of Liquid Fuels," WADC Tech. Rept. 56-344 (1957)
8. Scientific and Technical Aerospace Reports (NASA)
9. Spray Literature Abstracts, vol. I, II (ASME)
10. Technical Abstract Bulletin (Dept. of Commerce)
11. Technical Translations (Dept. of Commerce)

APPENDIX A

INJECTOR MODELS AND TEST EQUIPMENT

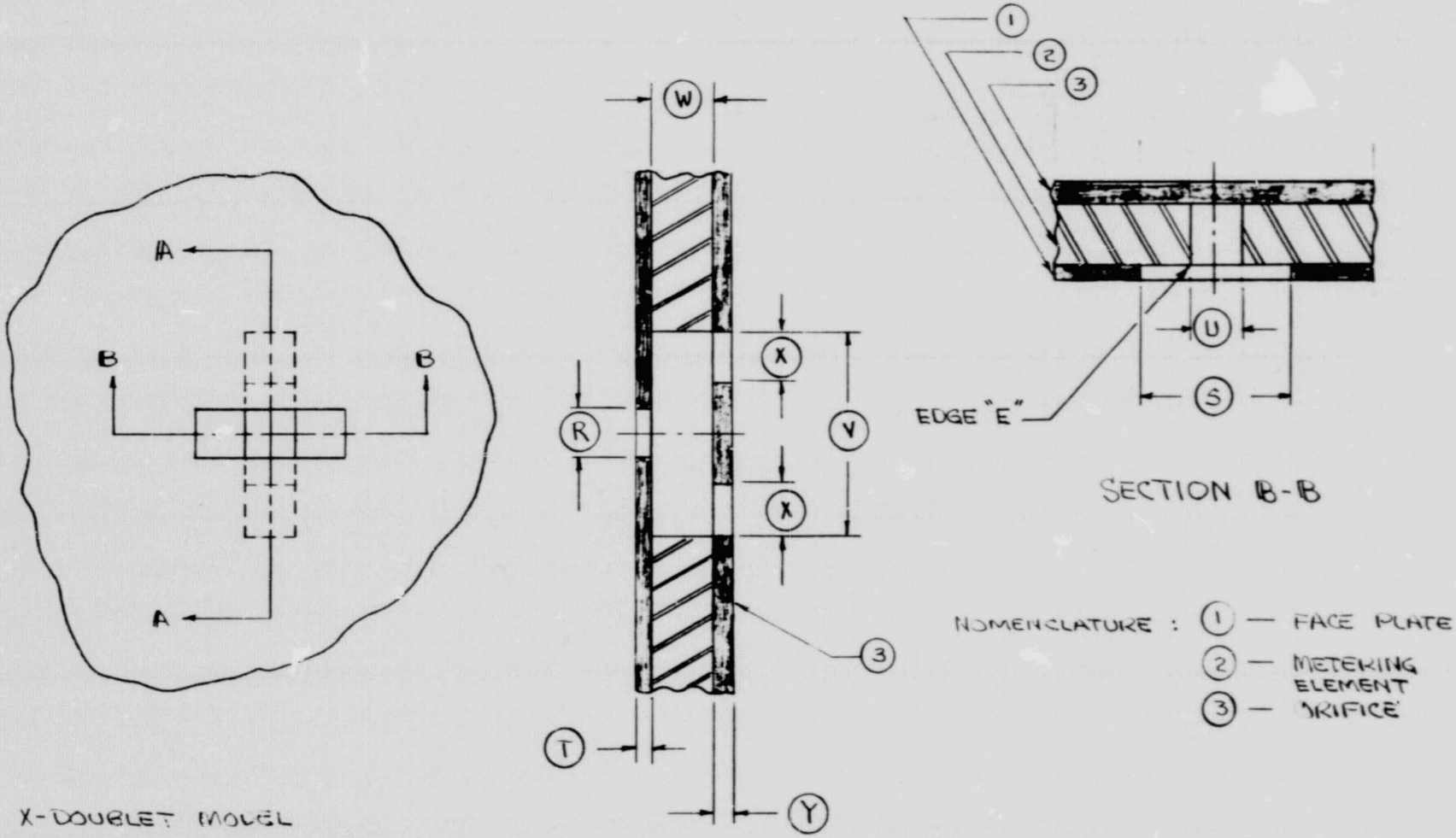

Figure A.1 X-Doublet Model

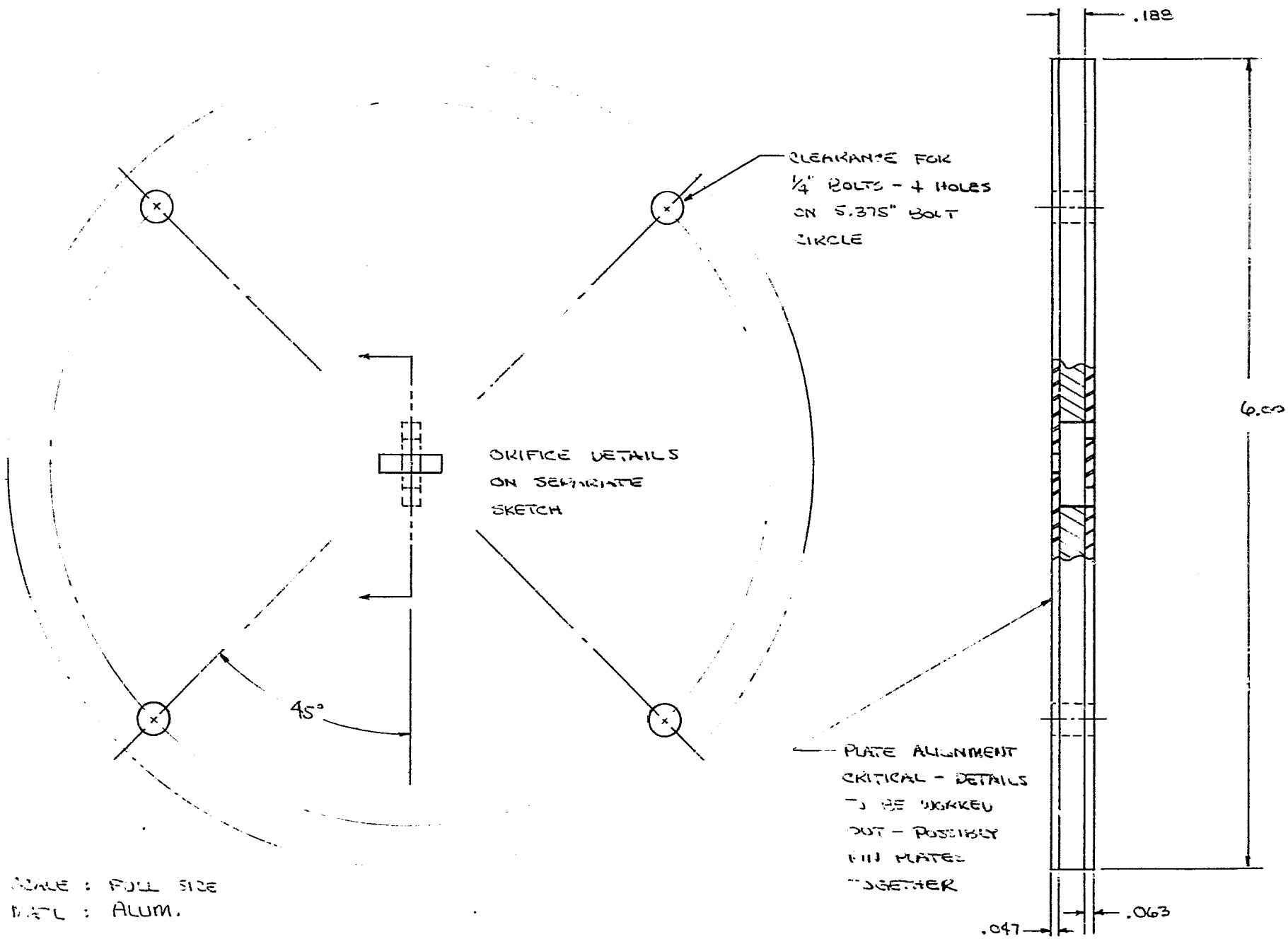

Figure A.1 continued

Figure A.1 continued

TABLE A.1

Injector Assemblies

Injector	Nominal Dimensions (in.)							
	R	S	T	U	V	W	X	Y
XD-P	.020	.060	.006	.020	.080	.024	.020	.008
XD-M1	.156	.469	.051	.156	.625	.190	.156	.062
XD-M2	.156	.469	.051	.156	.625	.090	.156	.062
XD-M3	.156	.469	.051	.156	.625	.259	.156	.062
XD-M4	.156	.469	.051	.156	.625	.190	.156	.121
XD-M5	.156	.469	.051	.156	.625	.190	-	-
XD-M6	.156	.469	.051	.156*	.625*	.190	.156	.062
XD-M7	.156	.469	.051	.156	.938	.190	.156	.062

* Outlet edge of metering element beveled 0.05 in. x 45°, see edge "E" in sketch.

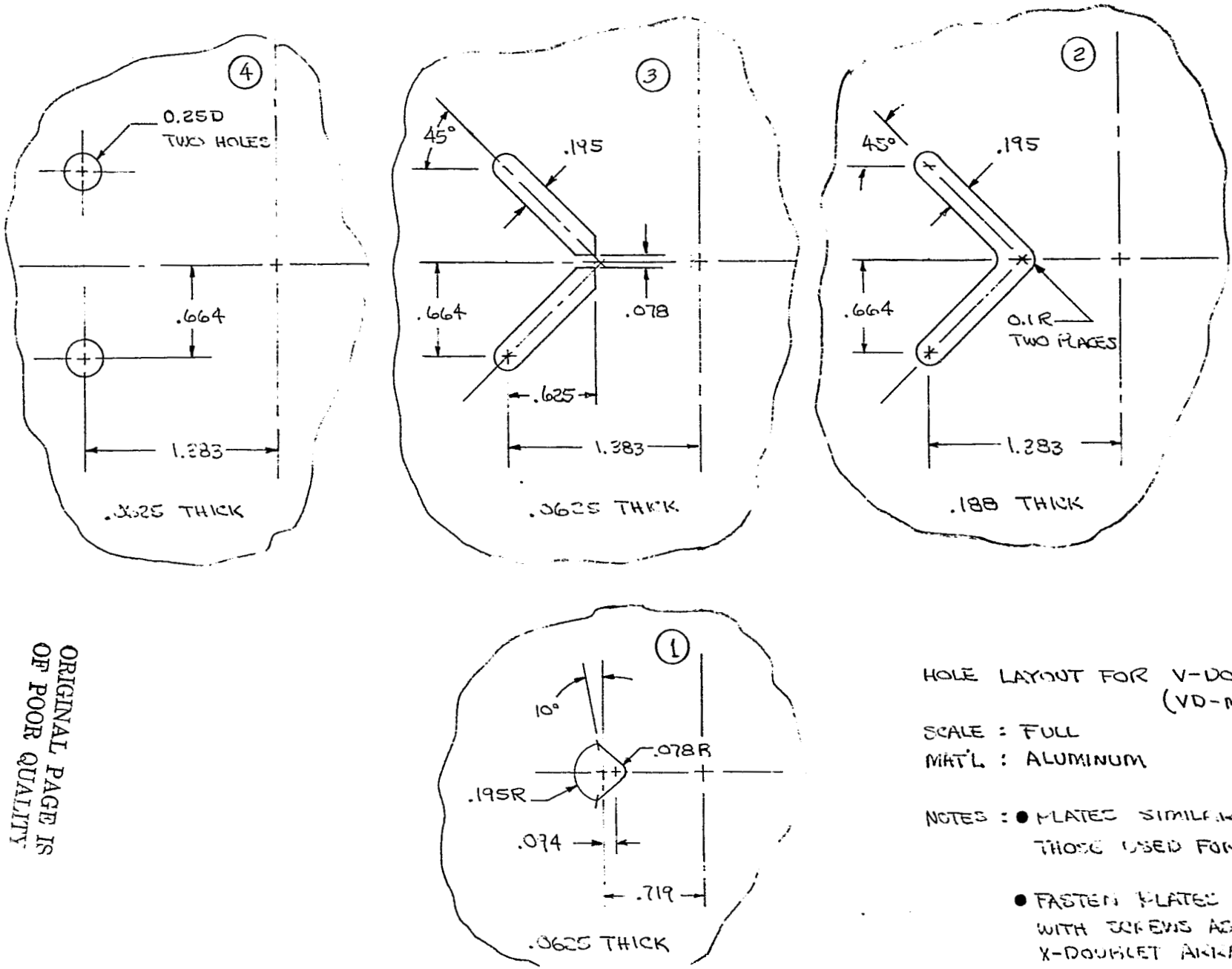

Figure A.2 V-Doublet Model

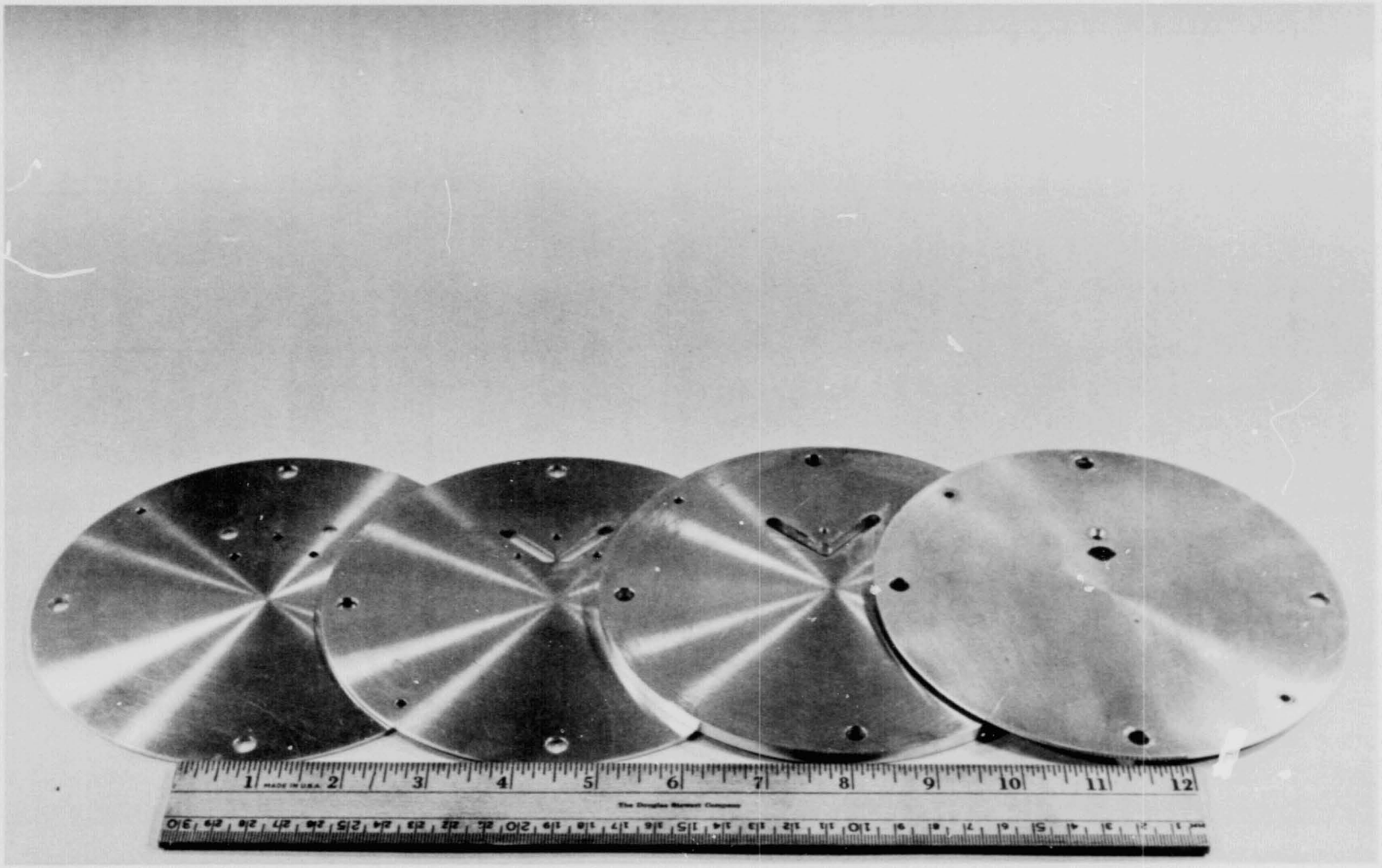

Figure A.3 V-Doublet Assembly

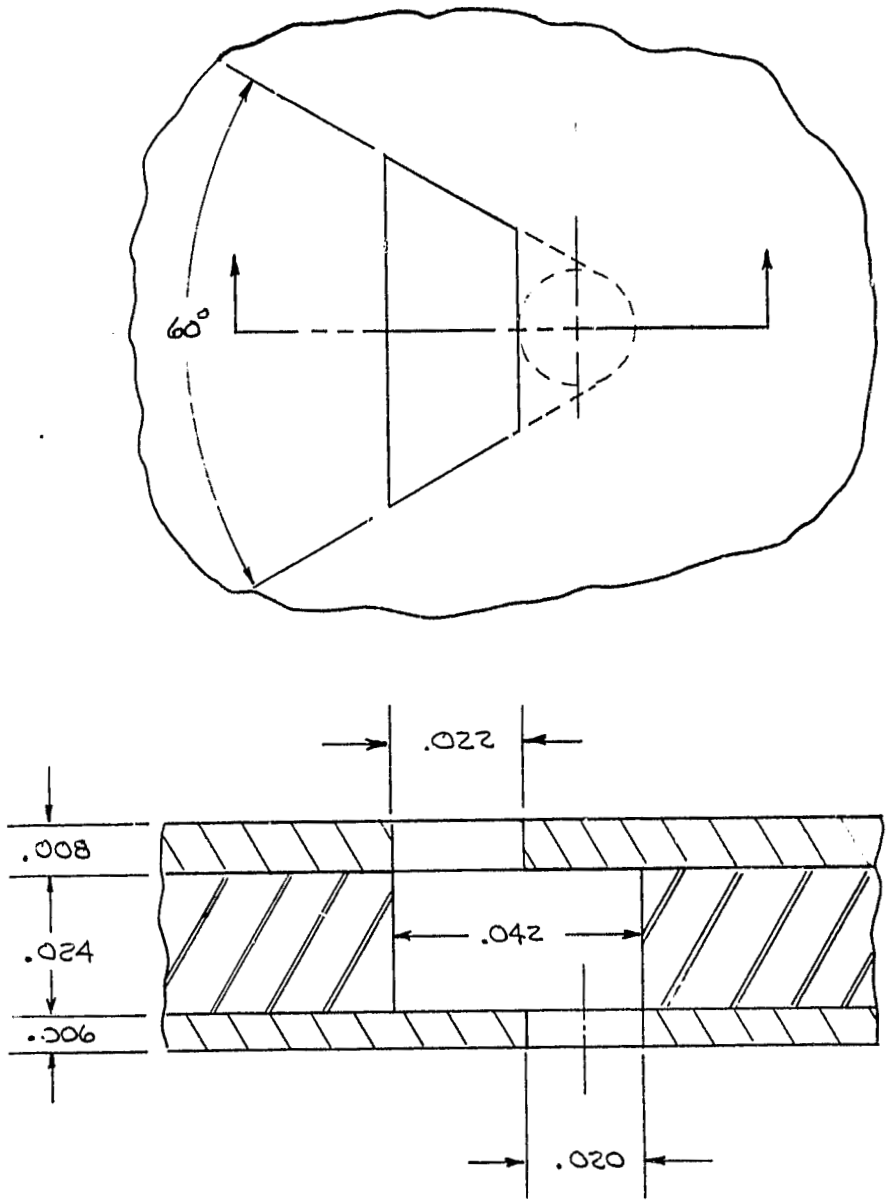

SPLASH - PLATE PROTOTYPE

SCALE : 31¼ - to - 1

Figure A.4 Splash-Plate Prototype

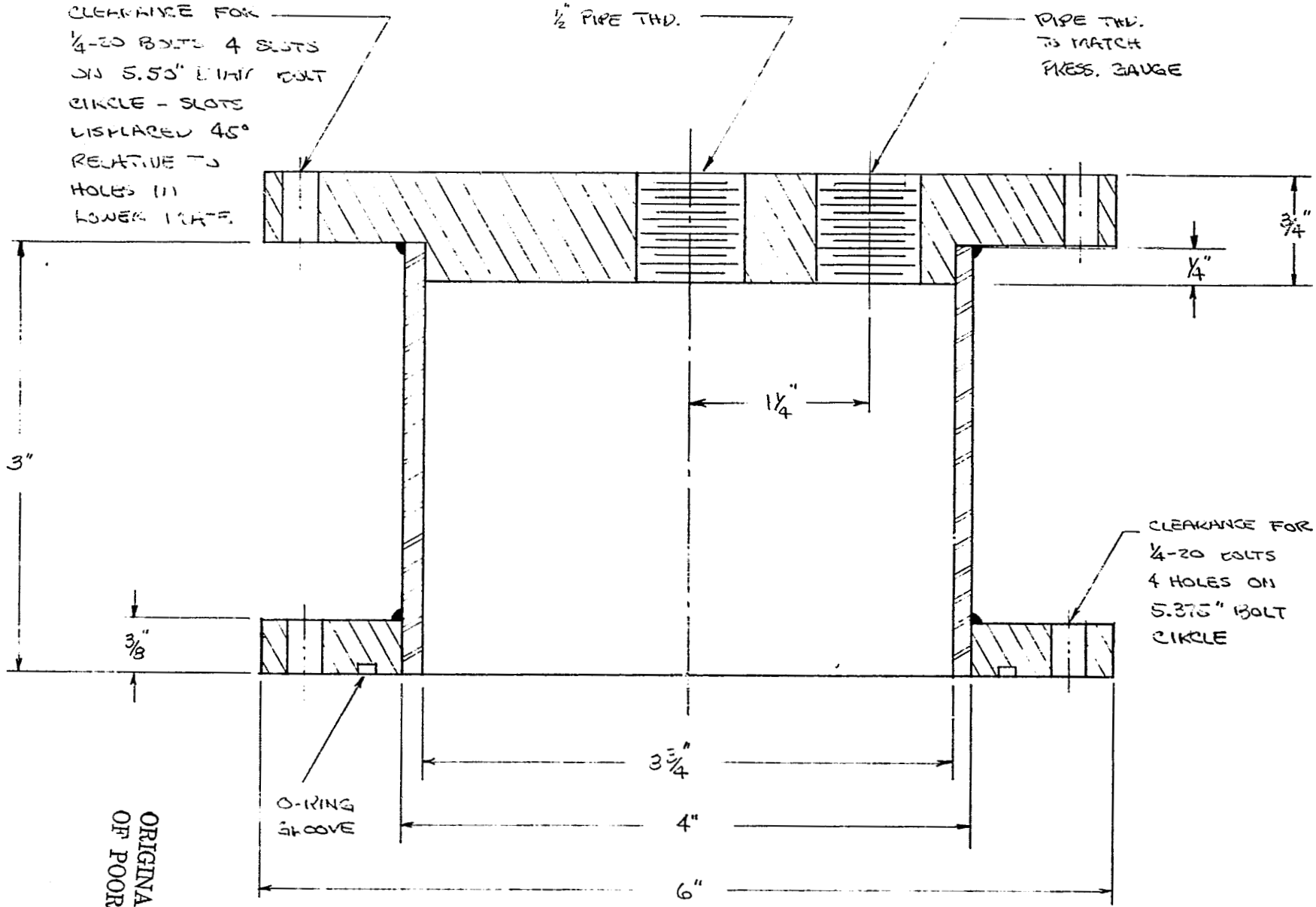

Figure A.5 Plenum Chamber and Injector Model Mounting

SCALE : FULL SIZE

MAT'L : ALUM.

DIMENSIONS NOT CRITICAL ON CYLINDER

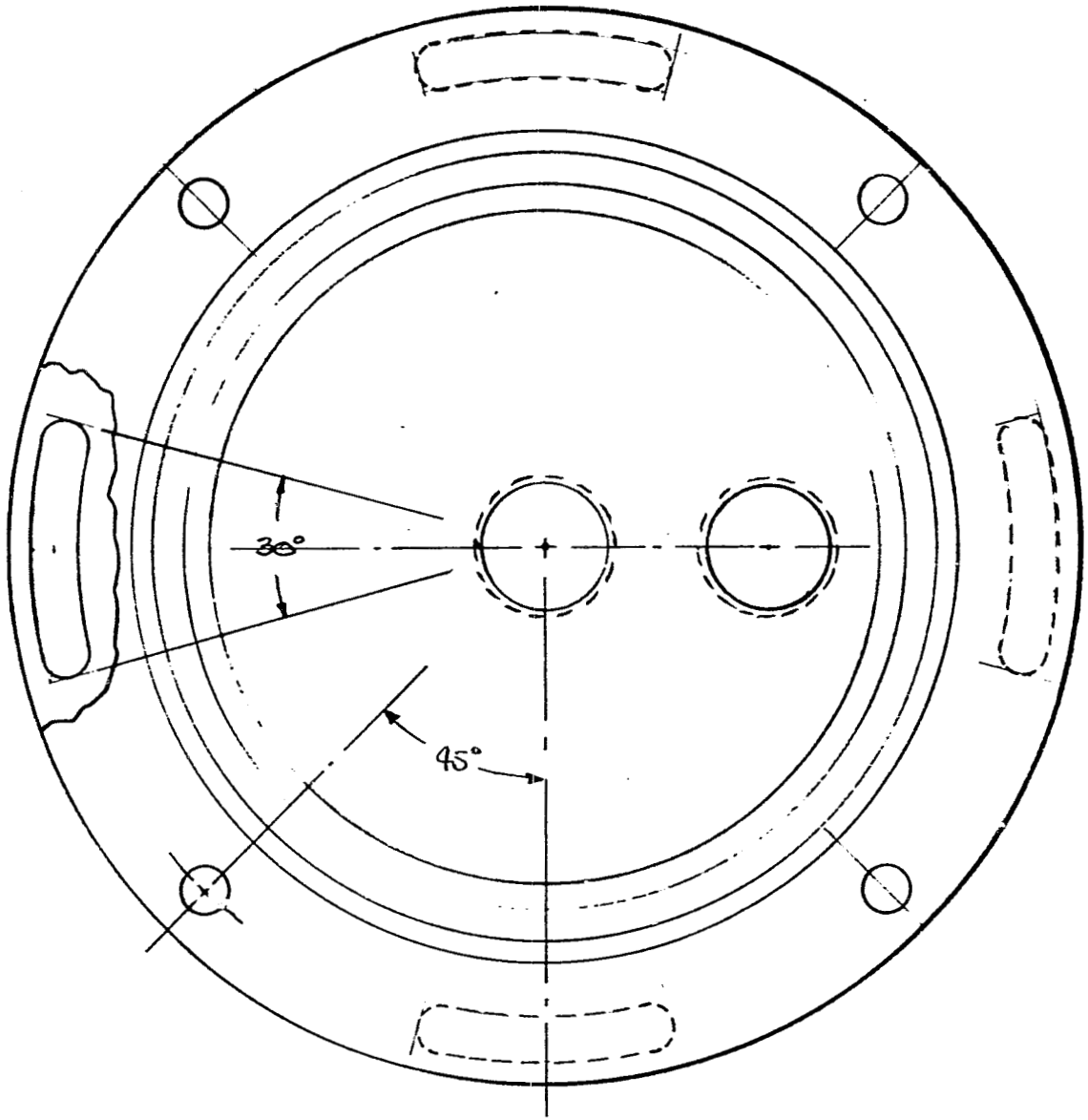

Figure A.5 continued

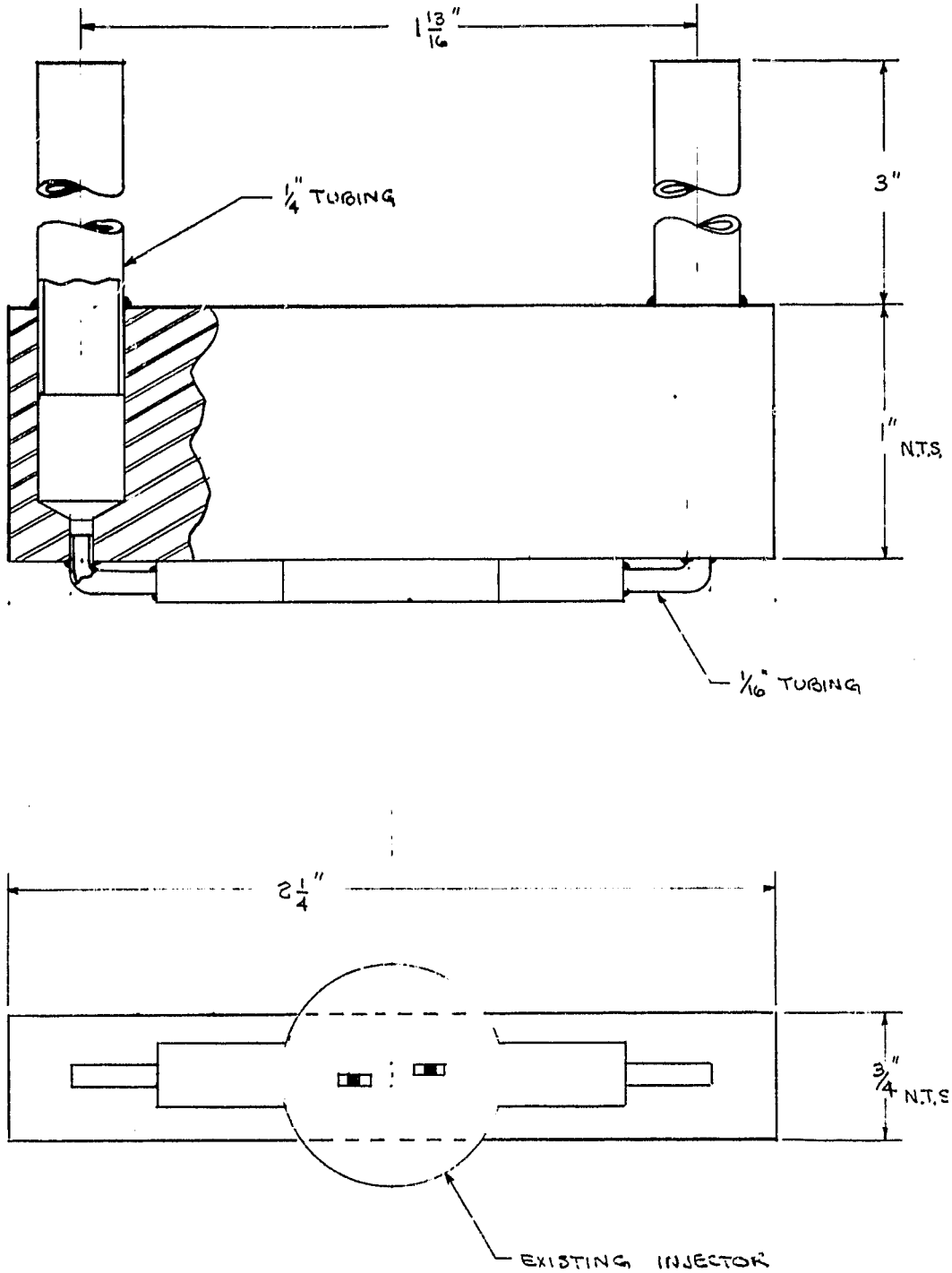

SCALE 2" = 1" MATERIAL: BRASS, ALUM., OR S. STEEL
NO. REQ'D: 4

NOTES:
- SOLDER OR WELD TUBING TO ADAPTER BLOCK AND ADAPTER BLOCK TO INJECTOR - DO NOT OVERHEAT INJECTOR.
- DIMENSIONS NOT CRITICAL

Figure A.6 Mounting for Prototype Injector

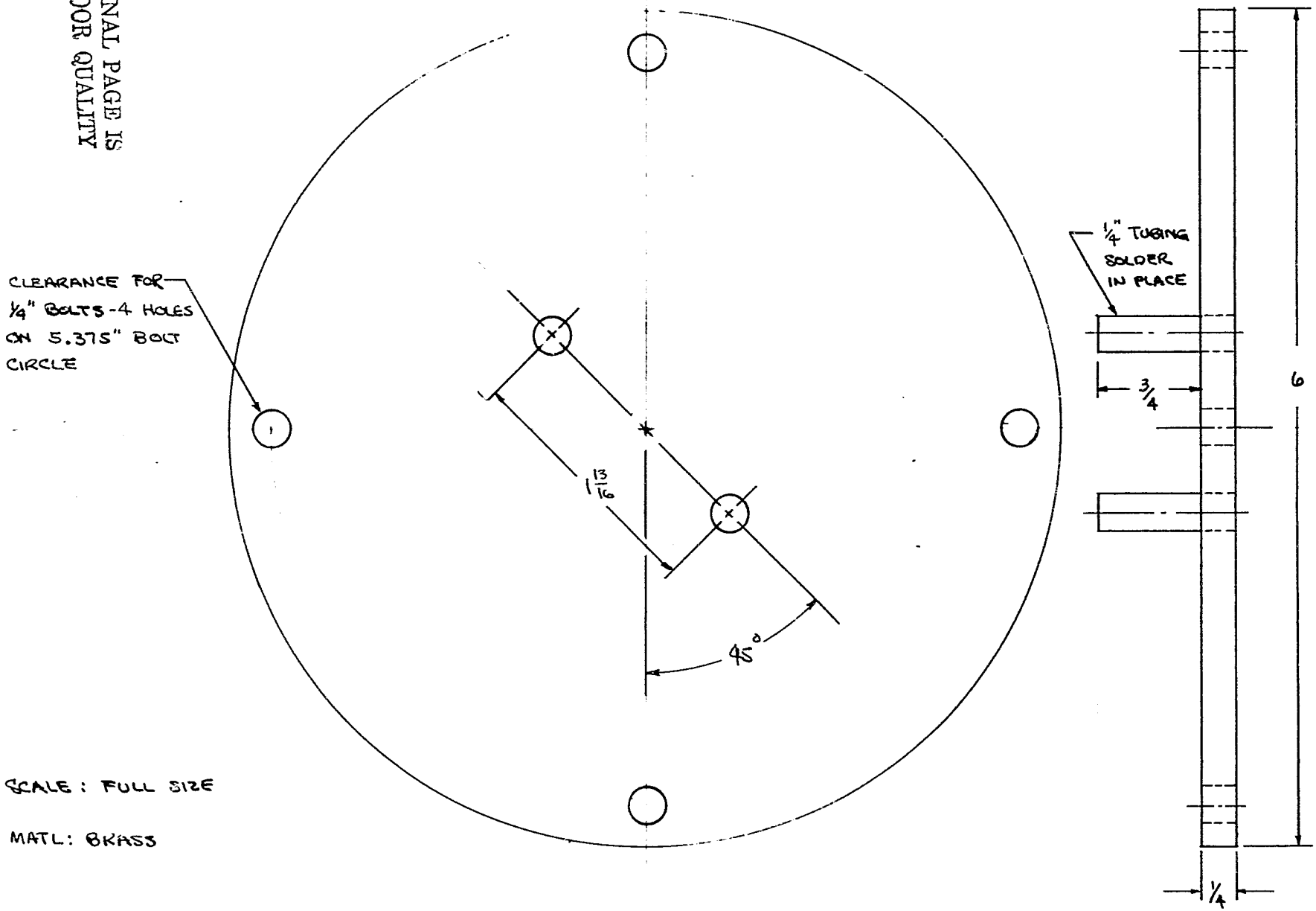

Figure A.7 Plenum Chamber Adapter Plate for Prototype Injectors

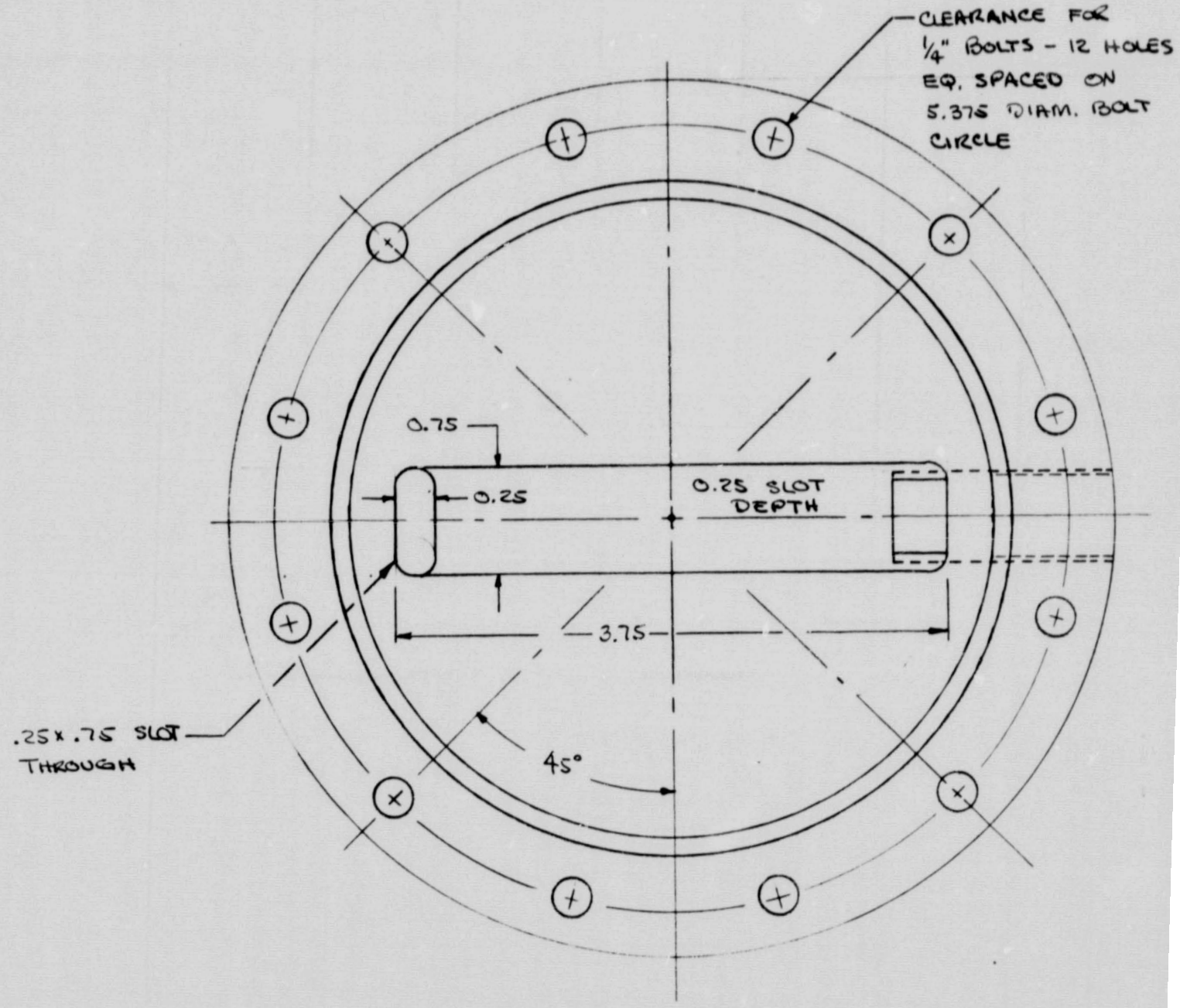

SCALE : FULL SIZE
MAT'L : ALUM.
NO. REQ'D : 1

Figure A.8 Cross-Flow Manifold

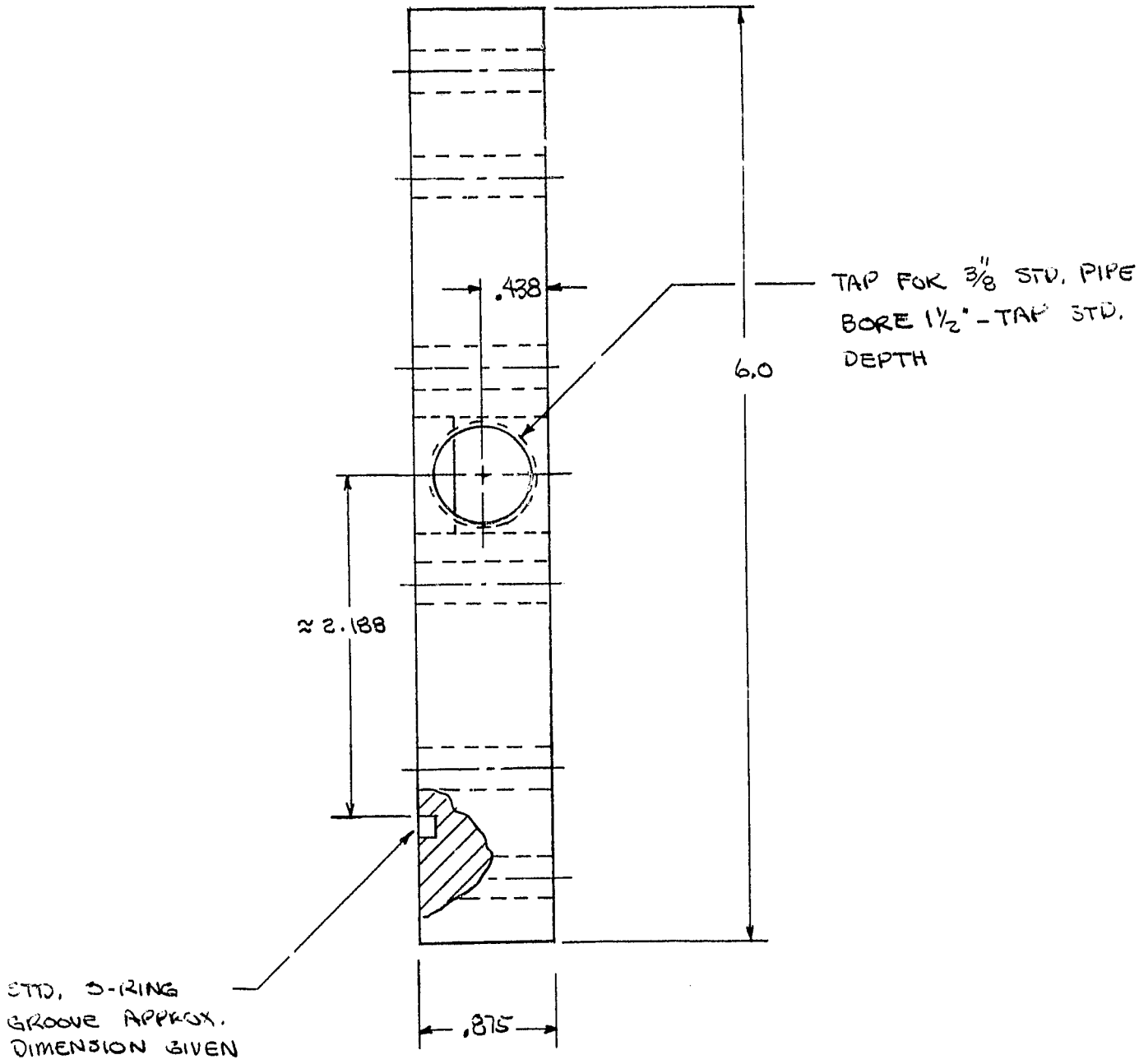

Figure A.8 continued

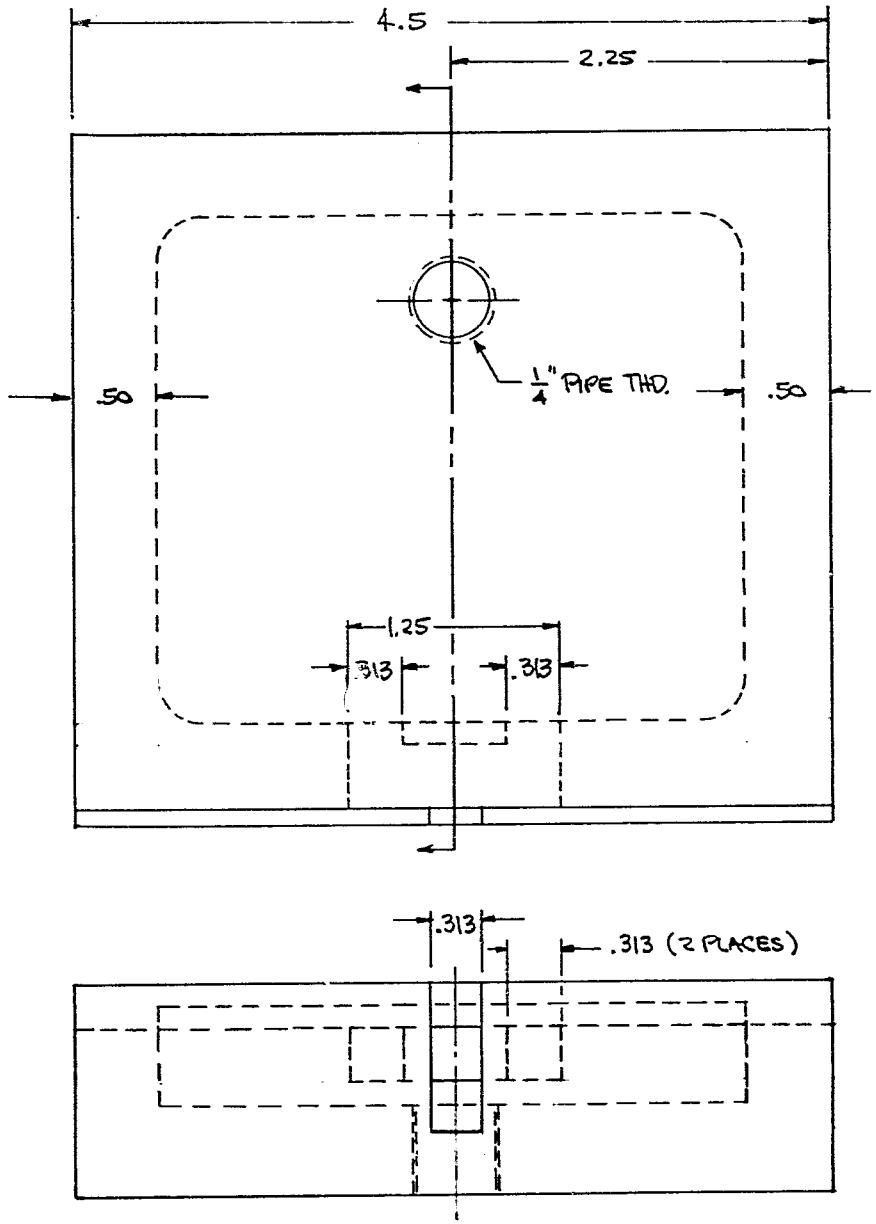

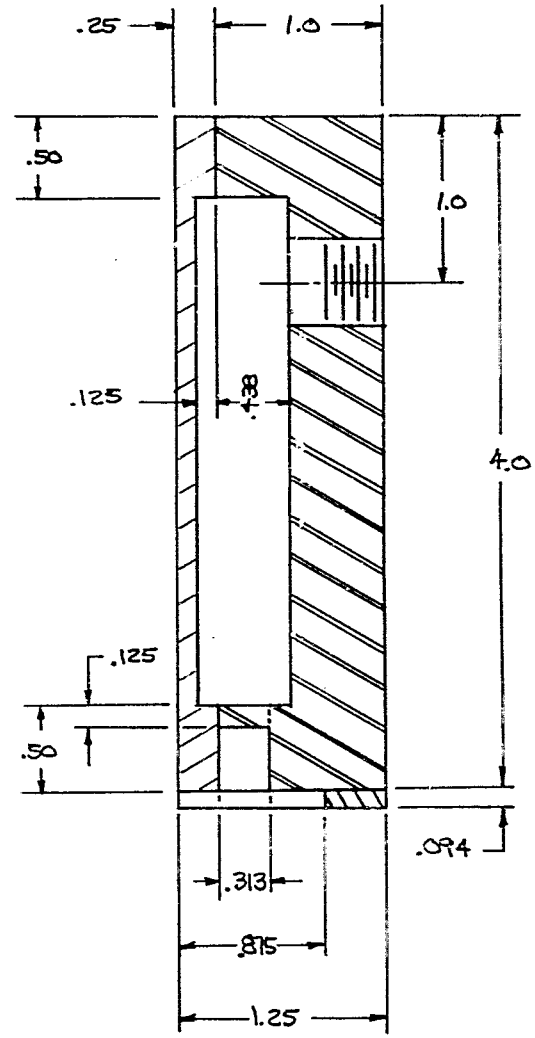

NOTES:

ASSEMBLY CONSISTS OF THREE COMPONENTS WHICH ARE TO BE GLUED TOGETHER.
ASSEMBLY MUST BE TRANSPARENT.

X-DOUBLET : FLOW VISUALIZATION MODEL
SCALE : FULL
MAT'L: CLEAR ACRYLIC PLASTIC
NO. REQ'D : 1

4-7-75

Figure A.9 Internal Flow Visualization Model

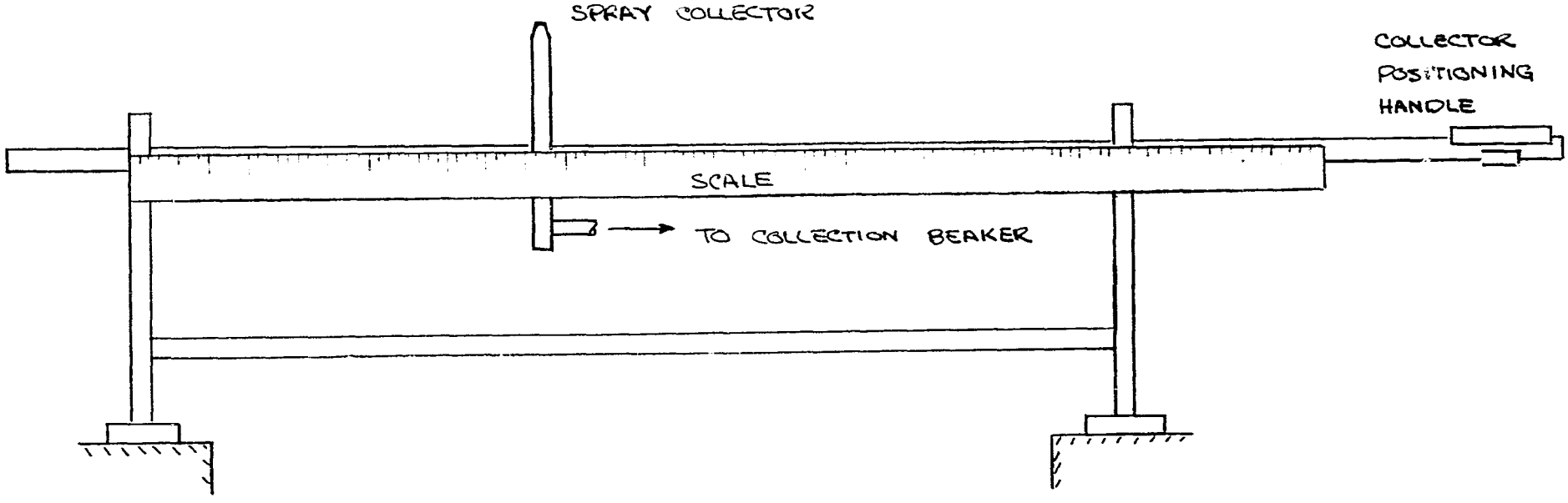

Figure A.10 Spray Collection Apparatus

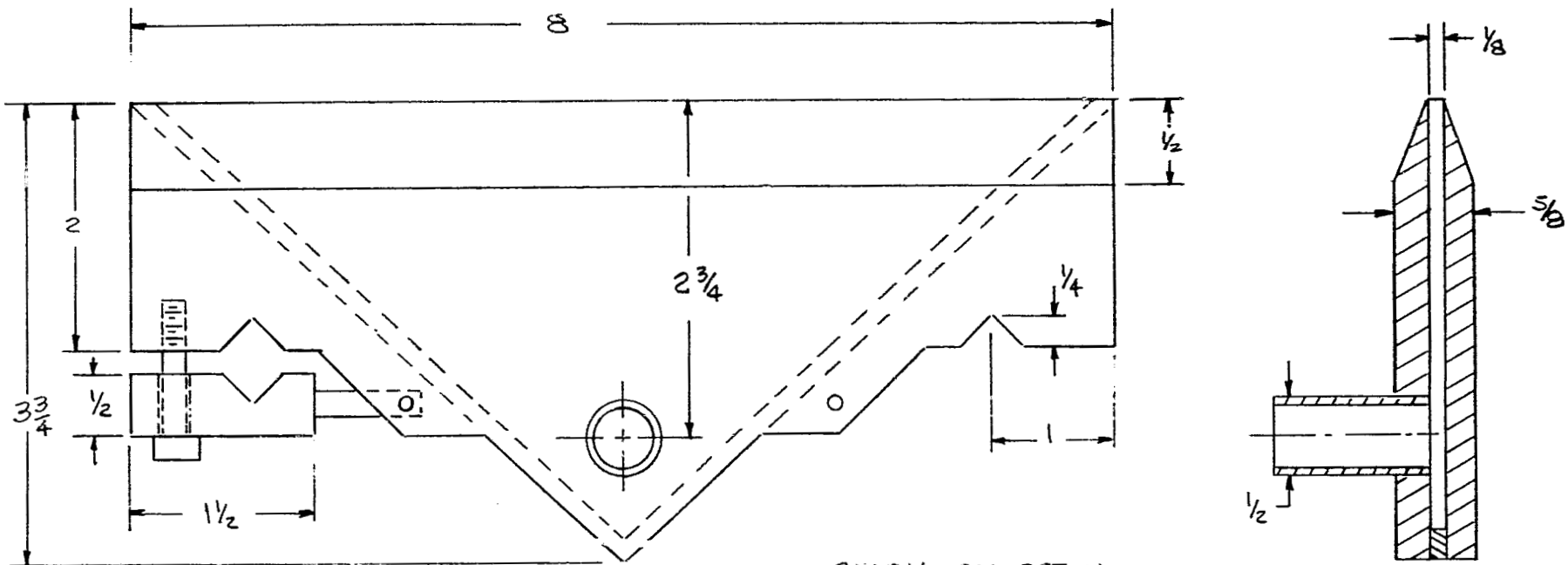

SPRAY COLLECTOR
SCALE: 3/4
MAT'L = ACRYLIC PLASTIC
(ONLY MAJOR DIMENSIONS SHOWN)

Figure A.10 continued

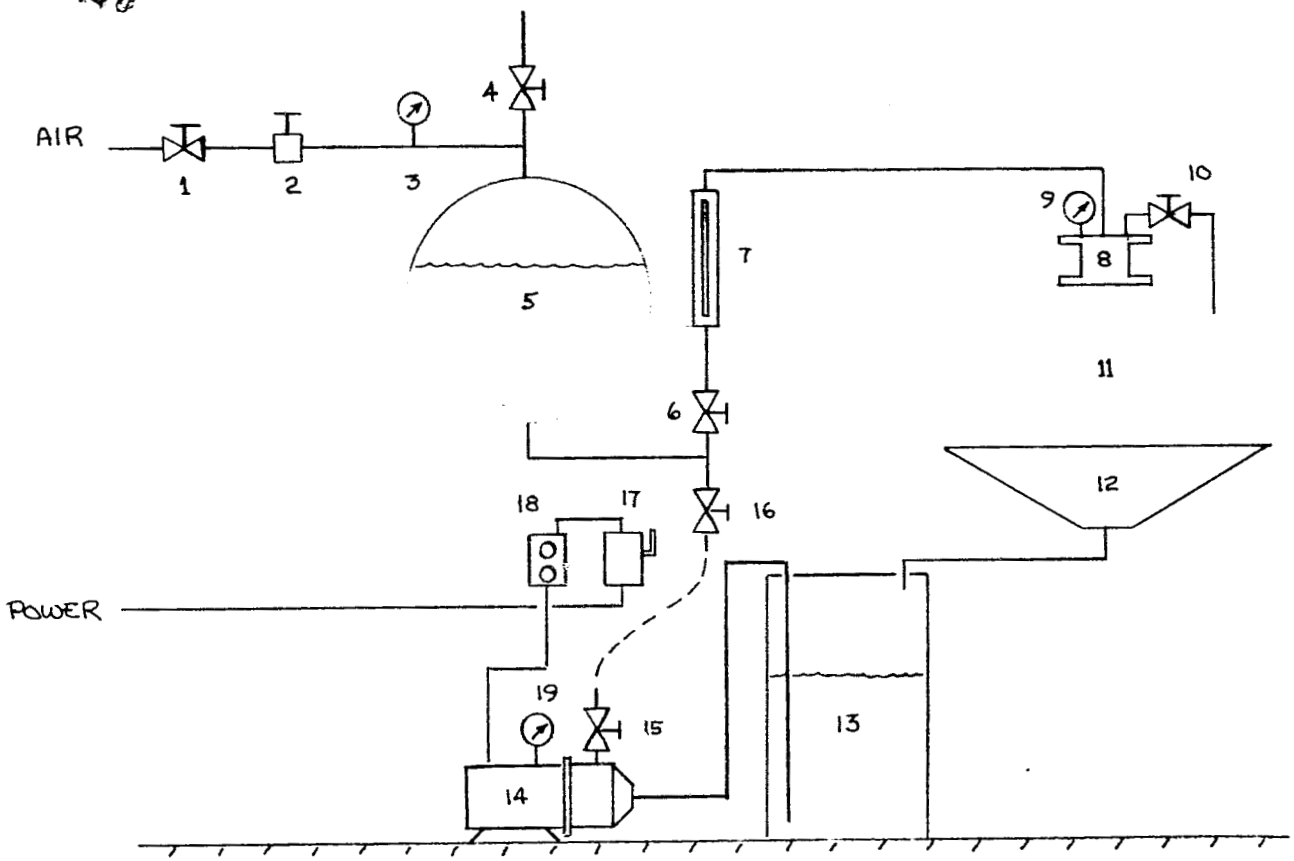

1. AIR SUPPLY VALVE
2. PRESSURE REGULATOR
3. RESERVOIR PRESSURE GAUGE
4. PRESSURE RELIEF VALVE
5. 82-GAL. RESERVOIR
6. FLOW CONTROL VALVE
7. ROTAMETER
8. INJECTOR MOUNT
9. INJECTOR PLENUM PRESSURE GAUGE
10. AIR BLEED VALVE
11. SPRAY FIELD
12. SPRAY COLLECTOR
13. HOLDING TANK
14. PUMP
15. PUMP VALVE
16. DRAIN / RETURN VALVE
17. FUSE BOX & MASTER SWITCH
18. START / STOP SWITCH
19. PUMP PRESSURE VALVE

Figure A.11 Test Facility Schematic

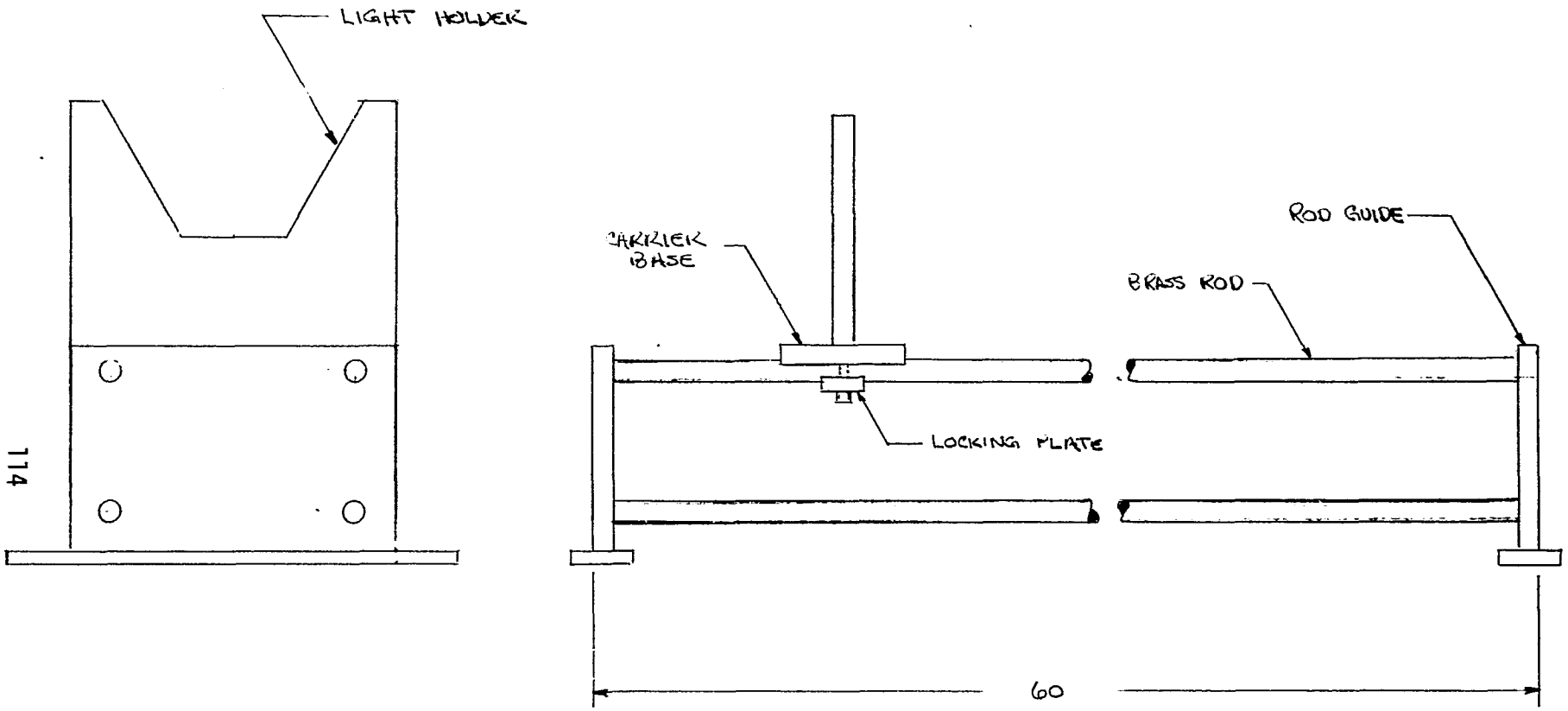

INSTRUMENT CARRIER AND GUIDE ASSEMBLY

SCALE : 1/4

Figure A.12 Instrument Carrier

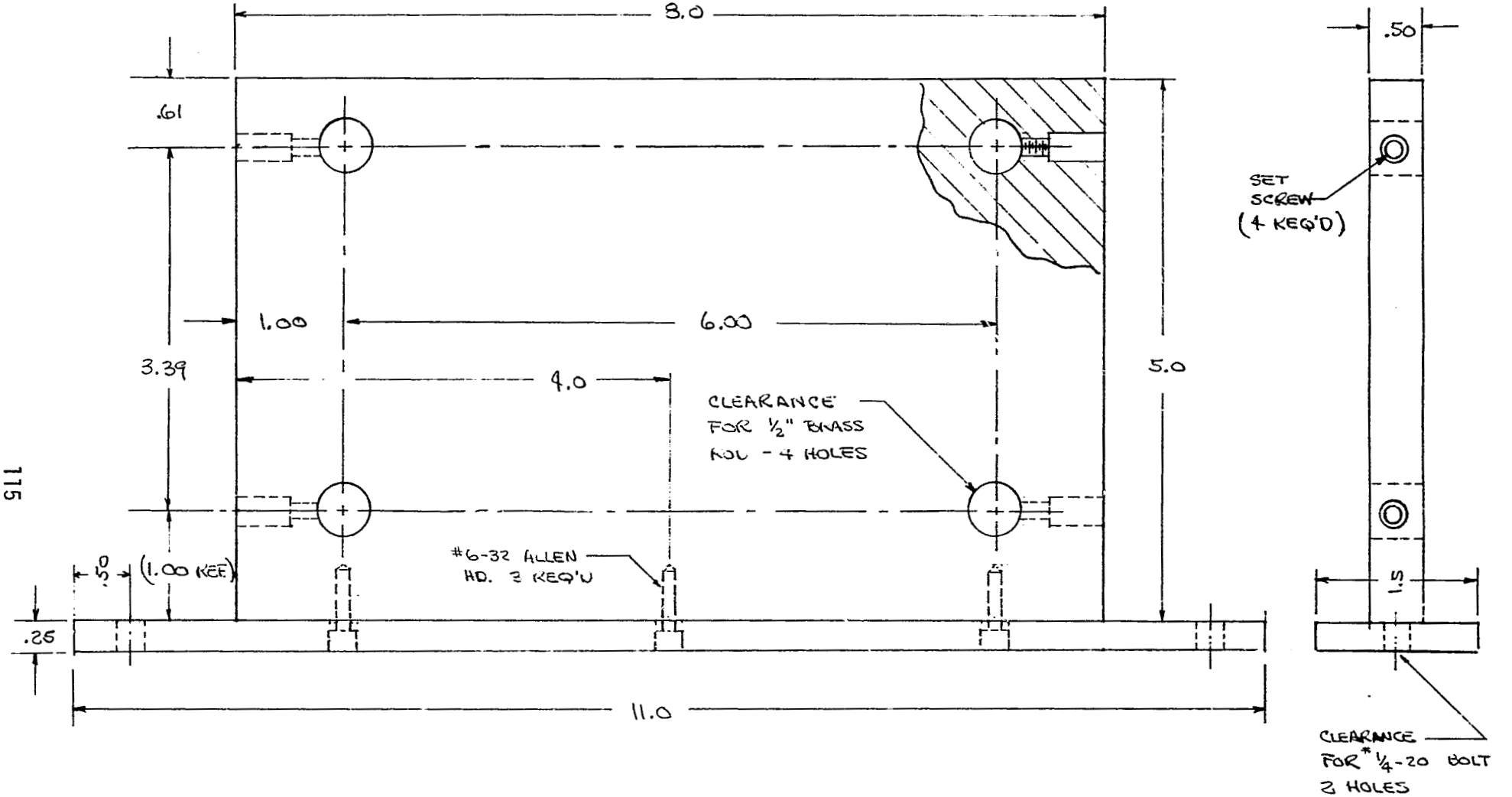

ROD GUIDE
NO. REQ'D : 4
MAT'L : ALUM.
SCALE : 3/4
ALL DIMENSIONS IN INCHES

NOTES : 1. TWO UPPER RODS MUST BE PARALLEL AND AT THE SAME HEIGHT ABOVE THE BASE

2. BREAK ALL SHARP EDGES

ORIGINAL PAGE IS
OF POOR QUALITY

Figure A.12 continued

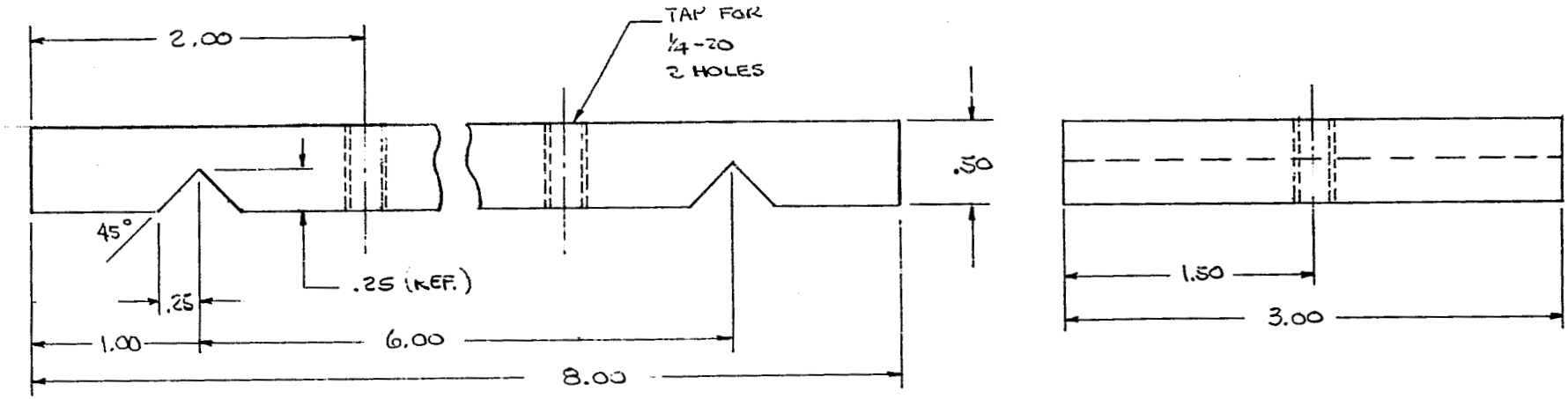

CARRIER BASE

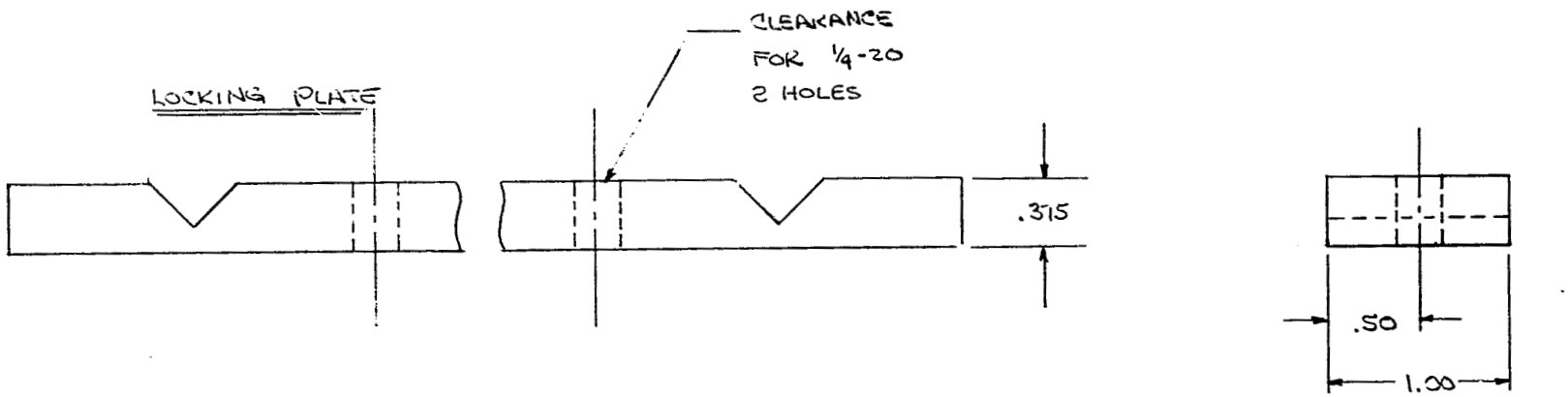

CARRIER

NO. REQ'D : 6

MAT'L : ALUM.

SCALE : FULL

ALL DIMENSIONS IN INCHES

NOTES : (1) CARRIERS MUST SLIDE SMOOTHLY ALONG GUIDES

(2) BREAK ALL SHARP EDGES

(3) UNLESS OTHERWISE SPECIFIED, DIMENSIONS OF LOCKING PLATE ARE SAME AS CARRIER BASE

4) CARRIER BASE TO BE DRILLED AND/OR TAPPED TO ALLOW MOUNTING OF SAMPLE HOLDERS

Figure A.12 continued

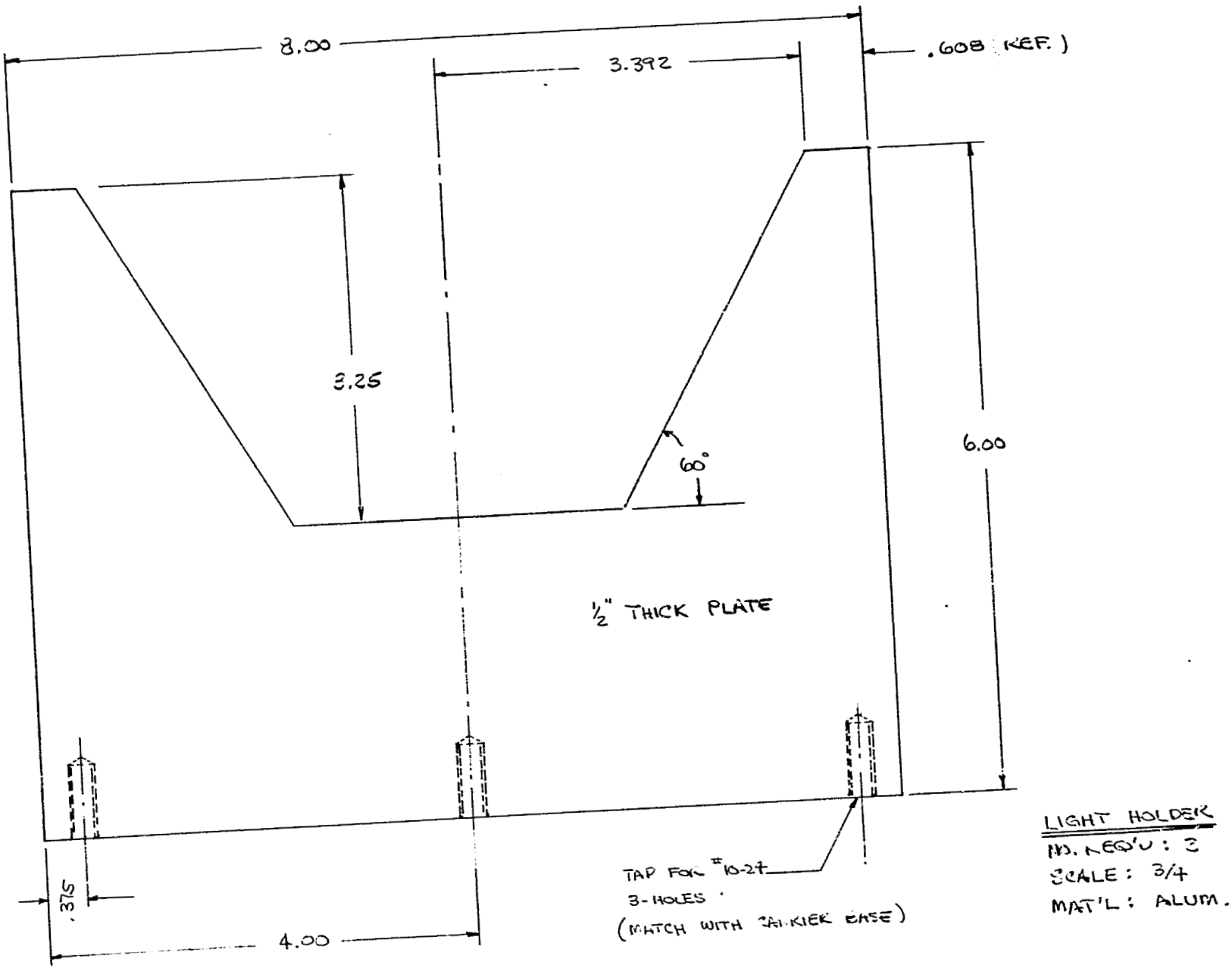

Figure A.12 continued

TABLE A.2

Test Facility - Major Components

Rotameters

Brooks
Instrument Div.
Emerson Electric Co.

Types: 1110-08H2B1A
1110-10H3B1A

Floats: 8RV8 & 8RV31
10RS-138 & 10RV-64

Camera

Grover
Burke & James, Inc.
w/Wollensak 190 mm f/4.5 lens

Plenum Pressure Gauges

Foxboro
Test Gauges
The Foxboro Co.

0-15 psi
0-60 psi

Stroboscope

Strobex
Model 127
Chadwick-Helmuth
Monrovia, Calif.

Pressure Regulator

Foxboro Airdron Regulator
Type 20
The Foxboro Co.

Reservoir

Sears-Roebuck and Co.
Glass Lined Hydro-Pneumatic Pump and Tank
82 gal. capacity
Model No. 153.2951 82

Pump

Sears-Robebuck and Co.
"Hydroglass" Convertible Deep Well Jet Pump
Model No. 390.25130

Table A.2 continued

250 mm scale, rib guide tubes, standard floats

Meter Size	Tube No.	ISA Tube Nomenclature	Float No.	Max. Flow Rate	
				Water (GPM)	Air (SCFM)*
8	R-8M-25-2	BR-½-27G10	8-RV-3	0.55	2.22
	R-8M-25-4	BR-½-35G10	8-RV-3	0.78	3.17
	R-8M-25-2	BR-½-27G10	8-RV-8	0.78	3.22
	R-8M-25-2	BR-½-27G10	8-RS-8	1.00	4.18
	● R-8M-25-4	BR-½-35G10	● 8-RV-8	1.09	4.45
	R-8M-25-2	BR-½-27G10	8-RV-14	1.04	4.28
	R-8M-25-2	BR-½-27G10	8-RS-14	1.32	5.48
	R-8M-25-4	BR-½-35G10	8-RS-8	1.40	5.86
	R-8M-25-4	BR-½-35G10	8-RV-14	1.45	5.88
	R-8M-25-2	BR-½-27G10	8-RV-31**	1.50	6.12
	R-8M-25-4	BR-½-35G10	8-RS-14	1.83	7.56
	R-8M-25-2	BR-½-27G10	8-RS-31**	1.93	7.76
	● R-8M-25-4	BR-½-35G10	● 8-RV-31**	2.06	8.32
	R-8M-25-4	BR-½-35G10	8-RS-31**	2.59	10.66
	R-8M-25-2	BR-½-27G10	8-LJ-48**	3.01	13.01
	R-8M-25-4	BR-½-35G10	8-LJ-48**	4.88	20.32
9	R-9M-25-1	BR-¼-14G10	9-RV-33	1.90	7.96
	R-9M-25-3	BR-¾-20G10	9-RV-33	2.53	10.45
	R-9M-25-1	BR-¼-14G10	9-RS-33	2.52	10.46
	R-9M-25-3	BR-¾-20G10	9-PS-33	3.24	13.45
	R-9M-25-1	BR-¼-14G10	9-RV-87**	3.09	12.66
	R-9M-25-1	BR-¼-14G10	9-RS-87**	4.01	16.84
	R-9M-25-3	BR-¾-20G10	9-RV-87**	3.92	16.25
	R-9M-25-3	BR-¾-20G10	● 9-RS-87**	● 5.12	21.20
	R-9M-25-1	BR-¼-14G10	9-LJ-160**	6.88	30.45
	R-9M-25-3	BR-¾-20G10	9-LJ-160**	9.65	44.18
10	● R-10M-25-1	BR-1-25G10	● 10-RV-64	4.54	18.05
	R-10M-25-1	BR-1-25G10	● 10-RS-64	5.64	23.65
	R-10M-25-3	BR-1-35G10	10-RV-64	6.28	25.76
	R-10M-25-1	BR-1-25G10	10-PV-139**	6.42	25.60
	R-10M-25-3	BR-1-35G10	10-RS-64	7.84	32.15
	● R-10M-25-1	BR-1-25G10	● 10-RS-138**	8.02	34.60
	R-10M-25-3	BR-1-35G10	10-RV-138**	8.84	36.10
	R-10M-25-3	BR-1-35G10	10-PS-138**	10.93	45.90
	R-10M-25-1	BR-1-25G10	10-LJ-238**	14.91	66.00
	R-10M-25-3	BR-1-35G10	10-LJ-238**	23.10	105.70
12	R-12M-25-4	BR-1½-17G10	12-RV-221	9.33	37.81
	R-12M-25-4	BR-1½-17G10	12-RV-343**	11.71	47.12
	R-12M-25-4	BR-1½-17G10	12-RS-221	12.46	50.65
	R-12M-25-4	BR-1½-17G10	12-RS-343**	15.43	62.75
	R-12M-25-5	BR-1½-35G10	12-RV-221	17.21	70.60
	R-12M-25-5	BR-1½-35G10	12-RV-343**	20.95	86.45
	R-12M-25-5	BR-1½-35G10	12-RS-221	22.40	91.85
	R-12M-25-5	BR-1½-35G10	12-RS-343**	26.90	112.00
	R-12M-25-4	BR-1½-17G10	12-LJ-740**	36.00	123.30
	R-12M-25-5	BR-1½-35G10	12-LJ-740**	67.40	293.50
13	R-13M-25-1	BR-2-18G10	13-RV-510	19.94	81.55
	R-13M-25-1	BR-2-18G10	13-RV-760	23.79	96.00
	R-13M-25-1	BR-2-18G10	13-RS-510	26.99	106.90
	R-13M-25-3	BR-2-30G10	13-RV-510	31.78	130.90
	R-13M-25-1	BR-2-18G10	13-RS-760**	31.85	131.00
	R-13M-25-3	BR-2-30G10	13-RV-760**	37.60	155.00
	R-13M-25-3	BR-2-30G10	13-RS-510	42.50	176.60
	R-13M-25-3	BR-2-30G10	13-RS-760**	49.55	227.70
	R-13M-25-1	BR-2-18G10	13-LJ-1594**	54.90	----
	R-13M-25-3	BR-2-30G10	13-LJ-1594**	99.40	----

* All air flows are at 14.7 psia and 70° F

** These floats are not recommended for gas service unless operating pressure downstream exceeds 30 psi

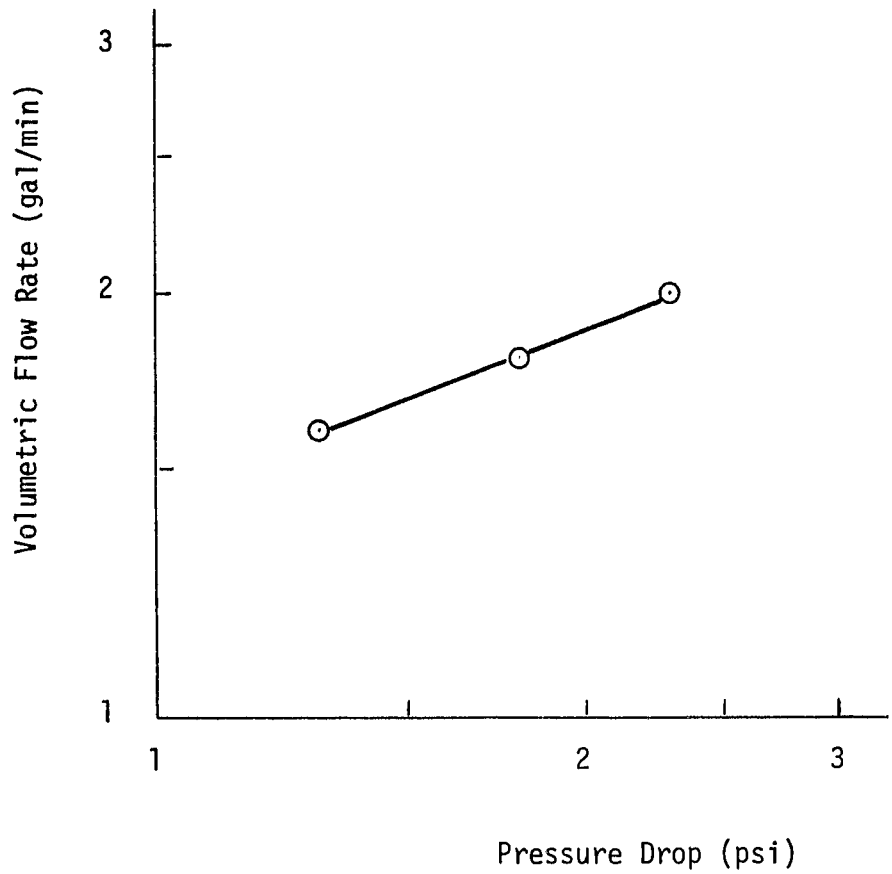

Figure A.13 Volumetric Flow Rate Versus Pressure Drop for V-Doublet Model (S.G. = 1.09)

APPENDIX B

FLUID PROPERTIES

Table B.1

Fluid Properties

Fluid	T (°F)	ρ (lbm/ft^3)	$\mu \times 10^4$ (lbm/ft-sec)	$\nu \times 10^5$ (ft^2/sec)	$\sigma \times 10^3$ (lb/ft)
MMH	70	54.2	5.4	1.00	2.30
MMH	200	50.6	2.3	0.45	1.85
N_2O_4	70	90.0	2.8	0.25	1.87
H_2O	70	62.4	7.1	1.14	5.00
24% Gly-H_2O*	70	66.1	14.4	2.18	4.96
34% Gly-H_2O	70	67.7	20.7	3.06	4.90

* 24% Glycerol on volume basis.

APPENDIX C

PHOTOGRAPHIC TECHNIQUES

Analysis of Shadowgraph Optics*

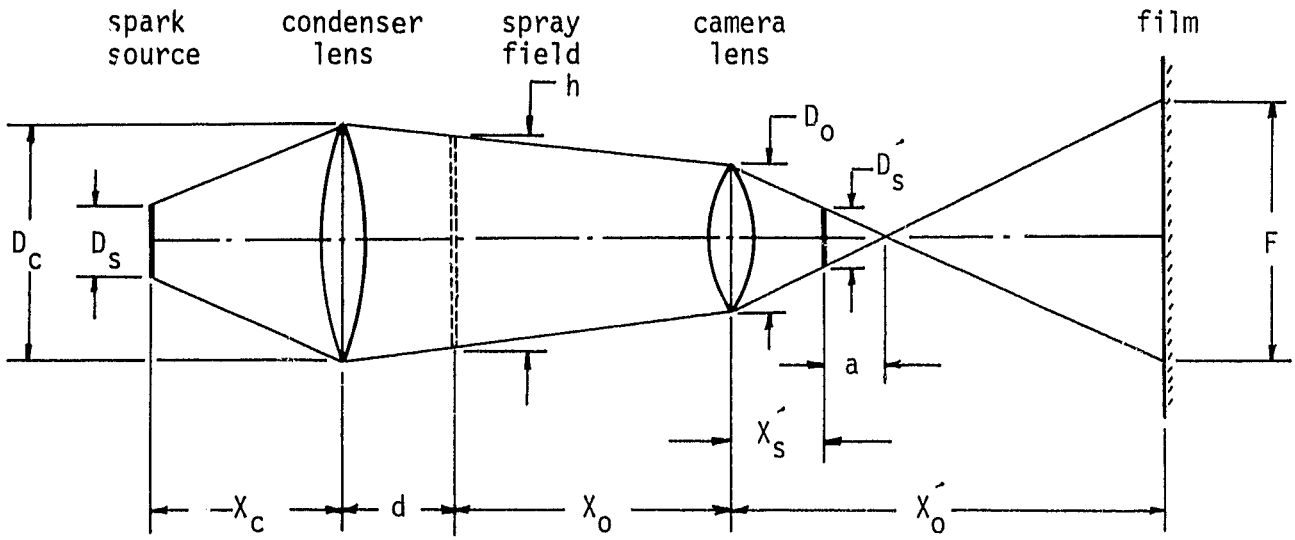

Image of Source Formed by Condenser Lens.

$$\frac{1}{X_c} + \frac{1}{X_c'} = \frac{1}{f_c}$$

$$X_c' = \frac{X_c f_c}{X_c - f_c} \tag{1}$$

Image size is given by $\left(\frac{X_c'}{X_c}\right) D_s$. This image lies to the right of the camera lens a distance X_s where

$$X_s = X_c' - (d + X_o). \tag{2}$$

---

* Ref. 2

This image forms a virtual image for the camera lens which then forms a real image at X_s' where

$$\frac{1}{-X_s} + \frac{1}{X_s'} = \frac{1}{f_o} \quad ,$$

$$X_s' = \frac{X_s f_o}{X_s + f_o} \tag{3}$$

The image size is given by

$$D_s' = \left(\frac{X_s'}{X_s} \right) \left(\frac{X_c'}{X_c} \right) D_s . \tag{4}$$

Image of the Spray Field.

$$\frac{1}{X_o} + \frac{1}{X_o'} = \frac{1}{f_o}$$

$$\frac{1}{x_o} + \frac{1}{mX_o} = \frac{1}{f_o} \qquad m \equiv \frac{X_o'}{X_o} = \text{magnification} = \frac{F}{h}$$

$$X_o = \left(\frac{m+1}{m} \right) f_o \tag{5}$$

$$X_o' = mX_o = (m+1)\, f_o \tag{6}$$

Condenser Lens.

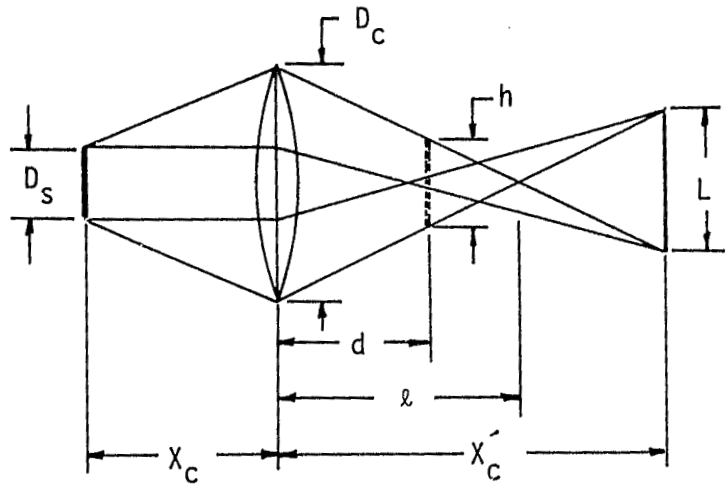

$$\frac{h}{\ell - d} = \frac{L}{X_c' - \ell} = \frac{D_c}{\ell} \quad , \quad L = D_s \left(\frac{X_c'}{X_c} \right)$$

$$h(X_c' - \ell) = L(\ell - d)$$

$$\ell(L + h) = X_c' h + Ld$$

$$\ell = \frac{X_c' h + Ld}{L + h} \tag{7}$$

$$L\ell = D_c(X_c' - \ell)$$

$$\ell(L + D_c) = X_c' D_c$$

$$\ell = \frac{X_c' D_c}{L + D_c} \tag{8}$$

Elimination of ℓ between (7) and (8) and substitution for L provides

$$D_c = \frac{X_c'}{X_c' - d}\left[h + d\,\frac{D_s}{X_c}\right] . \tag{9}$$

Camera Lens

$$\frac{D_s'}{a} = \frac{D_o}{X_s' + a} = \frac{F}{X_o' - (a + X_s')} .$$

Elimination of "a" provides

$$D_o = \frac{D_s' X_o' + X_s' F}{X_o' - X_s'} \tag{10}$$

Equations (1) through (10) are valid so long as $X_c' \geq d + X_o$. The quantities D_s, f_c, f_o, D_c, and D_o are constants in the apparatus used for the experiments described in this report. In addition, X_o' is limited by the bellows extension of the camera and F is limited by the film size, while d and X_o have minimum useful values due to spray impingment.

Equipment and Important Parameters

Spark-Shadowgraph System

1. Spark source

   Spark discharge of approximately 1.0 μ-sec. duration obtained by simultaneous discharge of five 0.05 μf capacitors across an ionized air gap. The spark source was borrowed from the laboratory of the Department of Aerospace Engineering of the University of Texas at Austin. Construction details are contained in Colthorp's thesis:

   J.R. Colthorp, "The Design and Analysis of a Single Station Free-Flight Ballistics Range," M.S. Thesis, The University of Texas at Austin, August 1963.

2. Camera

   Grover View Camera

   190 mm f/4.5 Wollensak Alphax lens

   Setting: f/4.5 for prototypes, spark discharge determines exposure time.

3. Condenser lens

   Compound lens

   2 3/4 in. diameter

   12 in. effective focal length

4. Film

   Kodak Tri-X sheet film (4" x 5"), ASA 320

processing:

Full strength Kodak Mierodol for 25 min at 70°F

No stop bath - water rinse

Kodak fixer for 2-3 min.

Wash

printing:

3 sec. - regular

3 sec. - burning in hot spot if necessary

Polycontrast F paper with 2 1/2 or #4 filter

Developed in GAF Vividol for 1 1/2-2 min.

Stop bath - acetic acid

Standard fixer for 2-3 min.

Wash

Ferrotype Gloss

5. Dimensions

$X_c = 13"$, $d = 9"$, $X_o = 15" = X_o'$

General Arrangement

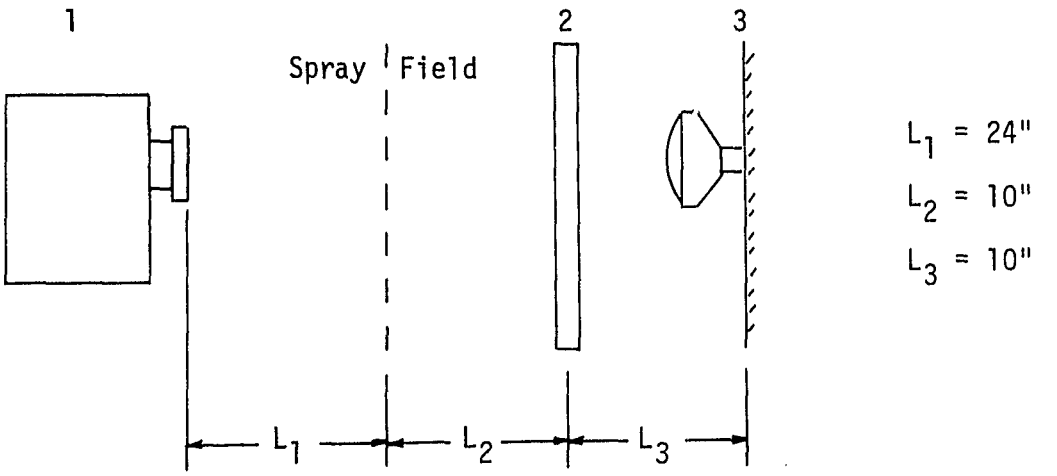

1. Fastex Camera

   Type WF3T w/13mm f/1.8 Wollensak lens

   #7278 Kodak Tri-X Reversal Film (ASA 160)

   1400 ft.-candles illumination at camera

   Operated with f/8 at 130 v.

   3500 frames/sec. average; 4000 frames/sec. for last 30 ft. of 100 ft. film roll.

2. Translucent acrylic plastic sheets. Three 1/4-inch thick sandblasted sheets plus one sheet of acetate film sandwiched between 1/4-inch plastic sheets.

3. Ten, 500 w photoflood lamps. See accompanying photograph.

Table C.1

High Speed Movie Records*

Movie No.	Injector	Specific Gravity	Flow Rate (gal/min)	Pressure Drop (psi)	Frames/sec (avg. - max.)
5	XD-M1	1.085	0.6	1.25	3500 - 4000
6	"	1.085	1.0	3.60	"
7	"	1.085	1.4	7.20	"
8	"	1.059	1.0	3.60	"

* Movies supplied to NASA representatives.

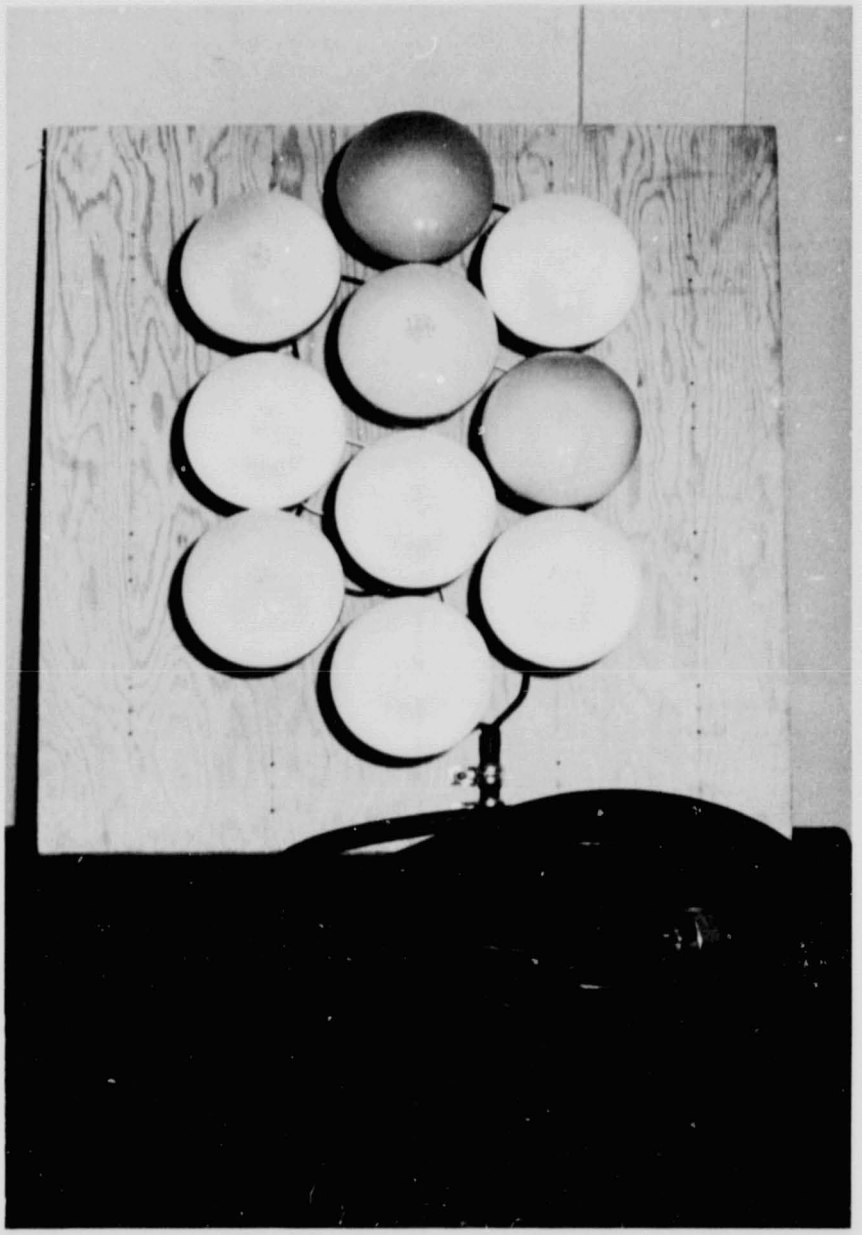

Figure C.1 Photoflood Arrangement for High Speed Movies

Stroboscopic Back-Lighting

General Arrangement

Generally same as for high speed movies, but with the following changes:

1. Camera

   Grover View Camera

   190 mm f/4.5 Wollensak Alphax lens

   Setting: f/8, stroboscopic discharge determines exposure time.

2. Stroboscope (replaces photofloods)

   Strobex — flash duration 50 μ-sec.

   Model 127 — 2400 ft.candles, 1 ft. from source

   Chadwick-Helmuth

   Monrovia, Calif.

3. Translucent plastic sheets

   Only two sandblasted sheets used.

4. Dimensions

   $L_1 = 30"$, $L_2 = 10"$, $L_3 = 21"$

5. Film

   Same as for spark-shadowgraph.

APPENDIX D

TABULATION OF DATA

RECORD OF PHOTOGRAPHS

Negative No.	Date	Injector	Flow Rate (gal/min)	Pressure Drop (psi)	Comments
1	11-13-74	XD-P	-	10	Water flow. Fuel side. Face View. Shadowgraph.
2	"	"	-	20	
3	"	"	-	30	
4	"	"	-	40	
5	"	"	-	50	
6	11-18-74	XD-P	-	10	
7	"	"	-	20	
8	"	"	-	30	
9	"	"	-	40	
10	"	"	-	50	
11	"	"	-	5	
12	"	"	-	30	11 shots superimposed.
13	"	"	-	30	5 shots superimposed.
14	"	-	-	-	Calibration for photos. 1 through 15.
15	"	-	-	-	"
16	12-2-74	XD-P	-	-	Calibration for photos. 16 through 25.
17	"	"	-	5	Side view. Alignment problem.

RECORD OF PHOTOGRAPHS contd.

18	"	"	-	10	
19	"	"	-	20	
20	"	"	-	30	
21	"	"	-	40	
22	"	"	-	50	
23	"	"	-	30	
24	"	"	-	20	
25	"	"	-	40	
26	12-10-74	XD-P	-	5	Side view. Operating correctly.
27	"	"	-	10	
28	"	"	-	20	
29	"	"	-	30	
30	"	"	-	40	
31	"	"	-	50	
32	"	"	-	30	
33	"	"	-	20	
34	"	"	-	-	Calibration for photos. 26 through 35.
35	"	"	-	-	"

RECORD OF PHOTOGRAPHS contd.

36	12-16-74	SP-P	-	20	Water Flow. Fuel side Face view. Shadowgraph.
37	"	"	-	30	
38	"	"	-	30	
39	"	"	-	40	
40	"	"	-	-	Calibration for photos. 36 through 40.
41	"	"	-	20	Side view.
42	"	"	-	30	
43	"	"	-	30	
44	"	"	-	40	
45	"	"	-	-	Calibration for photos. 41 through 45.
46A	2-11-75	XD-M1	0.20	0.20	Gly.-Water. SG. = 1.085. Face view. Back-lighted. Assembly 1-2-3, standard model.
47A	"	"	0.40	0.65	
48A	"	"	0.60	1.30	
49A	"	"	0.80	2.30	
49S	"	"	-	-	Calibration for photos. 46A through 49S.
46B	2-17-75	XD-M1	-	-	Calibration for photos. 46B through 52A.
46C	"	"	0.20	-	
47B	"	"	0.40	-	
48B	"	"	0.60	-	

RECORD OF PHOTOGRAPHS contd.

49B	"	"	0.80	-	
50A	"	"	1.00	-	
50B	"	"	1.00	-	
51A	"	"	1.20	-	
51B	"	"	1.20	-	
52A	"	"	1.40	-	
52B	2-19-75	XD-M1	-	-	Calibration for photos. 52B through 53D.
52C	"	"	1.40	-	
53A	"	"	0.80	-	
53B	"	"	1.60	-	
53C	"	"	1.60	-	
53D	"	"	1.60	-	
54	3-12-75	XD-M2	0.80	2.35	Modified XD. Assembly 1-2A-3. Spreading angle/2 in side view 20° ± 3°, photos. 54 through 57.
55A	"	"	1.00	3.75	
55B	"	"	1.00	3.75	
56	"	"	1.20	5.50	
57	"	"	1.40	7.50	
58A	"	XD-M3	0.80	1.95	Modified XD. Assembly 1-2B-3. Spreading angle/2 in side view 10° ± 4°, photos. 58A through 61.

RECORD OF PHOTOGRAPHS contd.

58B	"	"	0.80	1.95	
58C	"	"	0.80	1.95	
59	"	"	1.00	3.10	
60	"	"	1.20	4.50	
61	"	"	1.40	6.25	
62	"	XD-M4	0.80	2.05	Modified XD. Assembly 1-2-3A. Spreading angle/2 in side view 14° ± 3°, photos. 62 through 65.
63	"	"	1.00	3.45	
64	"	"	1.20	4.95	
65	"	"	1.40	6.75	
66	"	XD-M5	0.80	1.45	Modified XD. Assembly 1-2. Spreading angle/2 in side view 0° ± 1°, photos. 66 through 69.
67	"	"	1.00	2.35	
68	"	"	1.20	3.45	
69	"	"	1.40	4.70	
70A	"	-	-	-	Calibration for photos. 54 through 70B.
70B	"	-	-	-	"
71	3-24-75	-	-	-	Calibration for photos. 71 through 75B.
72	"	XD-M3	0.80	1.95	Modified XD. Assembly 1-2B-3.
73	"	"	1.00	3.20	
74	"	"	1.20	4.50	

RECORD OF PHOTOGRAPHS contd.

75A	"	"	1.40	6.30	
75B	"	"	1.40	6.30	
76	4-23-75	XD-M1	-	-	Calibration for photos. 76 through 79B.
77	"	"	0.60	1.30	Standard XD. SG = 1.059. Gly.-Water.
78A	"	"	1.00	3.65	
78B	"	"	1.00	3.65	
79A	"	"	1.40	7.20	
79B	"	"	1.40	7.20	
80A	4-30-75	XD-M1	-	-	Calibration for photos 80A through 84.
80B	"	"	-	-	"
81A	"	"	-	3.20	Cross-flow.= 1.13 gal/min. Total flow = 2.0 gal/min. S.G. = 1.059. flow → o/o →
82A	"	"	1.07	-	No cross-flow. flow → o/o
82B	"	"	1.07	-	" "
82RA	"	"	.87	2.65	No cross-flow. flow → o/o
82RB	"	"	.87	2.65	" "
83	"	"	-	3.25	Cross-flow - 1.12 gal/min. Total flow = 2.0 gal/min. flow → o o →
84	"	"	.88	2.75 (?)	No cross flow. flow → o o

RECORD OF PHOTOGRAPHS contd.

85	5-20-75	-	-	-	Calibration for photos. 85 through 92.
86	"	XD-M6	0.6	0.7	S.G. = 1.085. Modified x-doublet. Metering element of XD-M1 beveled .05" x 45° on outlet side.
87	"	"	1.0	2.1	"
88	"	"	1.4	4.5	"
89	"	XD-M1	0.82	2.44	S.G. = 1.085. For direct comparison with prototype photographs.
90	"	"	1.00	3.66	"
91	"	"	1.14	4.88	"
92	"	"	1.28	6.10	"
93	7-11-75	XD-M7	-	-	Calibration for pnotos. 93 through 99A.
94	"	"	1.0	3.2	S.G. = 1.09, Modified x-doublet. Orifice spacing increased 50% over XD-M1.
95	"	"	1.2	4.7	"
97	"	"	1.4/1.6	6.6/8.8	(Photo. not identified properly.)
99A	"	"	1.0	-	"

Calibration Data

Injector	S.G.	Flow Rate (grams/sec)	Pressure Drop (psi)
XD-P	1.0	1.99	10
		1.97	10
		2.37	15
		2.32	15
		2.67	20
		2.66	20
		3.01	25
		2.98	25
		3.32	30
		3.31	30
		3.63	35
		3.57	35
		3.77	40
		3.84	40
		4.05	45
		4.01	45
		4.32	50
		4.22	50
		4.43	55
		4.51	55

Injector	S.G.	Flow Rate (gal/min)	Pressure Drop (psi)
XD-M1	1.085	.2	.12
		.3	.35
		.4	.60
		.5	.95
		.6	1.25
		.7	1.75
		.8	2.35
		.9	2.90
		1.0	3.65
		1.1	4.30
		1.2	5.30
		1.3	6.20
		1.4	7.20
		1.5	8.35
		1.6	9.65
		1.7	11.10
		1.8	12.45
		1.9	14.00
		1.96	14.95
XD-M1	1.059	.4	.65
		.6	1.30

Calibration Data continued

SP-P	1.0	1.41	10
		1.39	10
		1.80	15
		1.94	15
		1.88	15
		1.97	15
		2.29	20
		2.27	20
		2.59	25
		2.55	25
		2.83	30
		2.82	30
		3.08	35
		2.98	35
		3.23	40
		3.20	40
		3.38	45
		3.38	45
		3.58	50
		3.56	50
		3.75	55
		3.72	55

		.8	2.25
		1.0	3.65
		1.2	5.25
		1.4	7.20
XD-M2	1.085	.8	2.35
		1.0	3.75
		1.2	5.50
		1.4	7.50
XD-M3	1.085	.8	1.95
		1.0	3.10
		1.2	4.50
		1.4	6.25
XD-M4	1.085	.8	2.05
		1.0	3.45
		1.2	4.95
XD-M5	1.085	.8	1.45
		1.0	2.35
		1.2	3.45
		1.4	4.70

Calibration Data continued

Injector	S.G.	Flow Rate (gal/min)	Pressure Drop (psi)
XD-M6	1.085	0.6	0.70
		1.0	2.10
		1.4	4.50
XD-M7	1.09	1.0	3.20
		1.2	4.70
		1.4	6.60
		1.6	8.80
VD-M1	1.09	1.6	1.30
		1.8	1.80
		2.0	2.30

Fan Spreading Angle Data

Negative No.	Injector	Angle (deg.)	Flow Rate (gal/min)	Pressure Drop (psi)	S.G.	$\left(\frac{\Delta p \ell}{\sigma}\right)$
1	XD-P	67		10	1.0	480
2		89		20		960
3		107		30		1440
4		99		40		1920
5		106		50		2400
6		67		10		480
7		84		20		960
8		104		30		1440
9		103		40		1920
10		107		50		2400
11		24		5		240
47B	XD-M1	29	.4	.60*	1.085	229
48B		49	.6	1.25		478
50B		104	1.0	3.70		1413
49B		89	.8	2.35		898
51A		107	1.2	5.30		2025
52A		111	1.4	7.30		2789
53B		106	1.6	9.70		3705

*Pressure data for XD-M1 read from calibration curve.

Initial Sheet Length Data

Negative No.	Injector	Actual Length* (in.)	$(\ell_i/\ell)^\dagger$	S.G.	$\left(\frac{\Delta p \ell}{\sigma}\right)$
1	XD-P	.48	24	1.0	480
2		.50	25		960
3		.53	26.3		1440
4		.50	25		1920
5		.51	25.5		2400
6		.50	25		480
7		.48	24		960
8		.50	25		1440
9		.50	25		1920
10		.48	24		2400
11		.43	21.5		240
47B	XD-M1	3.0	19.2	1.085	229
48B		3.8	24.4		478
49B		5.0	32.1		898
50B		4.5	28.8		1413
51A		4.7	30.1		2025
52A		5.0	32.1		2789
53B		5.2	33.3		3705

*Actual length as measured on photograph.

†Sheet length ℓ_i nondimensionalized with respect to orifice size ℓ.

Mass Distribution Data

x (cm)	$\dot{m}$ (gm/sec)	$\dot{M}$ (gm/sec)	h (cm)	w (cm)	$\left(\frac{x}{w}\right)$	$\left(\frac{\dot{m}}{\dot{M}}\right)$ x 100	plotting symbol
7	0.33	68.5	11.59	15.03	0.47	0.48	0
5	0.38				0.33	0.55	
3	0.94				0.20	1.37	
2	2.38				0.13	3.47	
1.5	3.33				0.10	4.86	
1	4.48				0.07	6.54	
0.75	5.06				0.05	7.39	
0.50	5.54				0.03	8.09	
-0.25	5.84				0.02	8.53	
0	5.79				0	8.45	
+0.25	5.26				0.02	7.68	
0.50	4.76				0.03	6.95	
0.75	4.18				0.05	6.10	
1	3.57				0.07	5.21	
1.5	2.54				0.10	3.71	
2	1.64				0.13	2.39	
3	0.74				0.20	1.08	
5	0.38				0.33	0.55	
7	0.31				0.47	0.45	
7	0.31	68.5	5.72	7.51	0.93	0.45	Δ
5	0.40				0.67	0.58	
3	0.82				0.40	1.20	
2	2.30				0.27	3.36	
1.5	4.01				0.20	5.85	
1	6.19				0.13	9.04	
0.75	8.00				0.10	11.68	
0.50	9.23				0.07	13.47	
-0.25	8.90				0.03	12.99	
0	8.27				0	12.07	
+0.25	6.90				0.03	10.07	

Mass Distribution Data contd.

0.50	5.15				0.07	7.52	
0.75	4.35				0.10	6.35	
1	3.43				0.13	5.01	
1.5	1.89				0.20	2.76	
2	1.07				0.27	1.56	
3	0.74				0.40	1.08	
5	0.37				0.67	0.54	
7	0.25				0.93	0.36	
7	0.45	95.9	11.59	15.03	0.47	0.47	□
5	0.53				0.33	0.55	
3	1.58				0.20	1.65	
2	3.22				0.13	3.36	
1.5	4.08				0.10	4.25	
1	5.71				0.07	5.95	
0.75	6.57				0.05	6.85	
0.50	7.53				0.03	7.85	
-0.25	7.30				0.02	7.61	
0	7.12				0	7.42	
+0.25	7.54				0.02	7.86	
0.50	6.92				0.03	7.22	
0.75	5.81				0.05	6.06	
1	5.36				0.07	5.59	
1.5	3.87				0.10	4.04	
2	3.03				0.13	3.16	
3	1.44				0.20	1.50	
5	0.52				0.33	0.54	
7	0.45				0.47	0.47	

Notation: x - distance from centerline to center of collector slot
$\dot{m}$ - mass collected/unit time in 1/8"-wide collector slot
$\dot{M}$ - total mass flow rate
h - distance from injector to collector
w - one-half spray field width

All data taken with model XD-M1 using SG = 1.085.

APPENDIX E

BLOCKED ORIFICE STUDIES

FLOW RATE VS. PRESSURE DROP
7.8 : 1 SCALE MODEL OF X-DOUBLET
GLYCEROL - WATER MIXTURE (S.G. = 1.085)

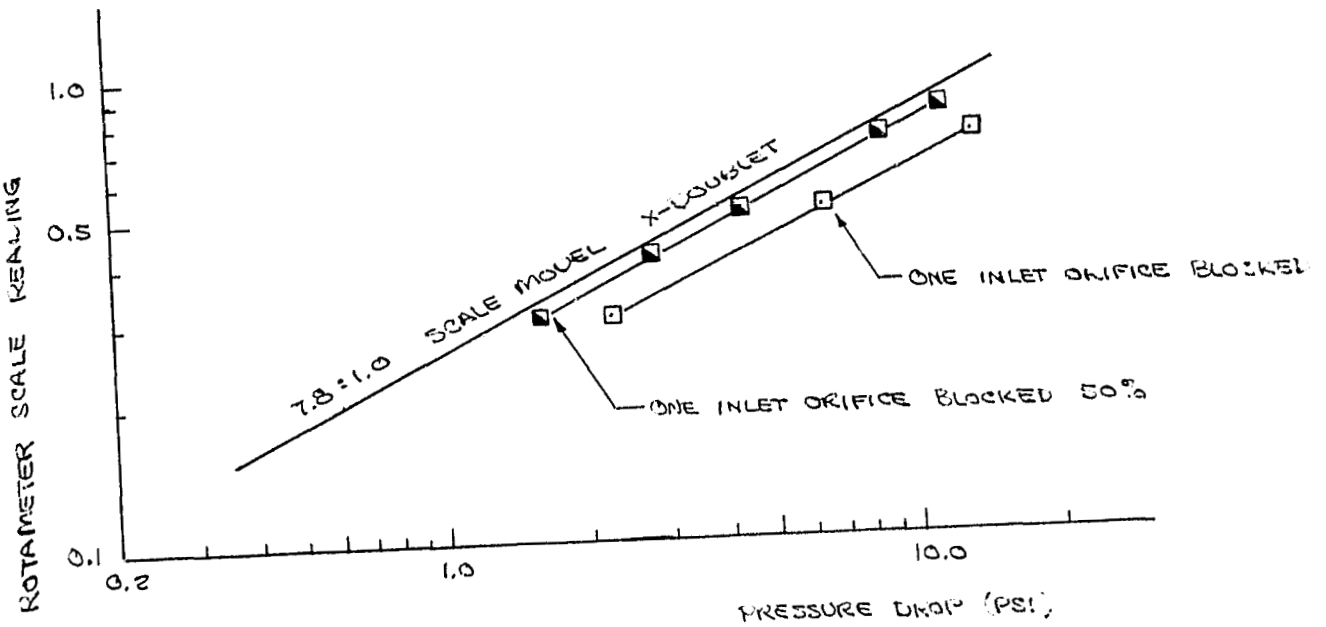

FLOW RATE (GAL/MIN) = SCALE READING × 2.0

PROTOTYPE FLOW RATE ≅ (MODEL FLOW RATE) × (.0489)

PROTOTYPE PRESS. DROP (PSI) ≅ (MODEL PRESS. DROP) × (8.2)

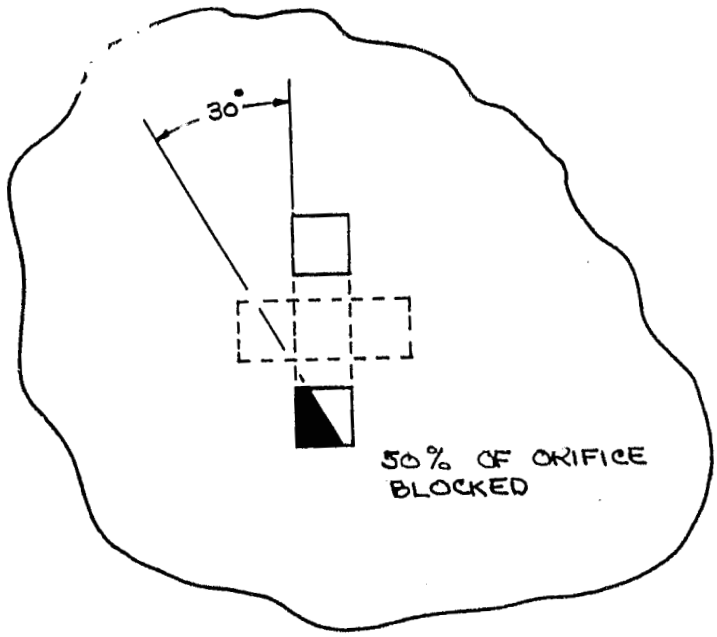

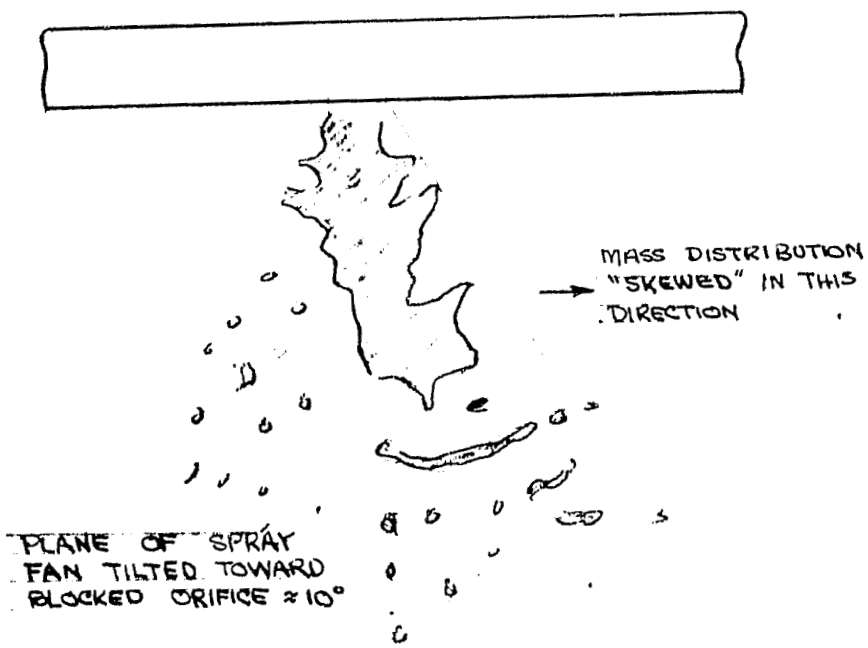

MODEL TEST - X DOUBLET

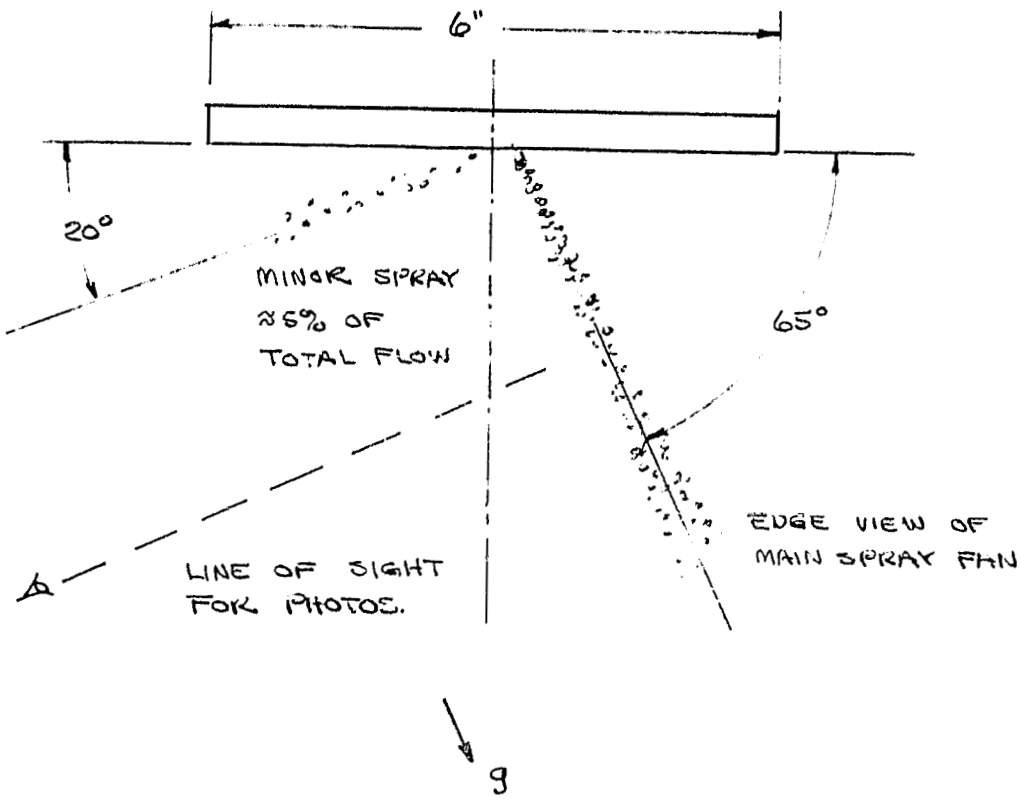

NOTE : Minor spray was blocked to allow photos to be taken. This caused large droplets which appear in photos.

One Inlet Orifice Completely Blocked

X-Doublet